INTERACTION NOTES

NOTE 464

APRIL 1988

Electromagnetic Penetration of Narrow Slot Apertures Having Depth

Larry K. Warne and Kenneth C. Chen

Sandia National Laboratories, Albuquerque, NM 87185

ABSTRACT

The problem of electromagnetic penetration of a narrow slot aperture in a thick, perfectly conducting plane is reduced to the solution of Hallén's integral equation with an equivalent antenna radius. The depth and width of the slot are assumed to be small compared to both the length of the slot and the wavelength. The equivalent radius is evaluated in terms of the solution to the transverse static problem. Simple approximations for the equivalent radius are also given. Hallén's integral equation is solved by both the Galerkin method with piecewise sinusoidal basis functions and by King's three–term method. Large slot depth–to–width ratios give rise to vanishingly small equivalent radii and thus large antenna resonance quality factors. The axial magnetostatic dipole moment of the slot is derived by means of Hallén's iteration method. A simple correction to the static field distribution in the slot is also given. This correction allows the depth to become somewhat larger relative to the wavelength.

ACKNOWLEDGMENT

The authors wish to thank T. E. Koontz, Sandia National Laboratories, who prepared the numerical figures. The authors also wish to acknowledge the helpful discussions with W. A. Johnson and M. E. Morris, Sandia National Laboratories, and E. M. Gurrola, currently at Stanford University.

I. INTRODUCTION

Electromagnetic penetration of apertures in thin, perfectly conducting planes has been studied in considerable detail. References can be found in the books by Lee [1] and Van Bladel [2]. However, apertures always have some depth, and many times, the depth is larger than the width. For example, Figure 1 shows a bolted joint between sections in the outer conducting shell of an object. The aperture has a length of approximately the bolt spacing because the conductors tend to bow when the bolts are tightened. The tortuous depth route is many times the width of the aperture.

Apertures that are infinitely long in thick, perfectly conducting planes have been considered by Harrington and Auckland [3]. Seely [4] has considered arbitrarily shaped apertures, which have small depth compared to the wavelength, in perfectly conducting planes by a modification of existing zero depth moment method codes. Seely's results show increasing slot quality factors with increasing depth.

This paper considers the slot with finite length, $\ell = 2h$, shown in Figure 2. The transverse dimensions, width w and depth d, are assumed to be small compared to both the length ℓ and the wavelength λ. A plane electromagnetic wave impinges on the slot from the half space $y < -\frac{d}{2}$. The problem is reduced to solving Hallén's integral equation with an equivalent antenna radius.

The problem is symmetrized in Section II by allowing a wave to also impinge from the half space $y > \frac{d}{2}$. The "even" excitation of the slot is dominant in the width and depth limits being considered. The field "local" to the slot for the "even" excitation is the same as the field in the transverse static solution corresponding to a cross section of the slot. Section III briefly reviews this two–dimensional static solution. Section IV replaces the

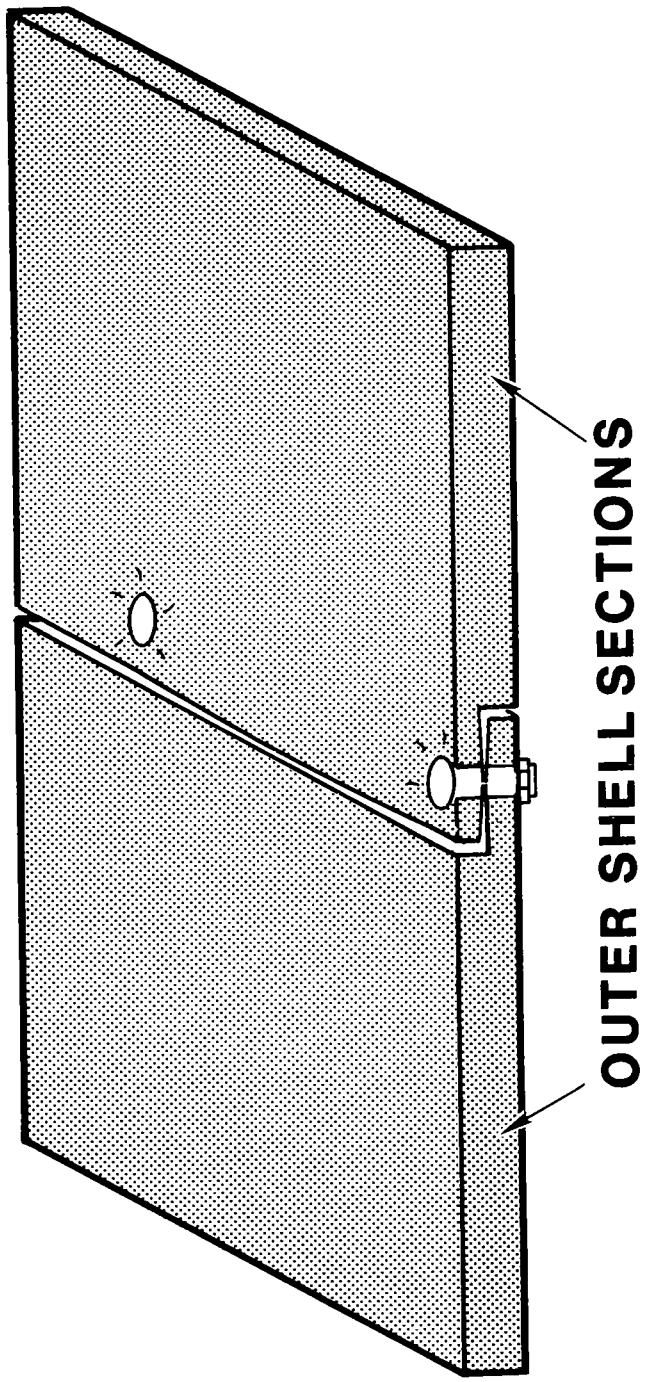

Figure 1. Bolted joint in the outer shell of a system. The conductors tend to bow between bolts, creating a slot aperture having depth.

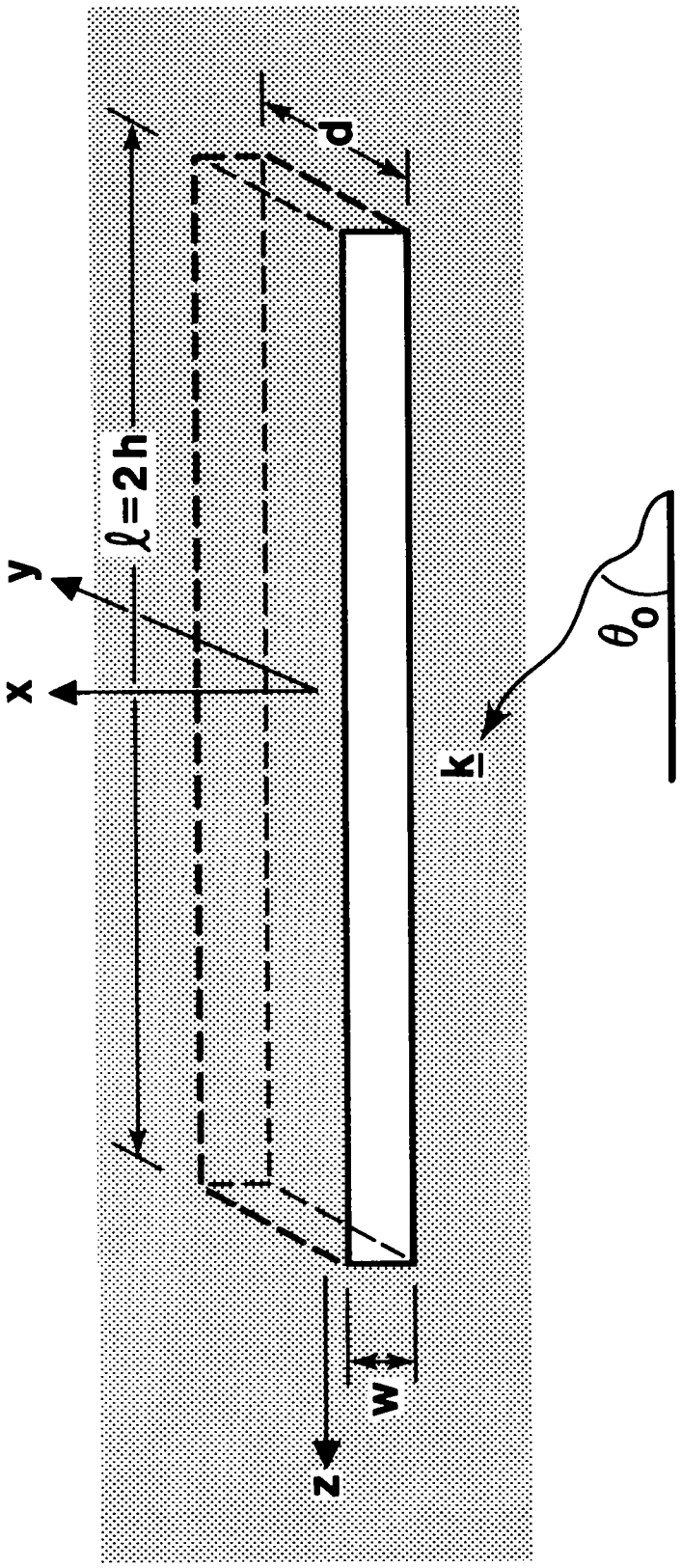

Figure 2. Rectangular slot aperture with length much larger than the width and depth. A plane electromagnetic wave impinges at an angle θ_o with respect to the axial or z direction.

slot by a magnetic cylinder antenna of appropriate equivalent radius, evaluated in terms of the transverse static solution. Section V introduces and gives the solution to Hallén's integral equation (which determines the magnetic current along the antenna or equivalently the voltage along the slot) by means of the Galerkin method with piecewise sinusoidal basis functions and by King's three–term method. Section VI determines the axial magnetostatic dipole moment of the slot by Hallén's iteration method. A simple approximate solution of the "odd" problem, the addition of which allows the depth to become somewhat larger relative to the wavelength, is carried out in section VII.

Appendix I gives a more rigorous derivation of Hallén's integral equation and the equivalent antenna radius starting from the integral equations of the narrow slot with depth [5]. A comparison is also given of the Galerkin solution to the "exact deep" integral equations and the approximate solutions mentioned above.

II. FORMULATION

A wave impinges on the slot in Figure 2 from the half space $y < -\frac{d}{2}$ with fields

$$\underline{E}^{inc} = \underline{E}_o \, e^{i\underline{k} \cdot \underline{r}}, \tag{1}$$

$$\underline{H}^{inc} = \underline{H}_o \, e^{i\underline{k} \cdot \underline{r}}, \tag{2}$$

where $\underline{H}_o = (\underline{k} \times \underline{E}_o)/(\omega\mu_o)$ and $\underline{E}_o$ are the vector amplitudes, $\underline{k} = k_x\underline{e}_x + k_y\underline{e}_y + k_z\underline{e}_z$ is the wave vector, $\underline{r} = x\underline{e}_x + y\underline{e}_y + z\underline{e}_z$ is the position vector, ω is the radian frequency, and time dependence $e^{-i\omega t}$ is used throughout.

The problem is scalarized by the following procedure. The fields can be expressed in terms of the electric vector potential [6]. However, because the slot is narrow

$$kw << 1, \; w << \ell, \tag{3}$$

the small axial electric field E_z, at the faces of the slot, $y=\pm d/2$, $0<x<w$, may be ignored. A magnetic surface current density [7]

$$\underline{K}_m = -\underline{n} \times (\underline{E}_2 - \underline{E}_1) \quad , \tag{4}$$

where $\underline{n}$ is the unit normal pointing from region 1 to region 2, on the surface of perfect conductors at the slot faces may replace the tangential electric fields. Because E_z is set to zero by conditions (3), the magnetic surface currents are z directed K_{mz}. The integral representation for the electric vector potential $\underline{A}_e$ in terms of these surface currents [7] thus has only a z component A_{ez}. The fields generated by the slot can thus be described by A_{ez}

alone.

The fields are obtained from the electric vector potential by means of [7]

$$\underline{D} = -\nabla \times \underline{A}_e \quad , \tag{5}$$

and

$$\underline{H} = -\nabla \varphi_m + i\omega \underline{A}_e \quad , \tag{6}$$

where the magnetic scalar potential, φ_m, is found from

$$\nabla \cdot \underline{A}_e = i\omega \mu_o \epsilon_o \varphi_m \quad , \tag{7}$$

and the constitutive relations are

$$\underline{D} = \epsilon_o \underline{E} \quad , \tag{8}$$

and

$$\underline{B} = \mu_o \underline{H} \quad . \tag{9}$$

The incident axial magnetic field excites the dominant modes of the slot, where

$$H_z^{inc} = H_{oz} e^{i\underline{k} \cdot \underline{r}} \quad , \tag{10}$$

and H_{oz} is the incident axial magnetic field amplitude. These modes account for the major penetration of the narrow slot.

It is convenient to symmetrize the problem by allowing a wave to impinge on the slot from the half space $y > \frac{d}{2}$. The odd and even short circuit (with the slot shorted) axial

magnetic fields can be written as

$$
\begin{aligned}
2\,H_z^{sc}(\underline{r}) &= H_{oz}\,[e^{i\underline{k}\cdot\underline{r}} + e^{i\underline{k}'\cdot(\underline{r}+d\underline{e}_y)}],\ y \le -\frac{d}{2}\,, \\
&= \mp\, H_{oz}\,[e^{i\underline{k}'\cdot\underline{r}} + e^{i\underline{k}\cdot(\underline{r}-d\underline{e}_y)}],\ y \ge \frac{d}{2}\,,
\end{aligned}
\tag{11}
$$

where $\underline{k}' = k_x\underline{e}_x - k_y\underline{e}_y + k_z\underline{e}_z$. The top (−) sign gives rise to the "even" problem, since E_x is even in y, and the bottom (+) sign gives rise to the "odd" problem, since E_x is odd in y. The field (11) evaluated at the slot faces yields

$$
\begin{aligned}
H_z^{sc} &= H_z^{inc}\,,\ y = -\frac{d}{2} \\
&= \mp\, H_z^{inc}\,,\ y = \frac{d}{2}\,,
\end{aligned}
\tag{12}
$$

where $$H_z^{inc} = \left[H_{oz}\, e^{-ik_y\frac{d}{2}}\right] e^{ikz\cos\theta_o}\,,$$

$k = \omega\sqrt{\mu_o\epsilon_o}$ is the magnitude of the wave vector, θ_o is the angle of incidence with respect to the z axis, and conditions (3) have been used to discard the x dependence. Notice that the quantity in parenthesis is the incident z component of the magnetic field at the center of the incident slot face.

The short circuit axial magnetic field (12) corresponds to a short circuit electric vector potential

$$
\begin{aligned}
A_{ez}^{sc} &= A_{ez}^{inc}\,,\ y = -\frac{d}{2}\,, \\
&= \mp\, A_{ez}^{inc}\,,\ y = \frac{d}{2}\,,
\end{aligned}
\tag{13}
$$

where $$A_{ez}^{inc} = -i \frac{\left[H_{oz}\, e^{-ik_y \frac{d}{2}}\right]}{\omega \sin^2\theta_o}\, e^{ikz\cos\theta_o} \ .$$

Figure 3 shows a cross section of the slot and depicts electric surface currents $\underline{K} = \underline{n} \times \underline{H}$, where $\underline{n}$ is the outward unit surface normal on the conductor. The "odd" problem has very small slot electric fields when the conditions

$$kd << 1,\ d << \ell, \tag{14}$$

hold. Notice that the slot may be shorted in this case without appreciably affecting the flow of surface current. The "even" problem, however, does result in substantial electric fields in the slot. This is obvious from the build up of surface charge on the slot walls in the "even" problem.

The fields in the vicinity of the slot in the "even" problem are static in nature when conditions (3) and (14) hold. The strategy for choosing an equivalent antenna radius, for the "even" problem, is to replace the slot by a simpler structure having the same "local" electrical properties. To do this, we need the "local" transverse static solution to the slot problem.

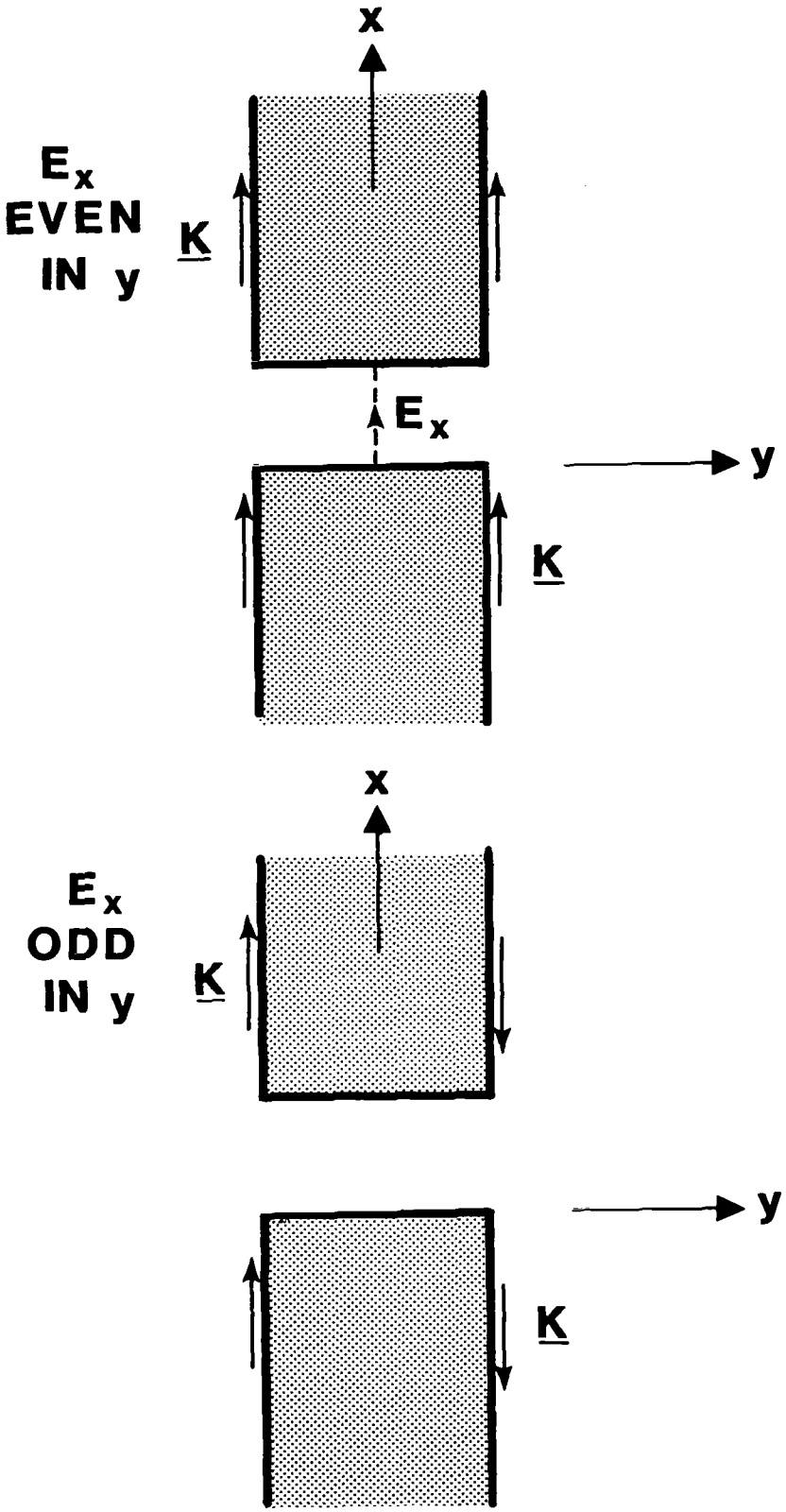

Figure 3. Cross section of rectangular slot aperture and two different parities of excitation with respect to the depth. The "even" problem has significant displacement current inside the slot.

III. TRANSVERSE STATIC SOLUTION

Figure 4 shows the slot cross section. The slot voltage in the "even" problem at a position z is

$$V(z) = \int_0^w E_x \, dx, \tag{15}$$

where the integration is, say, over the incident slot face $y = -\frac{d}{2}$. The "local" transverse electrostatic problem can thus be taken as having the left conductor ($x \leq 0$) at electrostatic potential V and the right conductor ($x \geq w$) at electrostatic potential 0.

The Schwarz – Christoffel transformation [8] can be used to transform the region surrounding the conductors in the $z = x + iy$ plane of Figure 4 to the upper half of a $z_1 = x_1 + iy_1$ plane. An exponential transformation can then be used to map the problem into a strip domain with uniform field (Note that the antenna mode consists of equal and opposite charges on the left and right conductors. Introduction of a second incident wave reflected in the $x = w/2$ plane [5] allows the problem to be decomposed into an antenna problem driven by the axial magnetic field and a problem driven by the transverse magnetic field and normal electric field). The electric field is given by

$$\underline{E} = -\nabla\varphi \quad , \tag{16}$$

where the electrostatic potential φ can be taken as the imaginary part of a complex potential W

$$\varphi = \text{Im } W \quad . \tag{17}$$

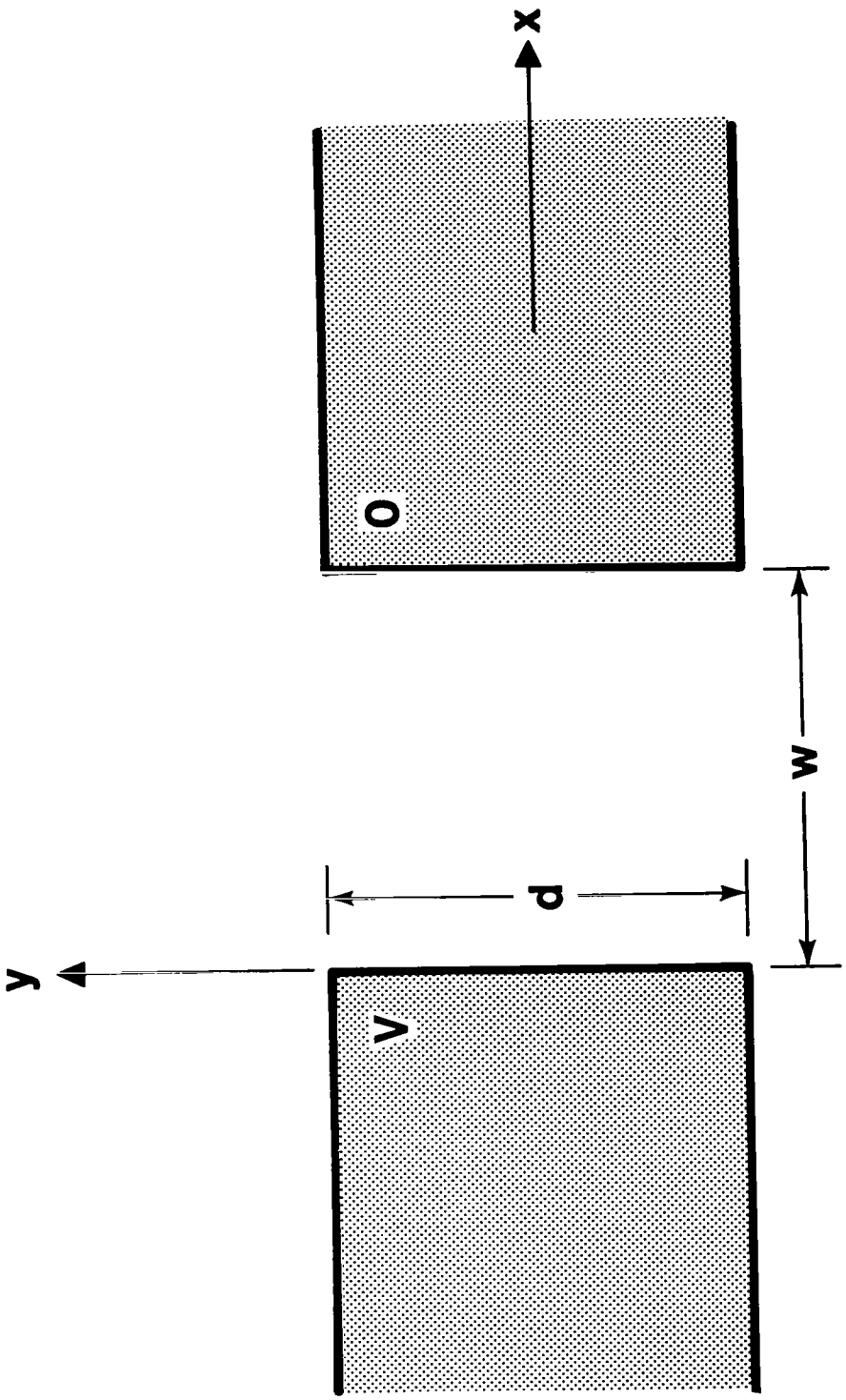

Figure 4. Rectangular slot cross section and electrostatic potentials for the "even" problem.

The complex potential from the conformal mapping is

$$W = \frac{V}{\pi} \ell n\left(\frac{z_1}{a_1}\right) \quad , \tag{18}$$

where [9]

$$z = C_1 \int_1^{z_1} \frac{\sqrt{(1-z_1^2)(1-p^2 z_1^2)}}{z_1^2} dz_1 + w - i\frac{d}{2} \ , \tag{19}$$

and a_1 is an arbitrary real constant. The usual principal value is taken for the branch of the square root of each linear factor in the integrand of (19). The parameter p is determined from the transcendental equation [9]

$$2\frac{d}{w} = -\frac{2E(p') - (1+p^2)\,K(p')}{2E(p) - (1-p^2)K(p)} \quad , \tag{20}$$

where

$$K(p) = \int_0^{\pi/2} \frac{d\theta}{\sqrt{1-p^2 \sin^2\theta}} \quad , \tag{21}$$

$$E(p) = \int_0^{\pi/2} \sqrt{1-p^2 \sin^2\theta}\ d\theta \quad , \tag{22}$$

are complete elliptic integrals of the first and second kinds, and

$$p' = \sqrt{1 - p^2}\,. \tag{23}$$

The constant C_1 is determined from p by means of the relation [9]

$$\frac{w}{2C_1} = (1-p^2)\,K(p) - 2E(p) \quad . \tag{24}$$

Figure 5 [9] shows a plot of p and $-C_1/w$ as a function of d/w. The asymptotic limit [9]

$$p \sim 4/e^{(2+\pi d/w)} \quad , d/w >> 1 \quad , \tag{25}$$

is also shown. The value of p approaches unity as $d/w \to 0$. The quantity $-C_1/w$ approaches $1/\pi$ for $d/w >> 1$ and the value 1/4 for $d/w \to 0$. Expansions for p and $-C_1/w$ that give accurate results over the full range of d/w are given in Appendix II.

Figure 6a shows the "local" electrostatic field lines. Figure 6b shows the corresponding orthogonal magnetostatic field lines.

The electric field can alternatively be derived from the z component of the electric vector potential by means of (5) and (8) where we may take

$$A_{ez} = -\epsilon_o \,\mathrm{Re}\, W. \tag{26}$$

The magnetic field may be determined from a magnetostatic scalar potential φ_m

$$H = -\nabla\varphi_m \quad , \tag{27}$$

where we may take

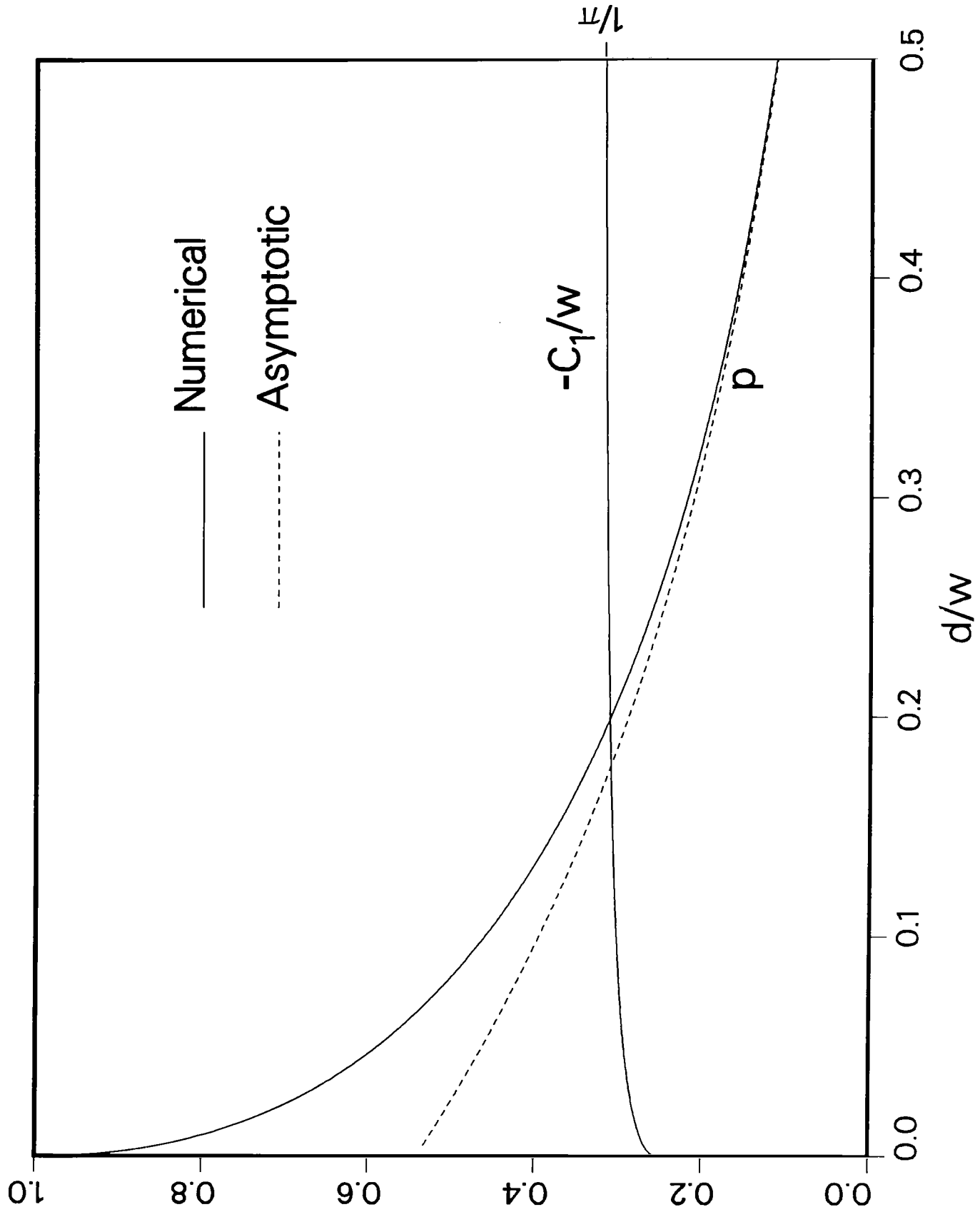

Figure 5. Parameters of conformal mapping solution of the electrostatic slot problem.

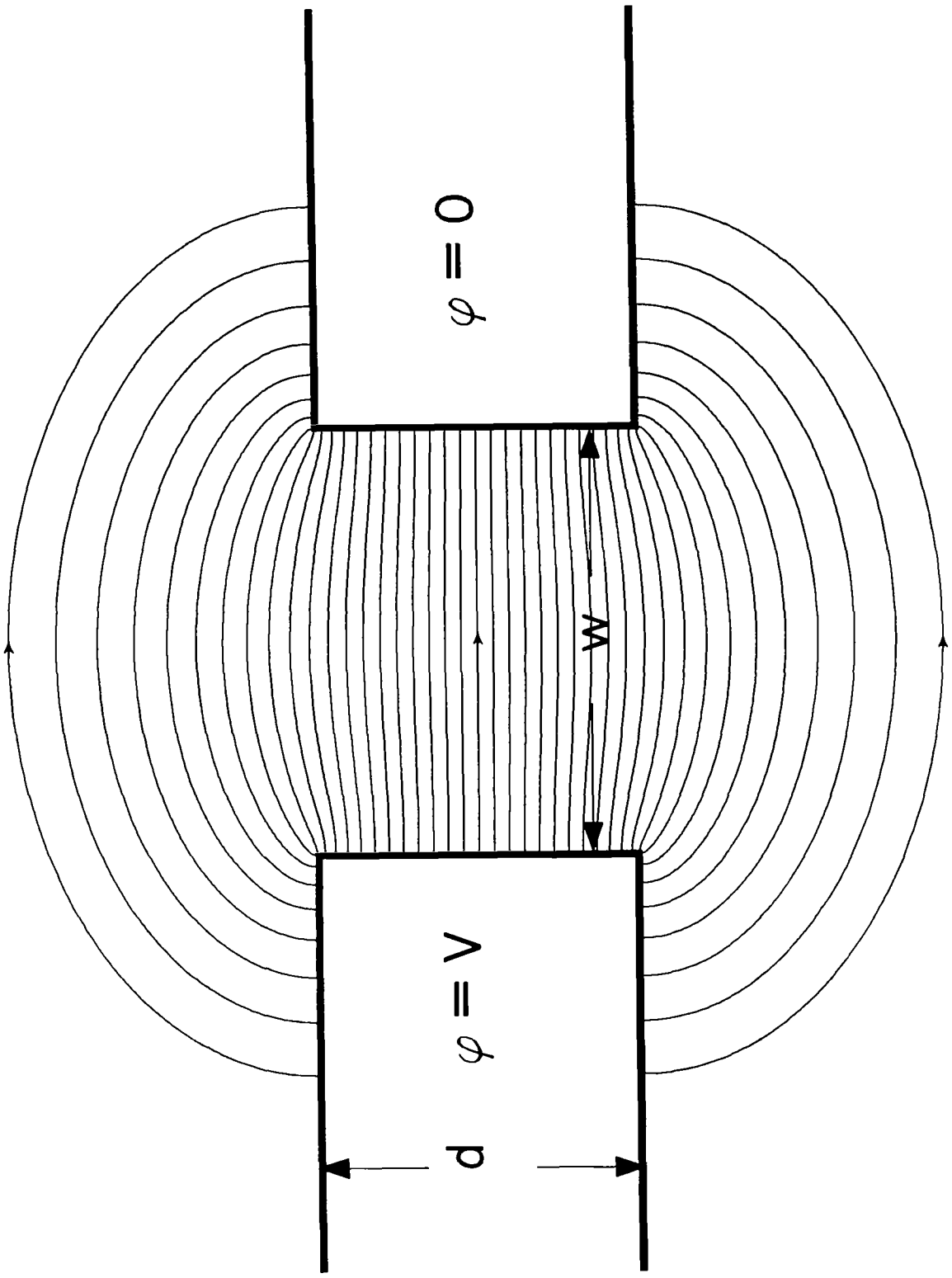

Figure 6. "Local" fields surrounding the slot are static in the "even" problem. (a) Electrostatic field generated by the potential difference V.

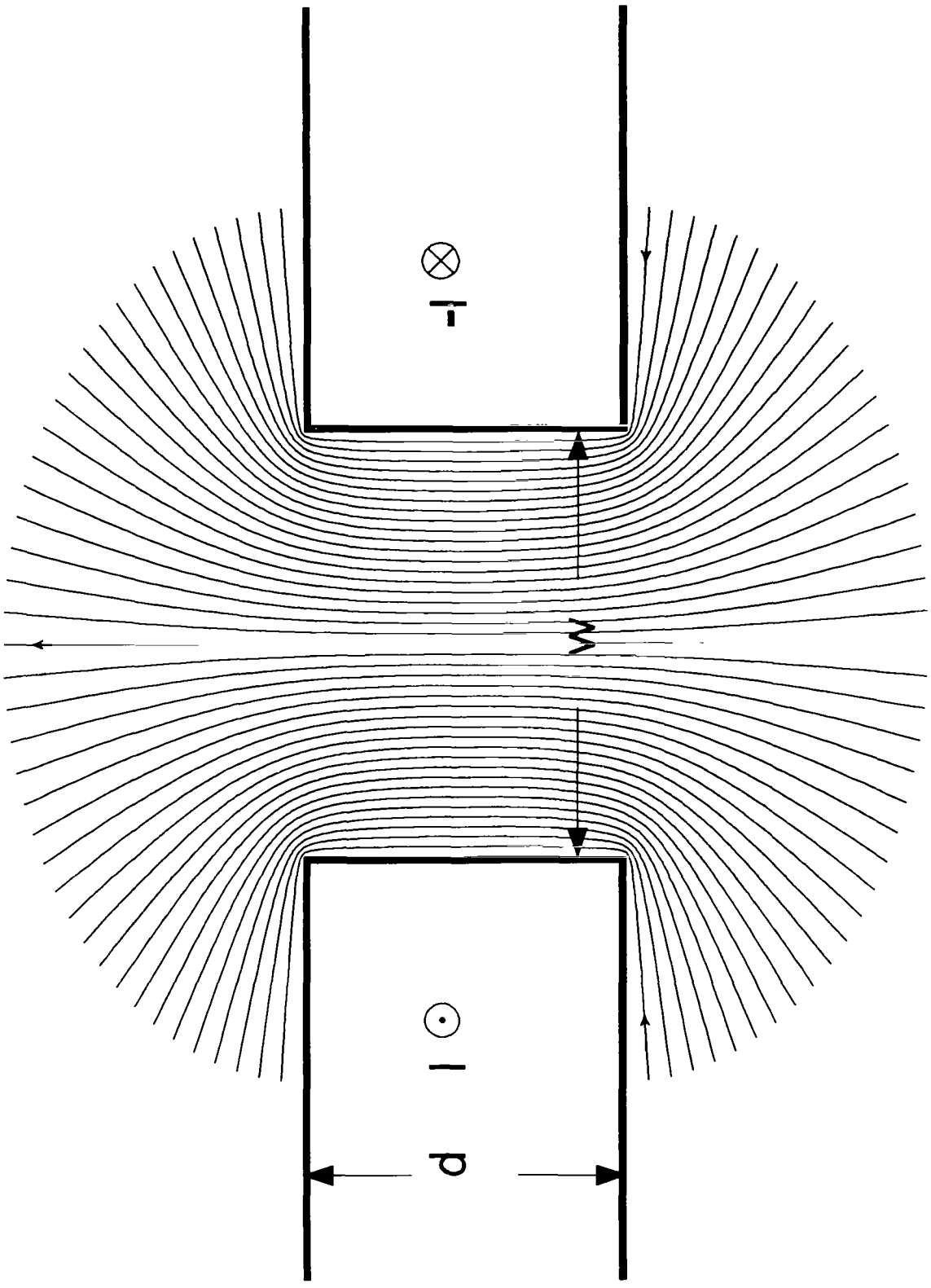

(b) Magnetostatic field generated by the axial current I.

$$\varphi_m = -\frac{1}{\mu_o} \operatorname{Re} W \quad , \tag{28}$$

and the voltage V, in (18), is replaced by the total magnetic flux per unit length $\bar{\Phi}$, passing through the slot in the y direction

$$\bar{\Phi} = \int_o^w B_y \, dx \quad .$$

IV. EQUIVALENT ANTENNA RADIUS

Consider the structure shown in Figure 7. The cylindrical surface is a perfect magnetic conductor. The two half planes are perfect electric conductors at different potentials. The exterior field at points distant (compared to the width) from the slot of Figure 4 is nearly identical to the field in Figure 7. Of course to make these exterior fields the same, the coordinate system in Figure 7 must be aligned with the center of one of the slot faces $y = \pm \frac{d}{2}$, in the slot problem of Figure 4, depending on which half space, $y \gtrless \pm \frac{d}{2}$, is being considered. We wish the antenna properties of the structure in Figure 7 to be the same as those of the "even" slot problem. The "local" fields of the "even" slot problem are approximately TEM [10]. If the "local" capacitance per unit length and the "local" inductance per unit length are made to agree with those of the slot, by choosing an appropriate equivalent radius, a, in Figure 7, then the antenna properties of this structure will be the same as those of the slot.

Let us choose a distance R characteristic of the extent of the "local" region such that

$$kR << 1, \ell >> R >> w \ . \tag{29}$$

Figure 8 shows the slot with the distance R marked on the left conductor. The charge per unit length Q_R, on the left conductor (out to the distance R on the exterior of the slot and including the interior wall of the slot), can be found by integrating the normal component of $\underline{D}$ over the metal surface. Using (5) and Stokes integral theorem this charge is

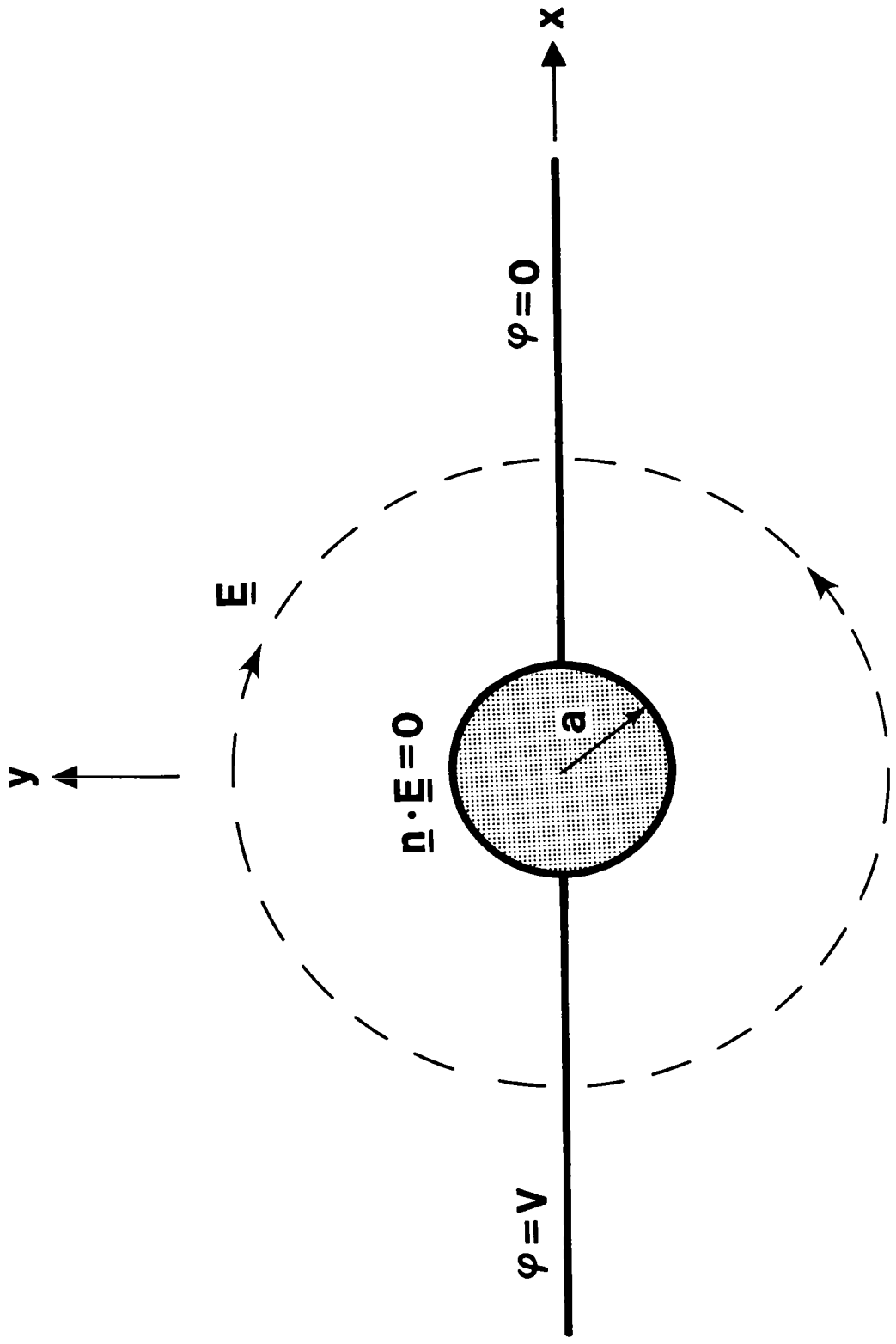

Figure 7. Perfect magnetic conducting cylinder of radius a sandwiched between two perfect electric conductors at different electrostatic potentials.

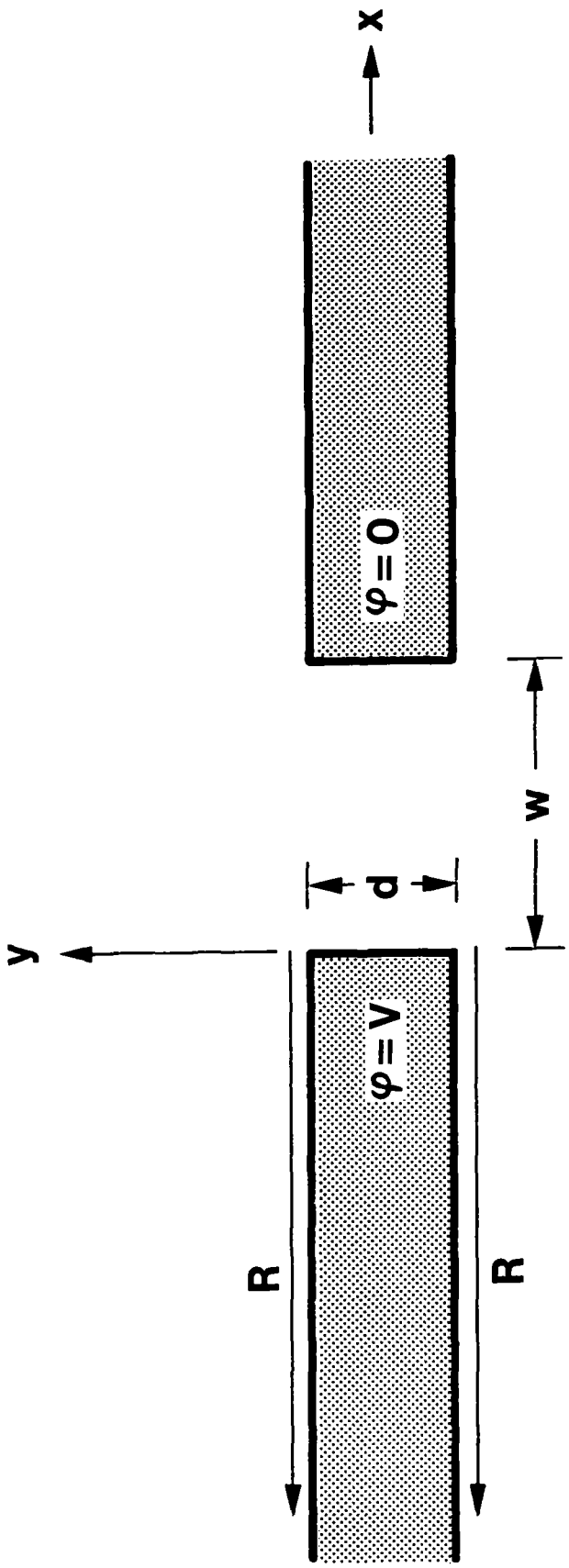

Figure 8. Rectangular slot cross section with distance R shown. The distance R is much larger than w, but much smaller than the slot length and the wavelength.

$$Q_R = -\oint_C \underline{A}_e \cdot \underline{d\ell} \ , \tag{30}$$

where the contour, C, bounds the surface over which the charge is desired. Because $\underline{A}_e$ has only a z component, from (30) we obtain

$$Q_R = A_{ez}(z = -R - i\,\frac{d}{2}) - A_{ez}(z = -R + i\,\frac{d}{2}) \ , \tag{31}$$

where the subscript z has the meaning of axial coordinate, whereas the argument z has the meaning of complex location $z = x + iy$ in the transverse plane.

The electric vector potential in (31) is obtained from (26). Expanding (19) at the locations indicated in (31) yields the asymptotic relations [5]

$$z_1 \sim \frac{R}{pC_1} \ , z = -R + i\,\frac{d}{2} \ , \tag{32}$$

$$z_1 \sim \frac{C_1}{R} \ , z = -R - i\,\frac{d}{2} \ , \tag{33}$$

where R is large (compared to w) and positive. Using (32) and (33) in (18) the electric vector potential (26) can be evaluated in (31) to give

$$Q_R \sim 2\epsilon_o \frac{V}{\pi} \ell n\left[\frac{R}{-C_1\sqrt{p}}\right] . \tag{34}$$

The local capacitance per unit length is simply

$$C_R = Q_R / V \ . \tag{35}$$

The charge per unit length, out to a radius R, on the left conductor of Figure 7 is

$$Q_R = 2\epsilon_o \int_a^R E_\phi \, d\rho = 2\epsilon_o \frac{V}{\pi} \ell n(\frac{R}{a}) \quad , \tag{36}$$

where ρ and ϕ are cylindrical coordinates, E_ϕ is the electric field in the lower half space, and the factor of 2 accounts for the upper surface of the conductor. Comparing (34) and (36), or the corresponding capacitances per unit length (35), we can make them equal by taking the equivalent radius to be

$$a = - C_1 \sqrt{p} \ . \tag{37}$$

This choice of equivalent radius, of course, also makes the "local" inductances per unit length,

$$L_R = \Phi / I_R \ , \tag{38}$$

equal. The current I_R, out to a large distance R on the left conductor, including the interior wall, is found from

$$I_R = \int_C \underline{H} \cdot (\underline{e}_z \times \underline{n}) \, d\ell \quad , \tag{39}$$

where the contour C extends over the left conductor surface, and $\underline{n}$ is the outward unit surface normal on the conductor.

Two limiting forms of the equivalent radius can be found from limiting values of p

and $-C_1/w$ as

$$a \sim \frac{w}{4} \ , \frac{d}{w} \to 0 \quad , \tag{40}$$

and using (25)

$$a \sim \frac{2}{\pi} w/e^{(1+\frac{\pi d}{2w})} \ , \frac{d}{w} >> 1. \tag{41}$$

A useful approximation to the equivalent radius can also be derived by considering Figure 9. The electric field surrounding the slot in a very thick plane is compared with a uniform interior field and the exterior field surrounding a slot in an infinitely thin conducting plane. The charge deposited on the conductors is well approximated by the composite uniform–thin slot field distribution. The thin slot exterior charge per unit length can be obtained from the limit ($\frac{d}{w} \to 0$) of (34) as

$$Q_R^> \sim 2\epsilon_o \frac{V}{\pi} \ell n(\frac{R}{w/4}) \ . \tag{42}$$

The uniform field interior charge per unit length is

$$Q_{unif}^< = \epsilon_o \frac{V}{w} d \ . \tag{43}$$

Adding (42) and (43) and comparing with (36) yields the approximate equivalent radius

$$a \approx \frac{w}{4} e^{-\frac{\pi d}{2w}} \ . \tag{44}$$

One way to compare the approximation (44), and the exact formula (37), is to compare the fatness parameter

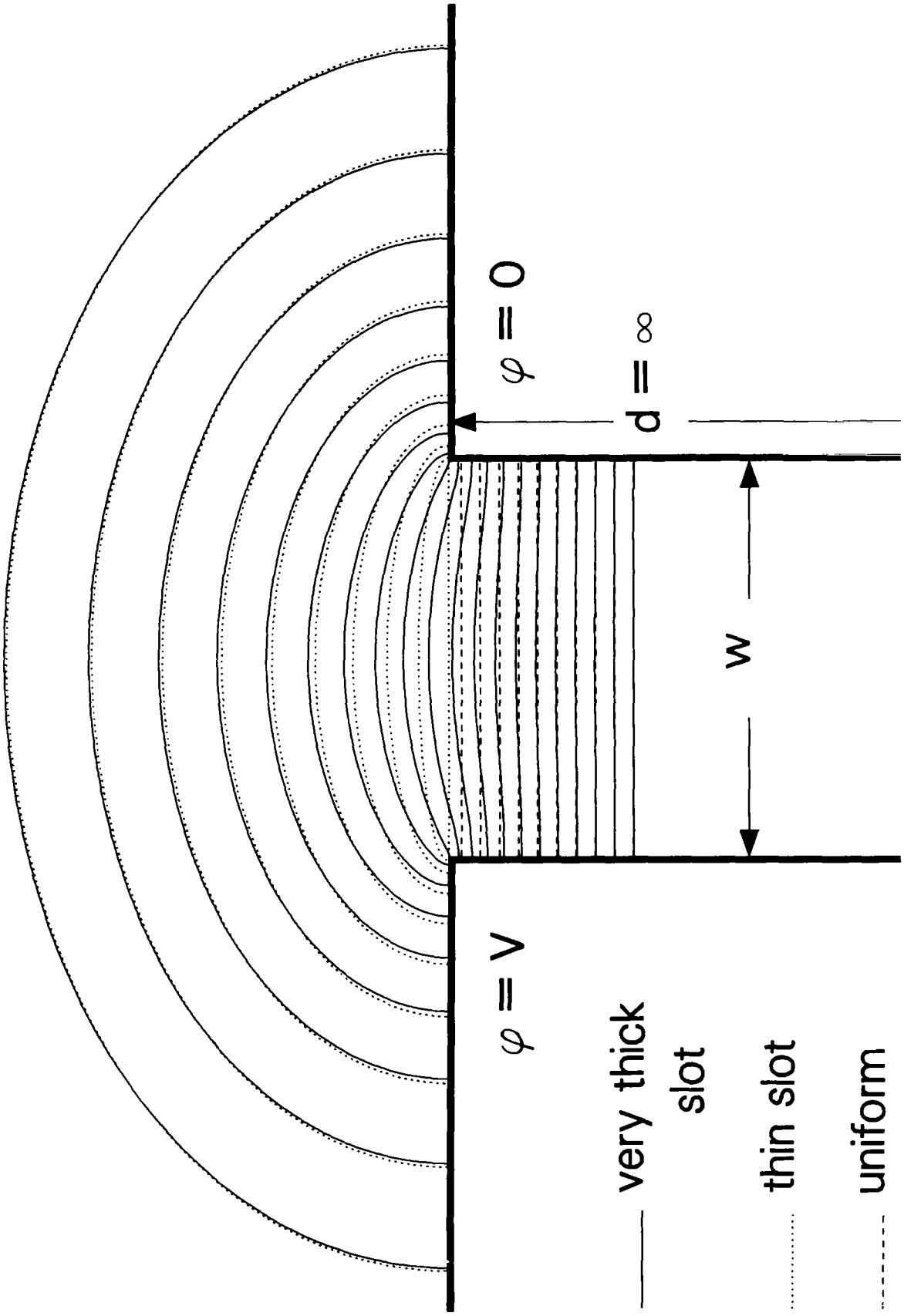

Figure 9. Electrostatic field surrounding a very thick slot. The exterior field surrounding an infinitely thin slot and an interior uniform field are superimposed.

$$\Omega = 2\,\ell n(\frac{2h}{a}) \quad , \tag{45}$$

using each of these two values for a. The reason for comparing Ω is that the fatness parameter is essentially the form the equivalent radius takes in slender antenna theory [11]. The fatness parameter is labeled as Ω_{ap} when (44) is used in (45). Figure 10 shows the ratio of Ω_{ap} to the true Ω for a slot with typical dimensions. The error in using approximation (44) is typically quite small. In fact, using (41) and (44) in (45), we obtain

$$\Omega - \Omega_{ap} \sim 2\,\ell n(\frac{\pi e}{8}) = .13 \quad , \frac{d}{w} >> 1 \quad . \tag{46}$$

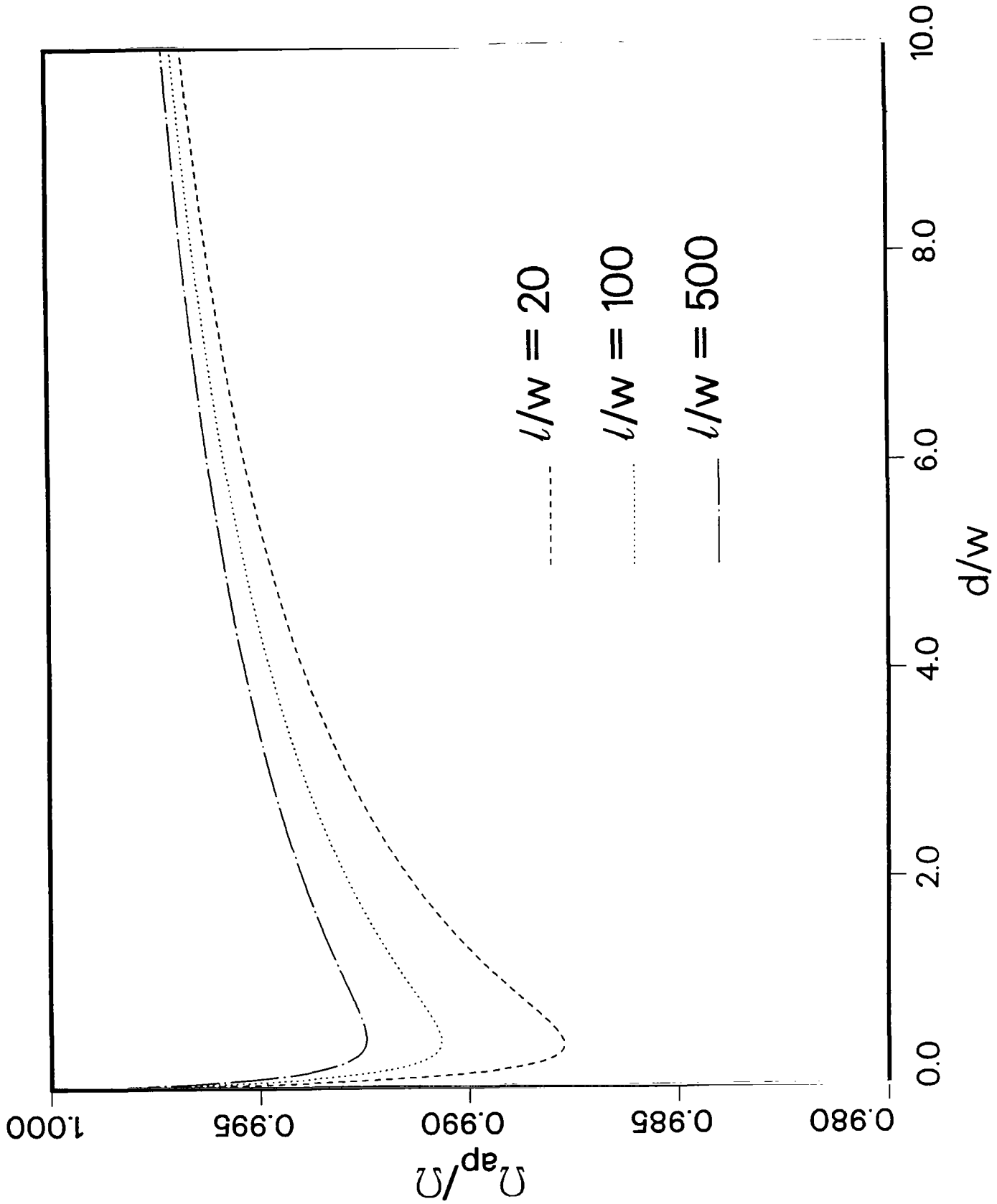

Figure 10. Ratio of antenna fatness parameters for typical slot dimensions. Ω_{ap} is determined from the approximate equivalent radius, whereas Ω is determined from the exact equivalent radius.

V. ANTENNA SOLUTION

Figure 11a shows a magnetic scattering antenna for which the tangential components of the magnetic field vanish on the surface. Figure 11b shows a cross section of the same antenna carrying total magnetic current I_m. If the magnetic current I_m is taken to be

$$I_m = -2V \quad , \tag{47}$$

then the "local" azimuthal electric field in the lower half of Figure 11b,

$$E_\phi = \frac{-I_m}{2\pi\rho} \quad , \tag{48}$$

is identical to that of Figure 7. The electric field in the upper half of Figure 11b is minus that of Figure 7.

The electric vector potential due to the current I_m [7], in Figure 11, is approximately

$$A_{ez} = \epsilon_o \int_{-h}^{h} I_m(z') \, G(\rho,z,z')dz' \quad , \tag{49}$$

where $$G(\rho,z,z') = \frac{e^{ikR}}{4\pi R} \quad ,$$

$$R = \sqrt{\rho^2 + (z-z')^2} \quad .$$

The approximation of assuming the current is confined to a zero radius filament has been

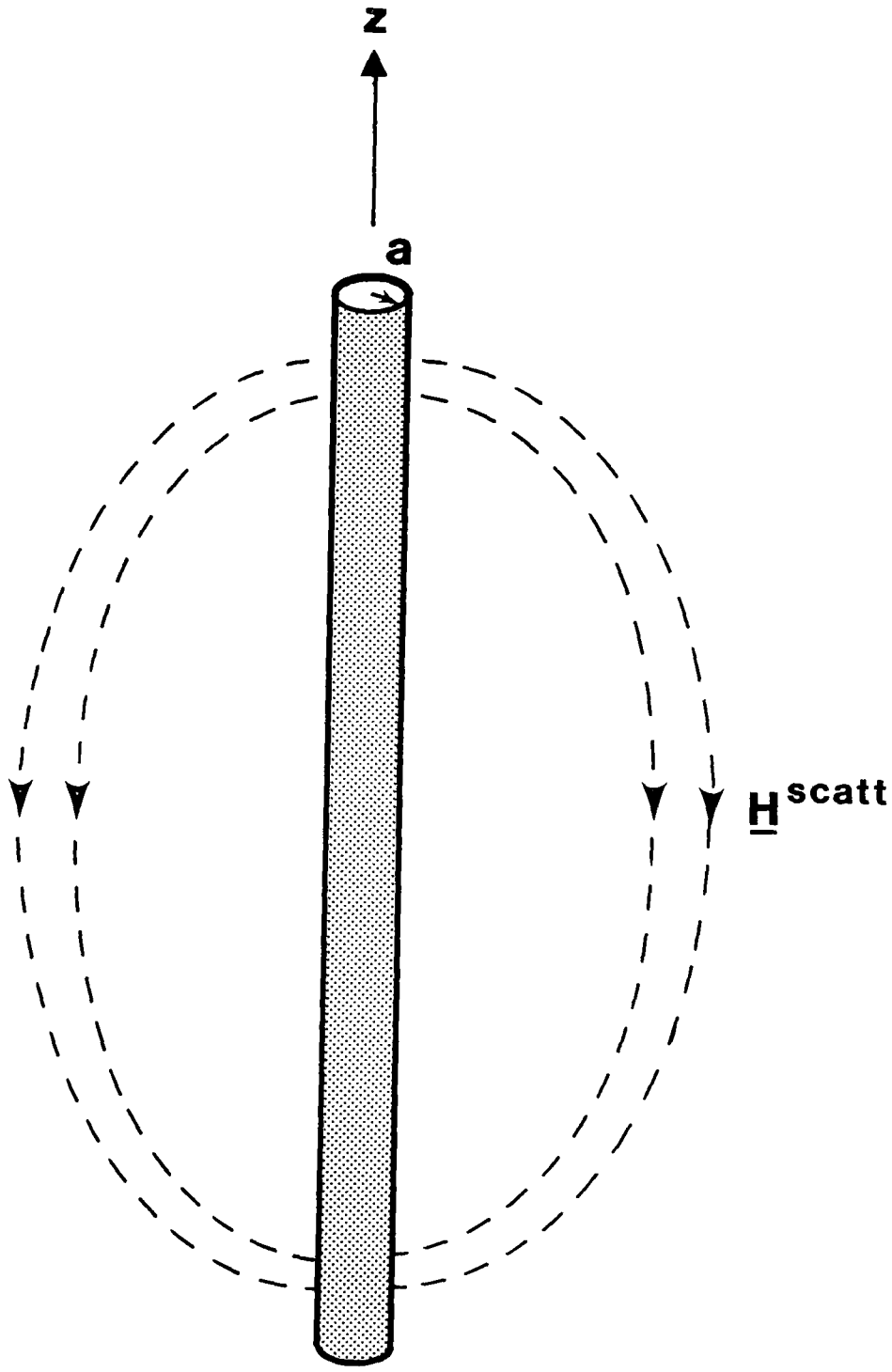

Figure 11. Magnetic scattering antenna of radius a. (a) Scattered magnetic field near the antenna.

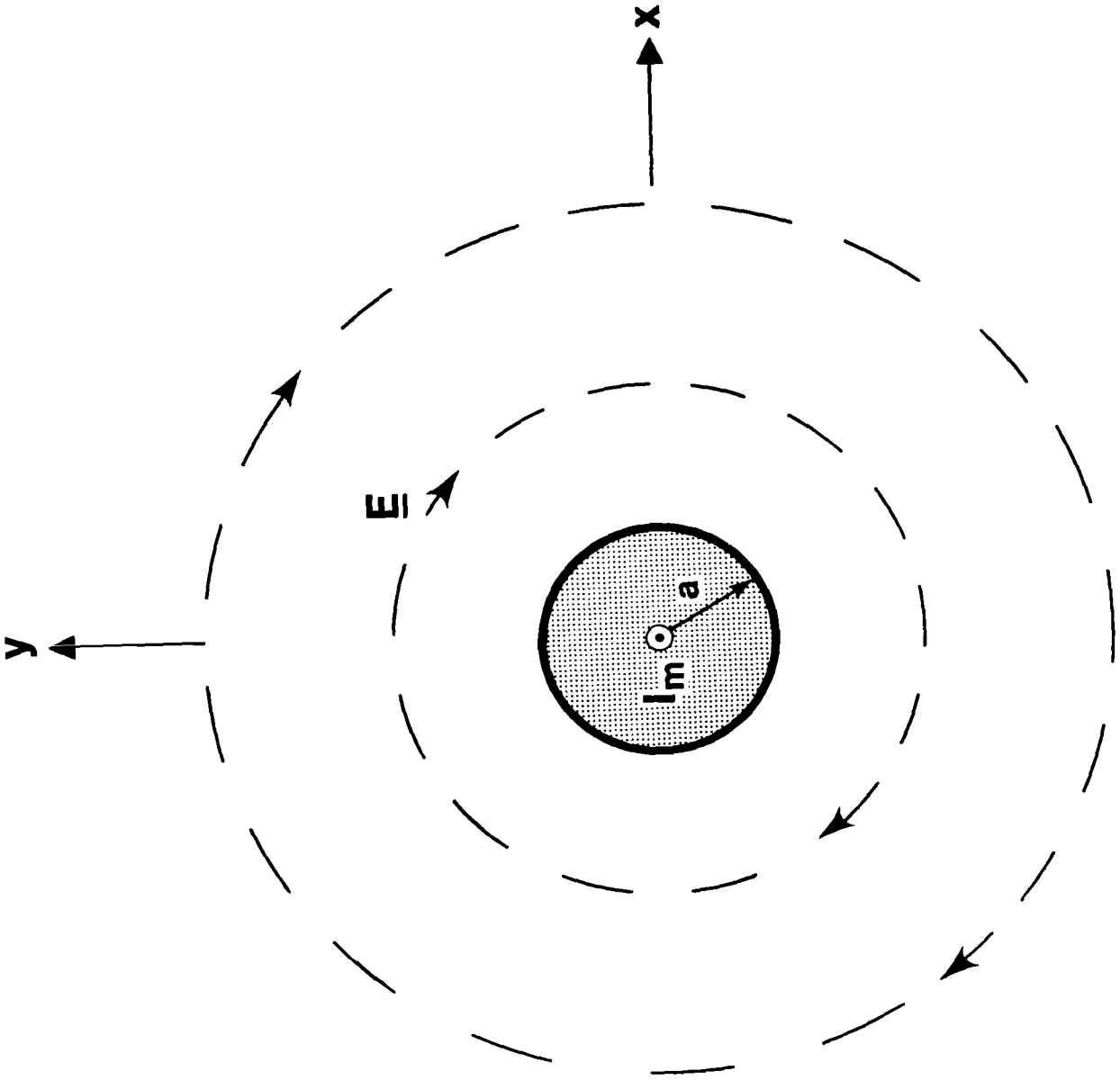

(b) Scattered electric field generated by the magnetic current I_m.

made in (49) [12]. Hallén's integral equation is obtained by requiring the total axial magnetic field, consisting of the sum of the incident field (10) and scattered field, to vanish on the surface $\rho = a$. The scattered magnetic field can be determined from the formula

$$H_z = \frac{i}{\omega\mu_o\epsilon_o}\left[\frac{\partial^2}{\partial z^2} + k^2\right] A_{ez} \quad , \tag{50}$$

where the scattered potential (49) is used in (50). Integration of the differential operator in (50) yields Hallén's integral equation

$$\epsilon_o \int_{-h}^{h} I_m(z') \frac{e^{ikR_a}}{4\pi R_a} dz' = -A_{ez}^{inc}(z) + C_o \cos kz$$

$$+ C_1 \sin kz \quad , \tag{51}$$

where C_o and C_1 are integration constants, $R_a = \sqrt{a^2 + (z-z')^2}$, and the incident electric vector potential at the antenna axis is

$$A_{ez}^{inc}(z) = -\frac{i}{\omega \sin^2\theta_o} H_{oz} e^{ikz\cos\theta_o} \quad . \tag{52}$$

The constants C_o and C_1 are evaluated by requiring

$$I_m(\pm h) = 0 \quad . \tag{53}$$

The scattered field resulting from the cylindrical structure in Figure 7 can also be represented by the magnetic current (47), in the illuminated half space $y < 0$. The total

axial field (50), where A_{ez} is now the sum of the scattered potential (49) and the short circuit "even" problem potential (13) (upper sign), again vanishes on the cylindrical surface $\rho = a$. Hallén's integral equation (51) thus also forms the basis of solution of the "even" slot problem with equivalent radius (37), and relation (47) yielding the voltage along the slot. Note that the short circuit potential of the "even" slot problem (13) is identical to the incident antenna potential (52), provided H_{oz} in (52) is interpreted as the axial magnetic field at the center of the incident slot face. Of course, as a result of condition (14) there is little difference in phase in the slot depth, but nevertheless the figures will be labeled to reflect the phase reference of H_{oz} being at the center of the incident slot face. The solution to (51) will be carried out by two standard methods.

King's three–term method [13] represents the solution to (51), for normal incidence, as

$$I_m(z) = -i4\pi \frac{\eta_o H_{oz}}{k\ Q} \left[\Psi_{dD} \left(\cos kz - \cos kh\right) - i\Psi_{dUI} \left(\cos\tfrac{1}{2}kz - \cos\tfrac{1}{2}kh\right) \right] \quad , \tag{54}$$

where $$Q = \Psi_{dD} \left[\Psi_{dUR} \cos kh - \Psi_U(h) \right] + i\Psi_{dUI}\Psi_D(h) \quad ,$$

and $\eta_o = \sqrt{\mu_o/\epsilon_o}$ is the impedance of free space. Integral representations for the various Ψ parameters are given in Appendix III. The Ψ parameters were evaluated by numerical integration; however, it should be noted that for the examples given, these integral representations can be approximated for small radius a in terms of standard sine and cosine integrals.

The Galerkin method with piecewise sinusoidal basis functions [14] represents the solution to (51) as

$$I_m(z) = \sum_{n=-N}^{N} I_{mn} F_n(z) \ , \tag{55}$$

where I_{mn} are coefficients and the basis functions are piecewise sinusoidal

$$F_n(z) = \frac{\sin(kz - kz_{n-1})}{\sin(kz_n - kz_{n-1})} \ , \quad z_{n-1} \leq z < z_n$$

$$= \frac{\sin(kz_{n+1} - kz)}{\sin(kz_{n+1} - kz_n)} \ , \quad z_n \leq z < z_{n+1} \tag{56}$$

$$= 0 \ , \text{otherwise.}$$

Appendix IV gives the linear system from which the coefficients I_{mn} are determined . The axial locations z_n lie along the antenna interval with

$$z_{\pm(N+1)} = \pm h. \tag{57}$$

Linear spacing

$$z_n = n\Delta \ , \ n = -N-1, \ldots, 0, \ldots, N+1 \ , \tag{58}$$

where $\Delta = h/(N+1)$, was used in the examples.

Appendices III and IV also give formulas for the power radiated by the magnetic current on the antenna. By symmetry, resulting from conditions (3) and (14), the radiated

power is approximately twice the transmitted power

$$P_{rad} = 2\, P_{trans} \quad . \tag{59}$$

Figure 12 gives normalized center voltage $\frac{V(0)}{\ell \eta_o H_{oz}}$ magnitude and normalized radiated power $\frac{P_{rad}}{\ell^2 S_o}$, where $S_o = \frac{1}{2}\,\eta_o |H_{oz}|^2$, for two slot examples. The value of antenna parameters, $\frac{h}{a}$ or Ω, identifies each of the two examples in Figure 12. Many sets of slot parameters $(\frac{\ell}{w}, \frac{d}{w})$ correspond to each of these antenna parameters. The particular case, $\frac{d}{w} = 0$, is listed in Figure 12. The number of basis functions in the Galerkin method (2N+1) was chosen to keep the spacing Δ no smaller than roughly four radii. The incident wave impinges normally ($\theta_o = \pi/2$) in all examples. The agreement between the King three–term solution and the Galerkin solution is quite good. The graphs in Figure 12 were terminated at an abscissa of $\frac{kh}{\pi} = \frac{5}{4}$, because the three–term method is only alleged to be valid up to this point [15].

Figure 13 gives the normalized center voltage magnitude and normalized radiated power from the Galerkin method for a slot with various depths. The peak values of the resonances are nearly independent of the depth, because the reactive components of the antenna, which this parameter strongly influences, cancel out at the resonances. The voltage and radiated power are greatly reduced away from resonance, as the depth increases relative to the width.

Notice that the value of kd, for the case $\frac{d}{w} = 25$, in Figure 13, approaches unity at the upper end of the $\frac{kh}{\pi}$ range. This violates one of the conditions (14). Nevertheless it will be demonstrated in Section VII that these results still give a reasonably good approximation to the slot voltage. This is not too surprising if one considers that the first

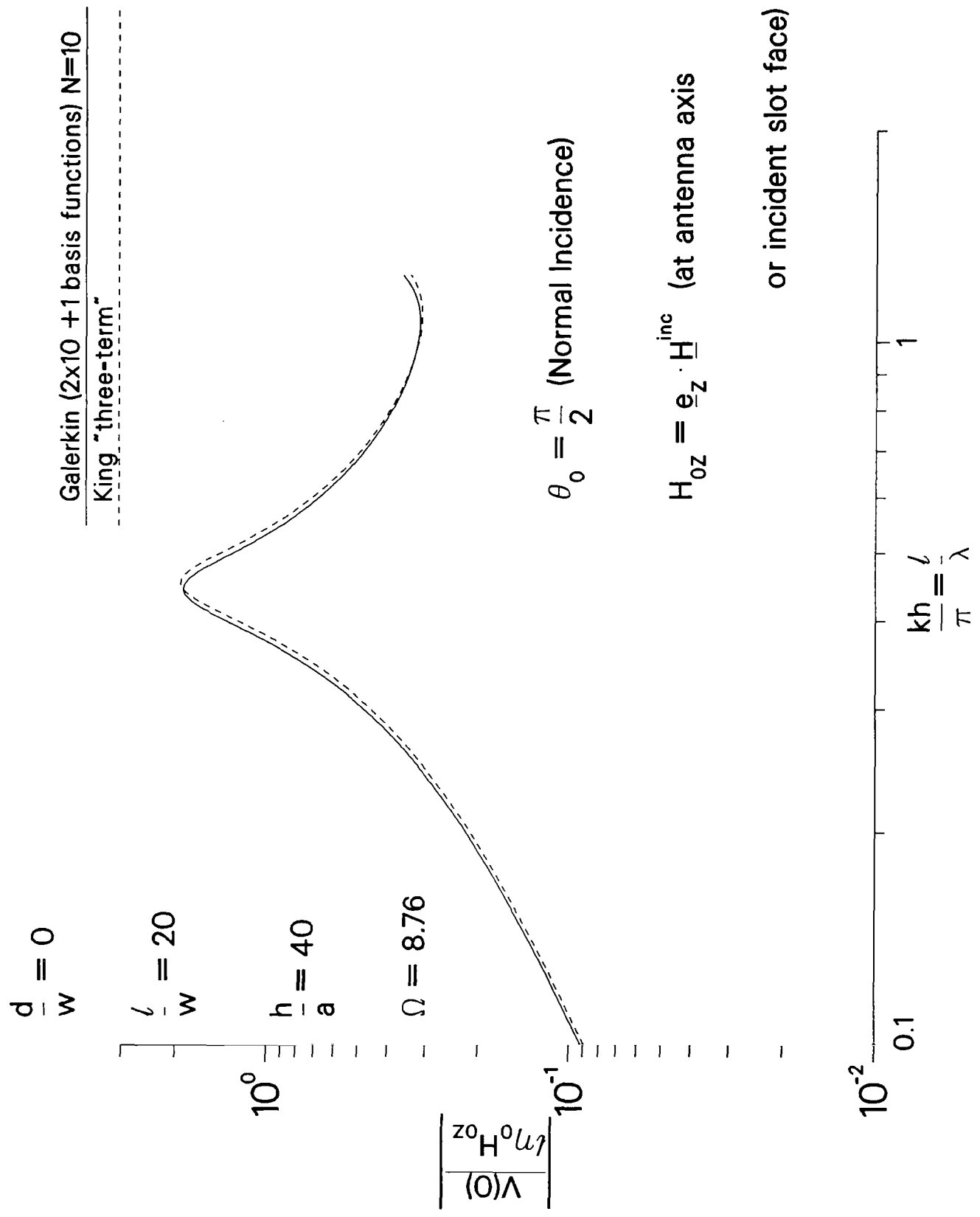

Figure 12. Normalized center voltage magnitude and normalized radiated power for two slot examples. Both the Galerkin solution and King three–term method are shown. (a) Center voltage magnitude $\Omega = 8.76$.

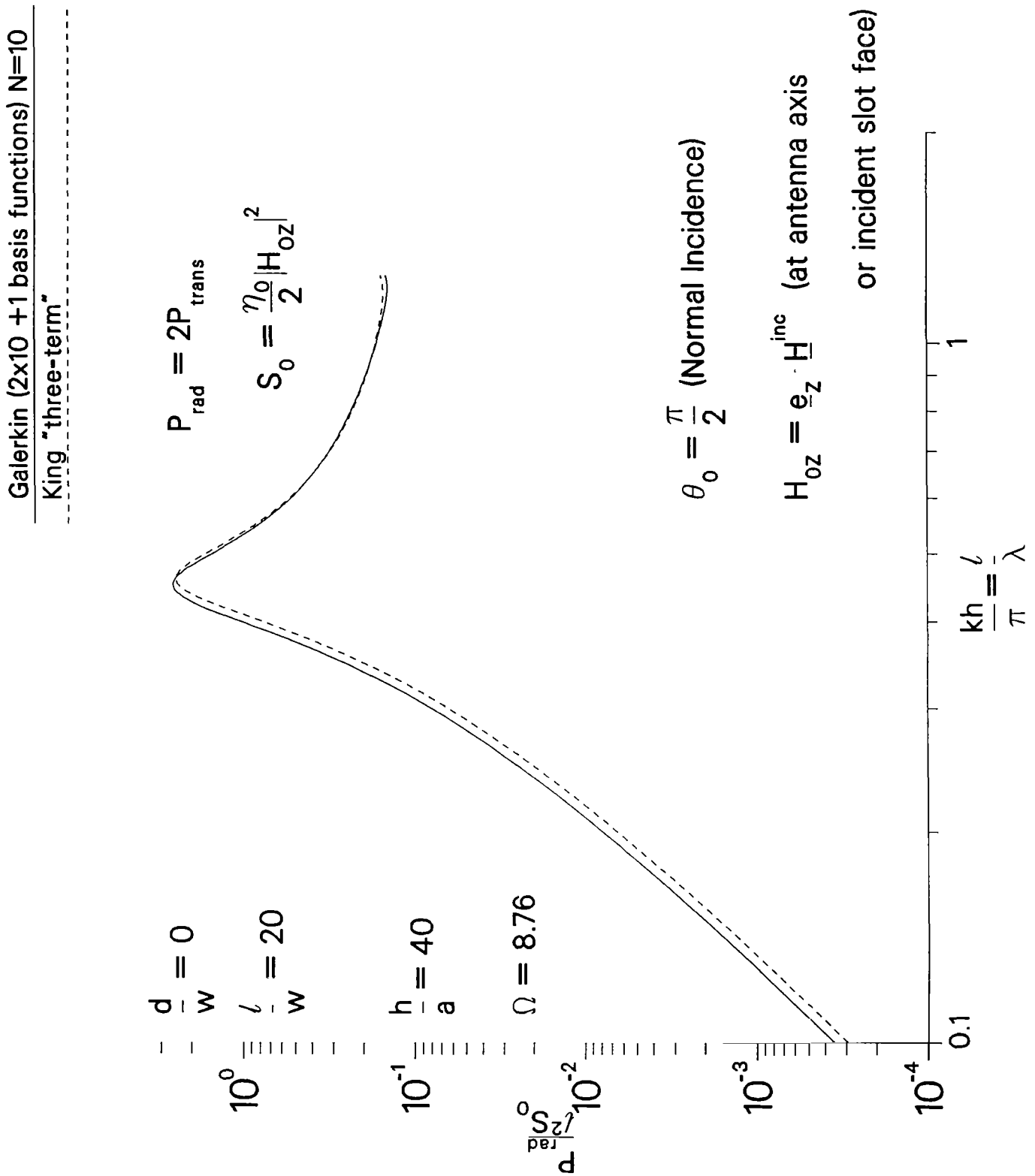

(b) Radiated power $\Omega = 8.76$.

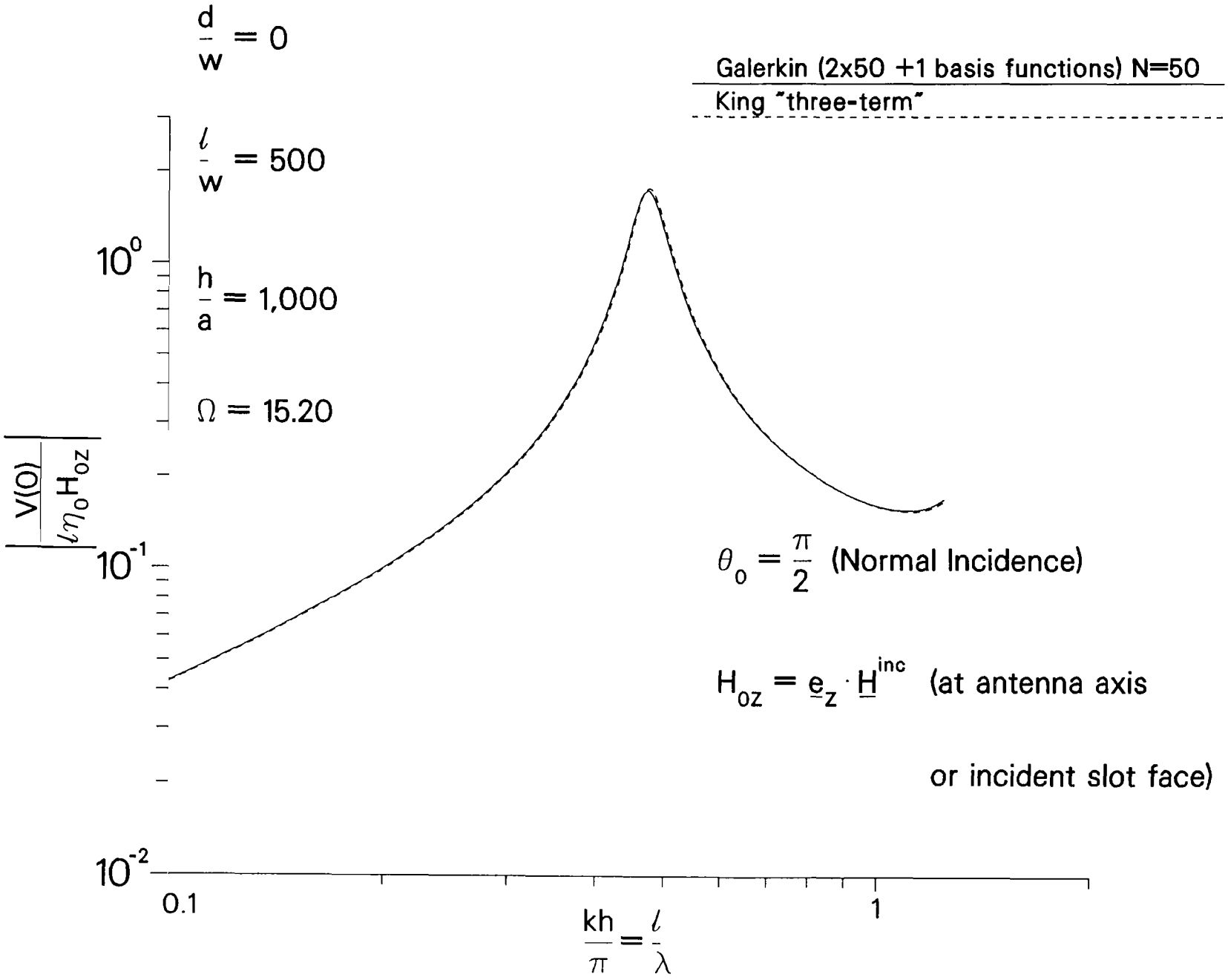

(c) Center voltage magnitude $\Omega = 15.20$.

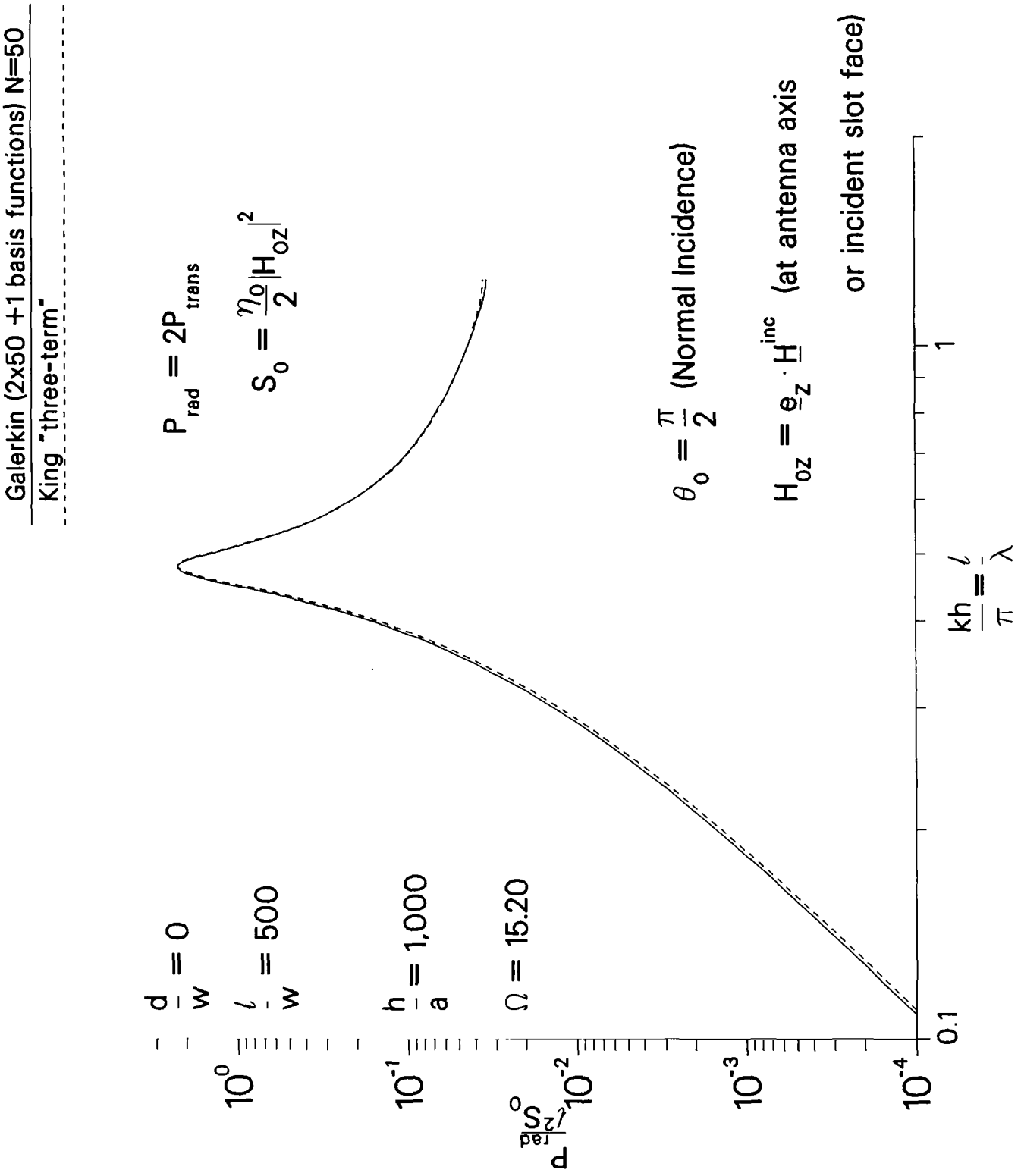

(d) Radiated power $\Omega = 15.20$.

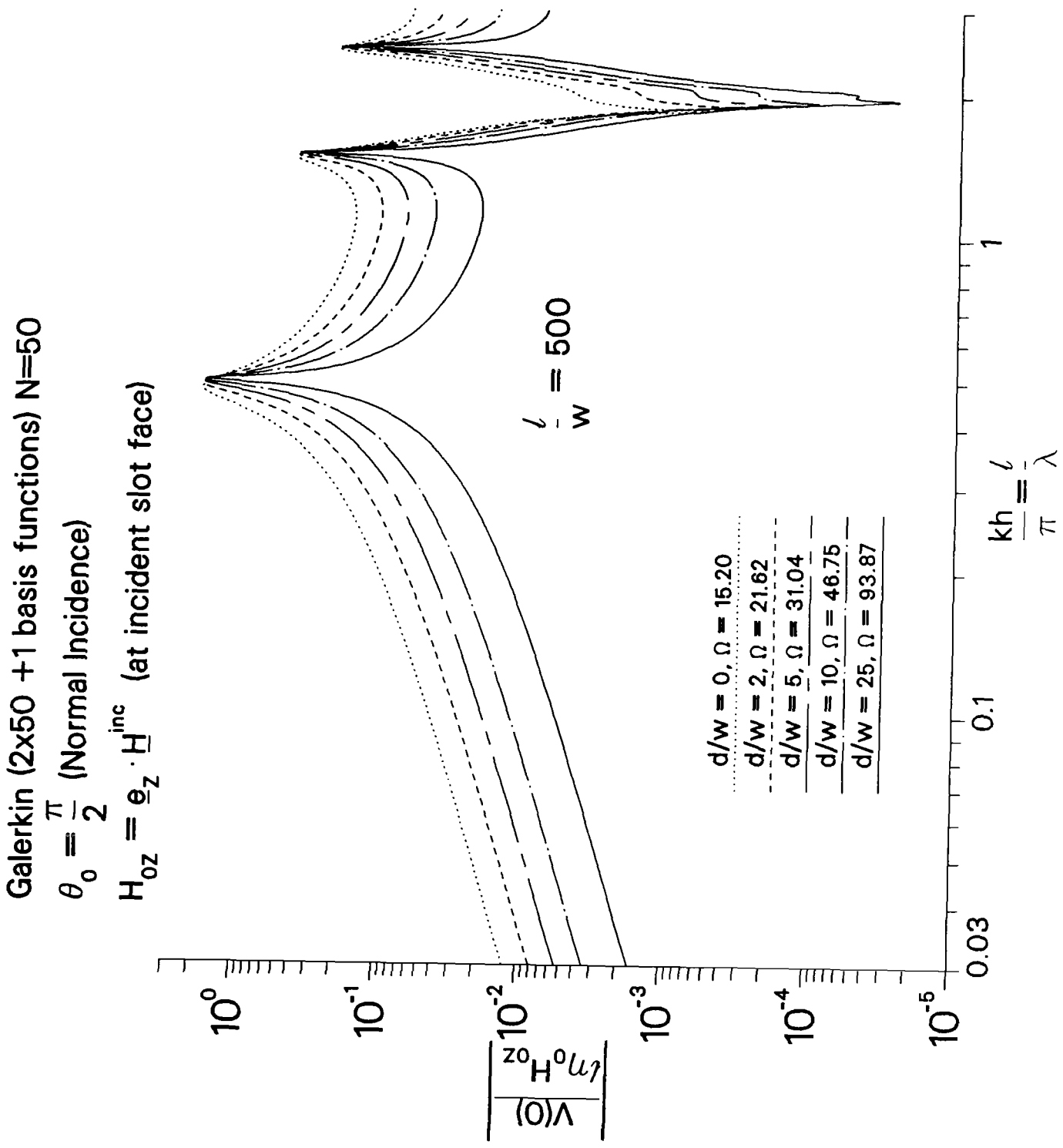

Figure 13. Galerkin solution for normalized center voltage magnitude and radiated power for a slot with $\ell/w = 500$ and varying depth. (a) Center voltage magnitude.

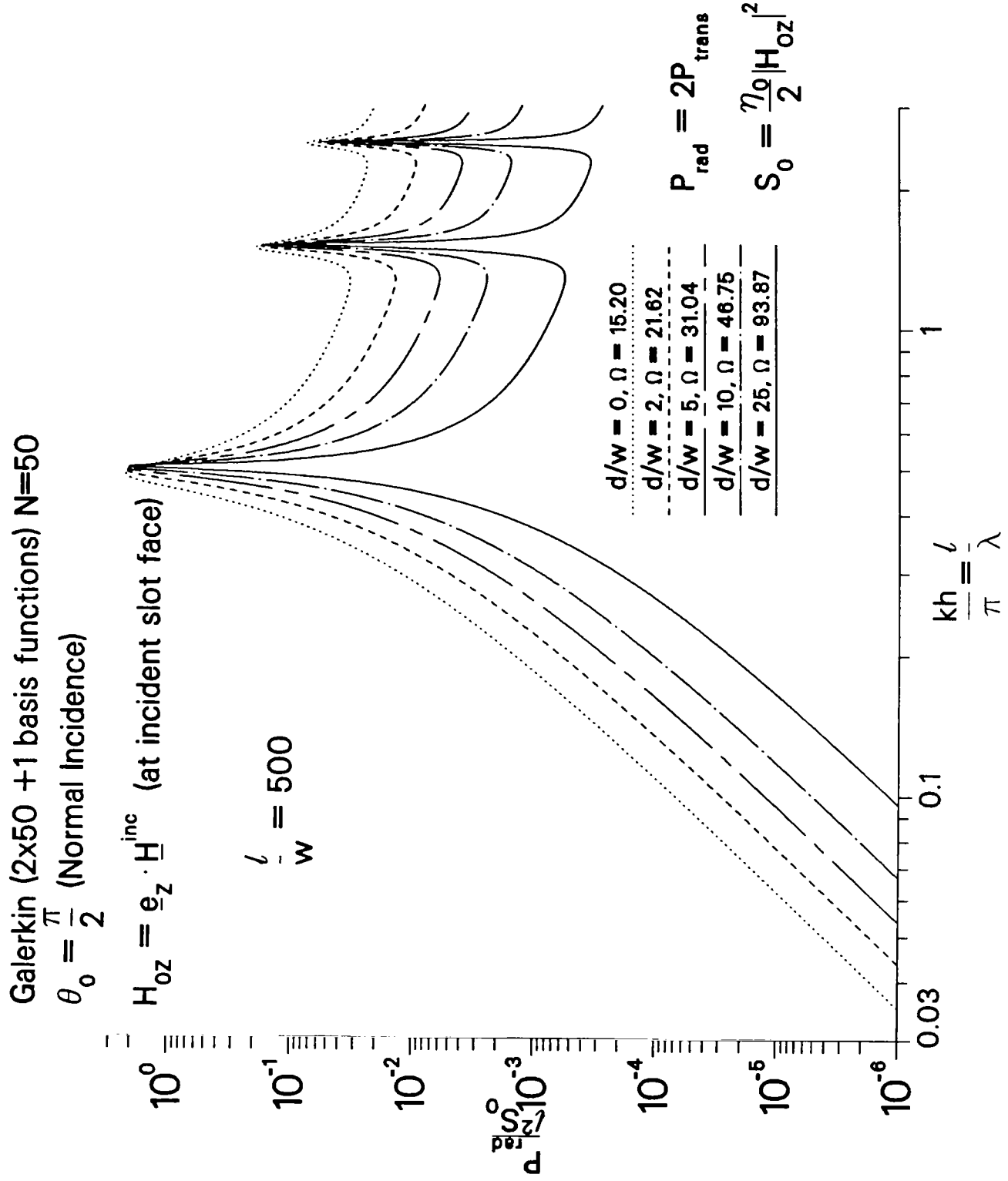

(b) Radiated power.

depth resonance of a slot, with $\frac{d}{w} >> 1$ and $\frac{\ell}{d} >> 1$, does not occur until kd $\approx \pi$ [16].

Figure 14 gives the normalized center voltage magnitude and normalized radiated power for several useful values of the fatness parameter Ω. Notice that the approximate fatness parameter from (44) and (45) has the simple form

$$\Omega_{ap} = 2\,\ell n(\frac{4\ell}{w}) + \pi\frac{d}{w} \quad , \tag{60}$$

where the first term is the exterior thin slot contribution and the second term is the uniform interior field contribution.

Duality may be invoked to relate the magnetic current I_m along the magnetic antenna to the electric current I along an electric antenna (both currents are defined to be positive if directed in positive z)

$$\frac{I_m(z)}{\mu_o H_{oz}} = \frac{I(z)}{\epsilon_o E_{oz}} \quad , \tag{61}$$

where E_{oz} is the z component of the incident electric field at the center of the axis of the electric antenna, and the angle of incidence θ_o must be the same in both electric and magnetic cases. Note that it is also possible to find an equivalent thin slot, by the same approach as taken in Section IV, and then use Babinet's principle [17] to transform to a strip and finally to an electrical antenna [12] with equivalent radius.

The "local" fields of the slot are found from the static solution, (16) and (27), once V(z) is known. From Faraday's Law

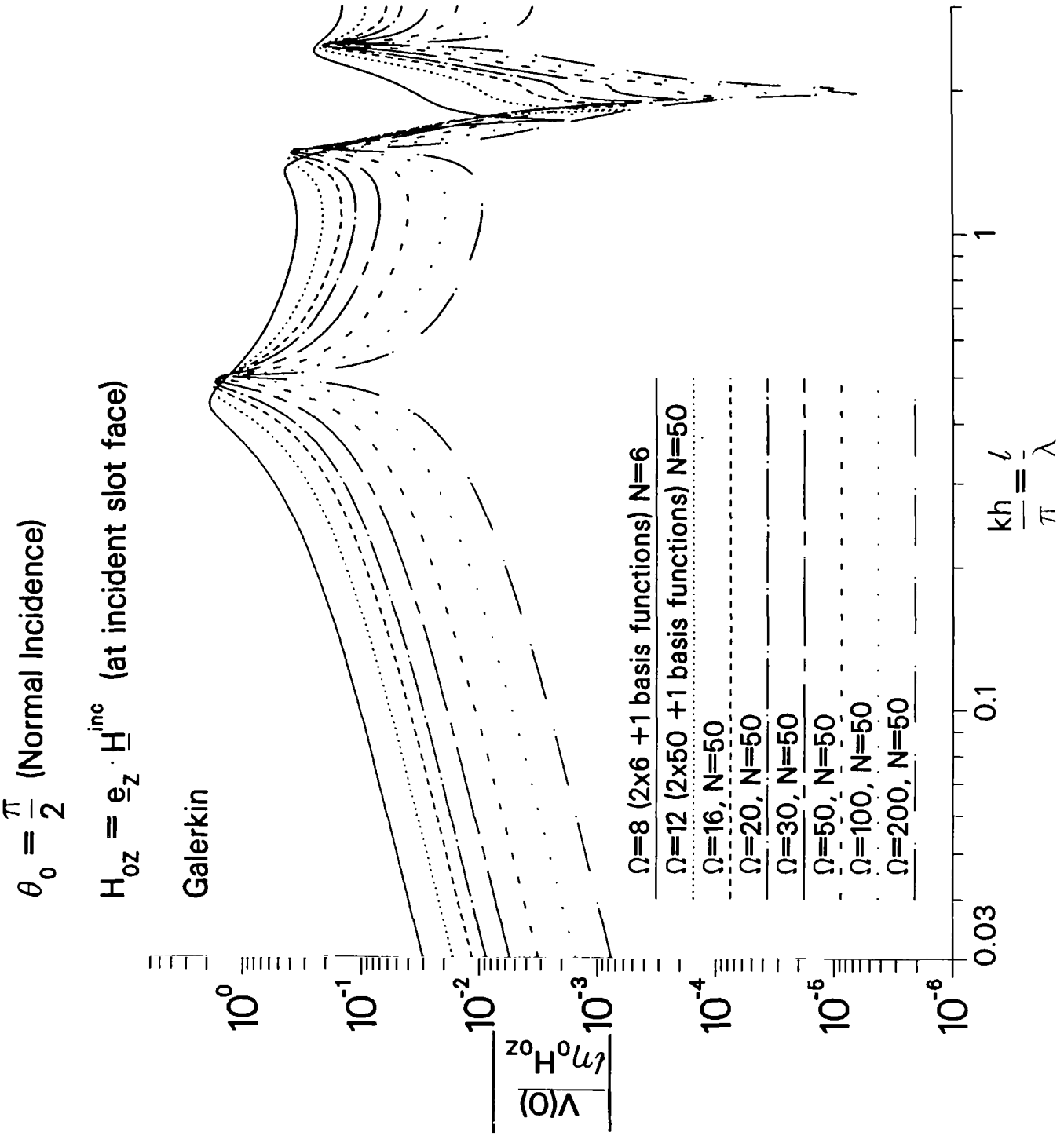

Figure 14. Galerkin solution for normalized center voltage magnitude and normalized radiated power for several useful values of the fatness parameter Ω. (a) Center voltage magnitude.

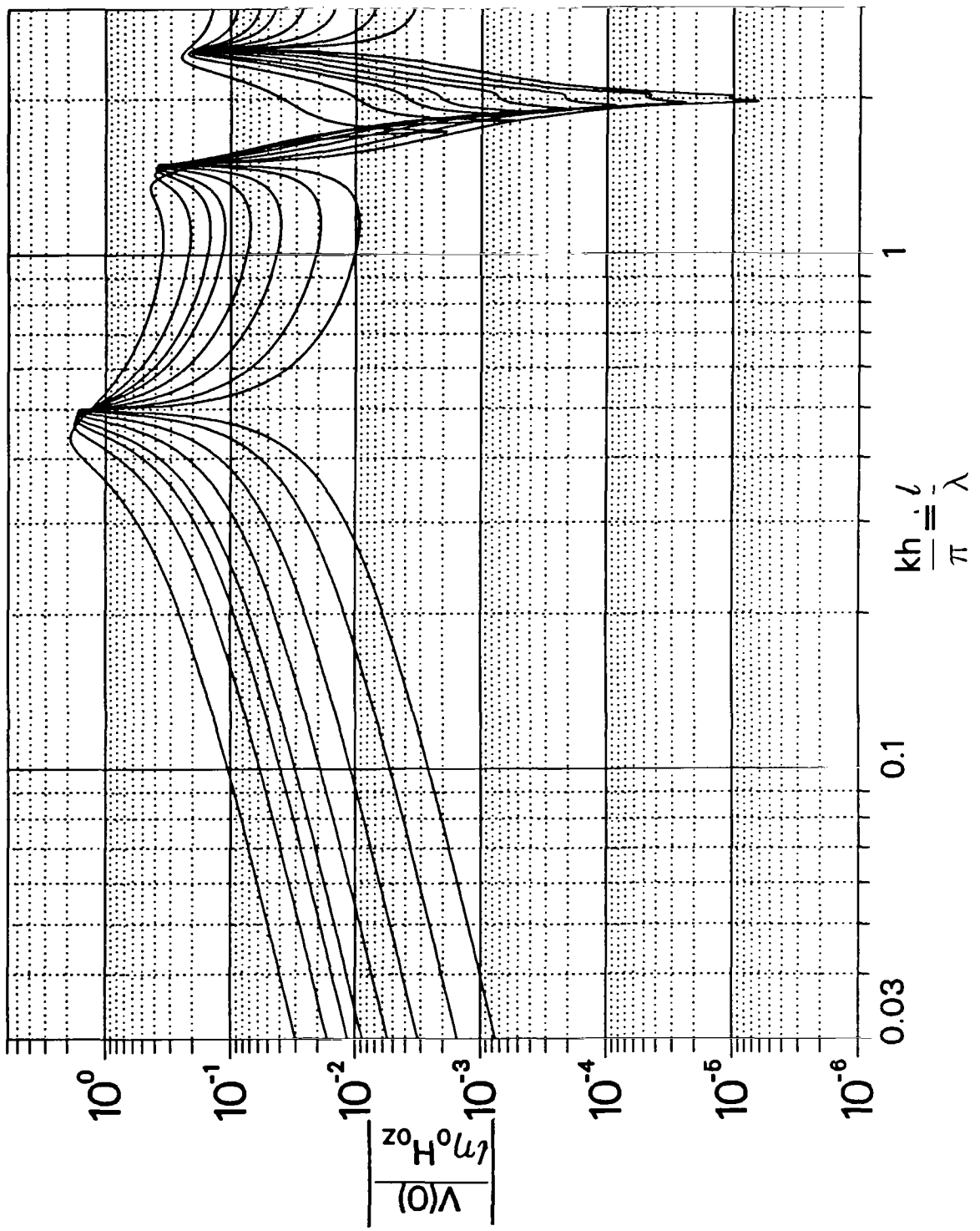

(b) Voltage with grid.

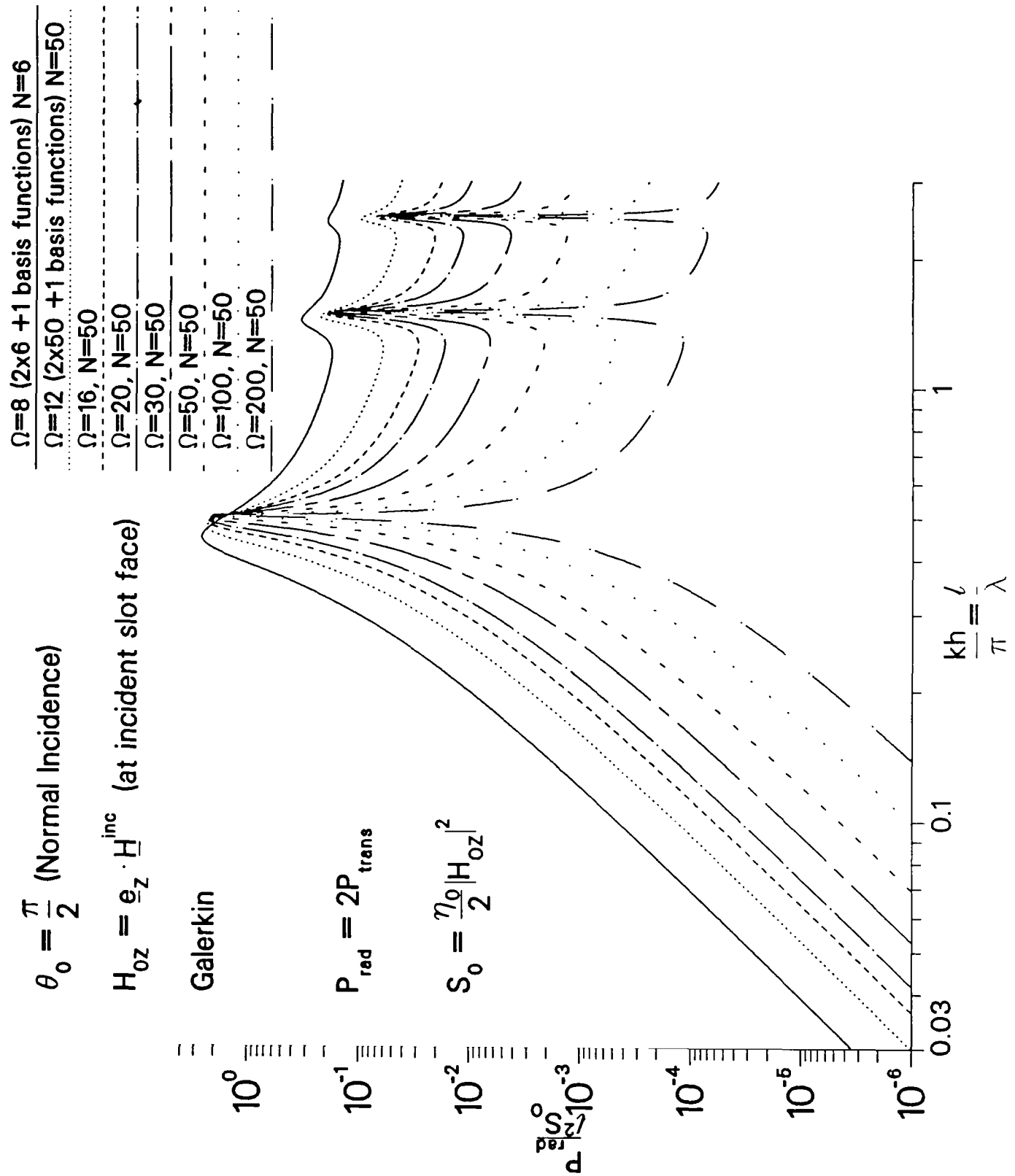

(c) Radiated power.

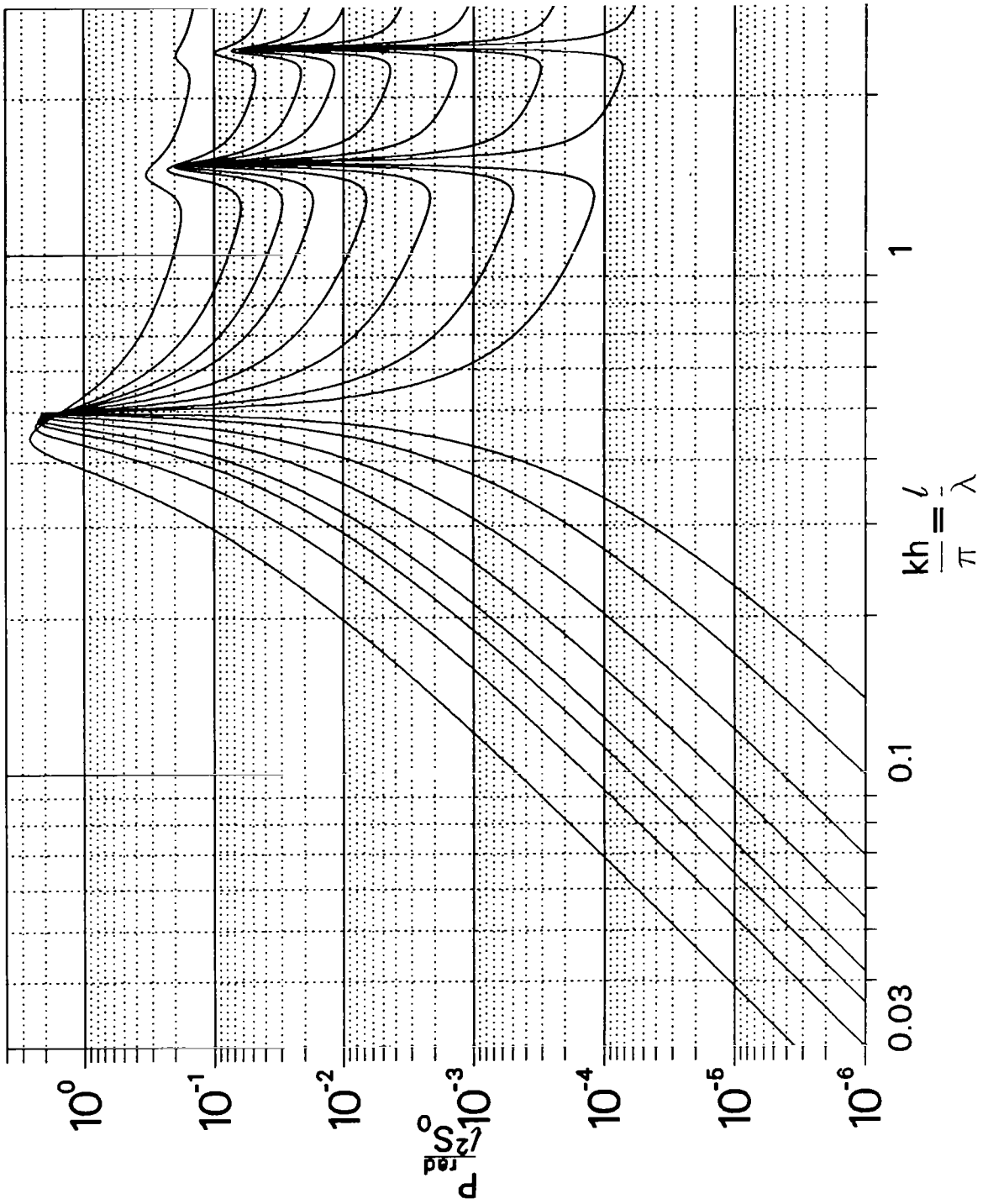

(d) Power with grid.

$$\oint_C \underline{E} \cdot \underline{d\ell} = i\,\omega \int_S \underline{B} \cdot \underline{n}\, dS \quad , \tag{62}$$

applied to a contour perpendicular to the slot cross section, of differential length, the magnetic flux per unit length is

$$\underline{\Phi}(z) = -\frac{i}{\omega}\frac{dV}{dz}(z). \tag{63}$$

The "nonlocal" fields of the slot can be determined from (5) through (9), where on the illuminated side of the slot the scattered potential is (49), and on the unilluminated side of the slot the potential is minus (49). The antenna coordinate system in (49), however, must be interpreted as having its origin at the center of whichever particular slot face, $y = \pm \frac{d}{2}$, corresponds to the half space of interest, $y \gtrless \pm \frac{d}{2}$.

VI. MAGNETOSTATIC DIPOLE MOMENT

Figure 15 shows the low frequency short circuit magnetic field impinging on the plane conductor and penetrating the slot. The dominant penetration of the slot at low frequencies involves the axial magnetic field. Bethe hole theory replaces the aperture in a plane by an equivalent dipole moment. The fields generated by the aperture in the far zone of the aperture are these dipole fields. The axial magnetostatic dipole moments of the slot with depth are shown in Figure 15. An asymptotic solution for these dipole moments will be given in terms of the large parameter Ω.

The magnetic scalar potential, resulting from the magnetic charge per unit length q_m along the dipole of Figure 11a, can be written as an integral [7]. Using the filamentary approximation for low frequencies we obtain

$$\varphi_m(\rho,z) = \frac{1}{\mu_o} \int_{-h}^{h} \frac{q_m(z')dz'}{4\pi R} \quad , \tag{64}$$

where $R = \sqrt{\rho^2 + (z - z')^2}$. Because the axial magnetic field must vanish along the antenna surface we obtain from (27) a static Hallén type equation

$$\frac{1}{\mu_o} \int_{-h}^{h} \frac{q_m(z')}{4\pi R_a} dz' = -\varphi_m^{inc}(z) = zH_{oz} \quad , \tag{65}$$

where $R_a = \sqrt{a^2 + (z-z')^2}$, H_{oz} is the axial component of the incident magnetic field at the antenna axis, and there is no integration constant on the right side of (65), because by symmetry the magnetostatic potential and magnetic charge per unit length are odd with respect to z. Following a static form of Hallén's iteration procedure [18], we add and

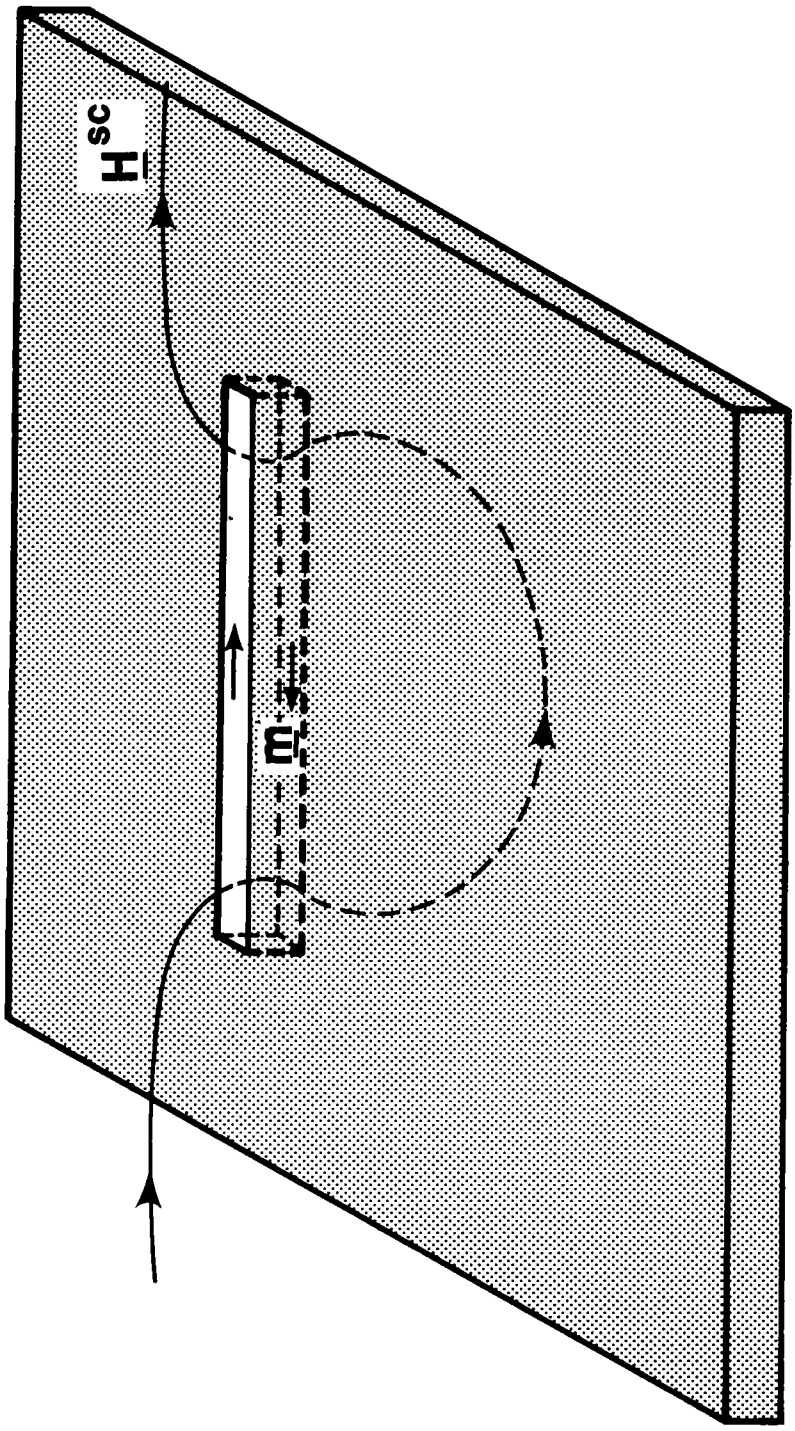

Figure 15. Magnetostatic field penetration of the thick slot. The equivalent axial magnetostatic dipole moments are shown.

substract $\frac{q_m(z)}{4\pi R_a}$ to the integrand of (65). This yields approximately

$$[\Omega + \ell n(1 - \frac{z^2}{h^2})]\, q_m(z) + \int_{-h}^{h} \frac{q_m(z') - q_m(z)}{|z-z'|}\, dz'$$

$$\approx 4\pi\mu_o z\, H_{oz} \quad . \tag{66}$$

Regarding Ω as a large parameter, (66) may be solved iteratively to generate an expansion for q_m. The zero order solution retains only Ω on the left side of (66). The first order solution is thus

$$q_{m1}(z) = \frac{4\pi\mu_o}{\Omega} H_{oz}\, z\left[1 + \frac{2}{\Omega} - \frac{1}{\Omega}\,\ell n\left[1 - \frac{z^2}{h^2}\right]\right] \quad . \tag{67}$$

The potential exterior to the slot is (64) on the illuminated side of the slot, but minus (64) on the unilluminated side of the slot. The same comments regarding the coordinate system in (64), as discussed at the end of Section V, apply here. Thus in the far zone, r>>h, the potential is

$$\varphi_m \sim \mp \frac{z}{4\pi\mu_o r^3} \int_{-h}^{h} q_m(z')z'dz' \quad , y \gtrless \pm \frac{d}{2} \quad . \tag{68}$$

Inserting (67) into (68) gives

$$\varphi_m \sim \mp \frac{h^3\ H_z^{sc}\ z}{6r^3(\frac{\Omega}{2} + \ell n\ 2 - \frac{7}{3})} \quad , y \gtrless \pm \frac{d}{2} \quad , \tag{69}$$

where the short circuit field is $H_z^{sc} = 2\ H_{oz}$, and terms of order $1/\Omega$ in the parenthesis have been dropped. The magnetostatic potential of a dipole of moment $\underline{m}$ is

$$\varphi_m = \frac{\underline{m} \cdot \underline{r}}{4\pi r^3} \cdot \tag{70}$$

Comparing (69) and (70) we may write the dipole moment as [1]

$$\underline{m} = -2\ \alpha_m\ H_z^{sc}\ \underline{e}_z\ , \tag{71}$$

where the polarizability α_m is given by

$$\alpha_m = \pm\ \frac{\ell^3 \pi}{24\ (\frac{\Omega}{2} + \ell n\ 2 - \frac{7}{3})}\ , y = \pm\frac{d}{2}. \tag{72}$$

The fatness parameter Ω is (45), with equivalent radius (37).

VII. "ODD" PROBLEM

The solution to the "odd" problem will now be estimated assuming conditions (3) and (14) still hold. The axial component of the magnetic field in the slot, away from the ends $z = \pm h$, is approximately the short circuit magnetic field, as illustrated by Figure 16a (angles near grazing incidence are not being considered). From the bottom sign in (12), the value is

$$H_z = H_{oz}\, e^{ikz\cos\theta_o} \quad , \tag{73}$$

where the amplitude H_{oz} is now assumed to be the incident magnetic field at the center of the incident slot face. Figure 16b shows the slot cross section with a contour for application of Faraday's law (62). The approximate result for the "odd" part of the voltage across the slot (15) is therefore

$$V(z) = -i\omega\mu_o\, y\, w\, H_{oz}\, e^{ikz\cos\theta_o} \quad , -\frac{d}{2} \le y \le \frac{d}{2} \, . \tag{74}$$

The "odd" contribution (74) thus forms a small correction to the "even" voltage discussed previously.

Figure 17 shows the curves $\frac{d}{w} = 10, 25$ from Figure 13a compared with those obtained by addition of (74) at the unilluminated and illuminated slot faces, $y = \pm d/2$. The agreement is quite good except in the vicinity of the minimum where the "even" center voltage becomes small. There is some deviation between the "even" voltage and the "combined" voltage near $\frac{kh}{\pi} = 3$, for $\frac{d}{w} = 25$. The quantity kd approaches unity in this region and one of the conditions (14), upon which both the odd and even solutions were based, is violated. Nevertheless, because the discrepancy is still rather small, it is

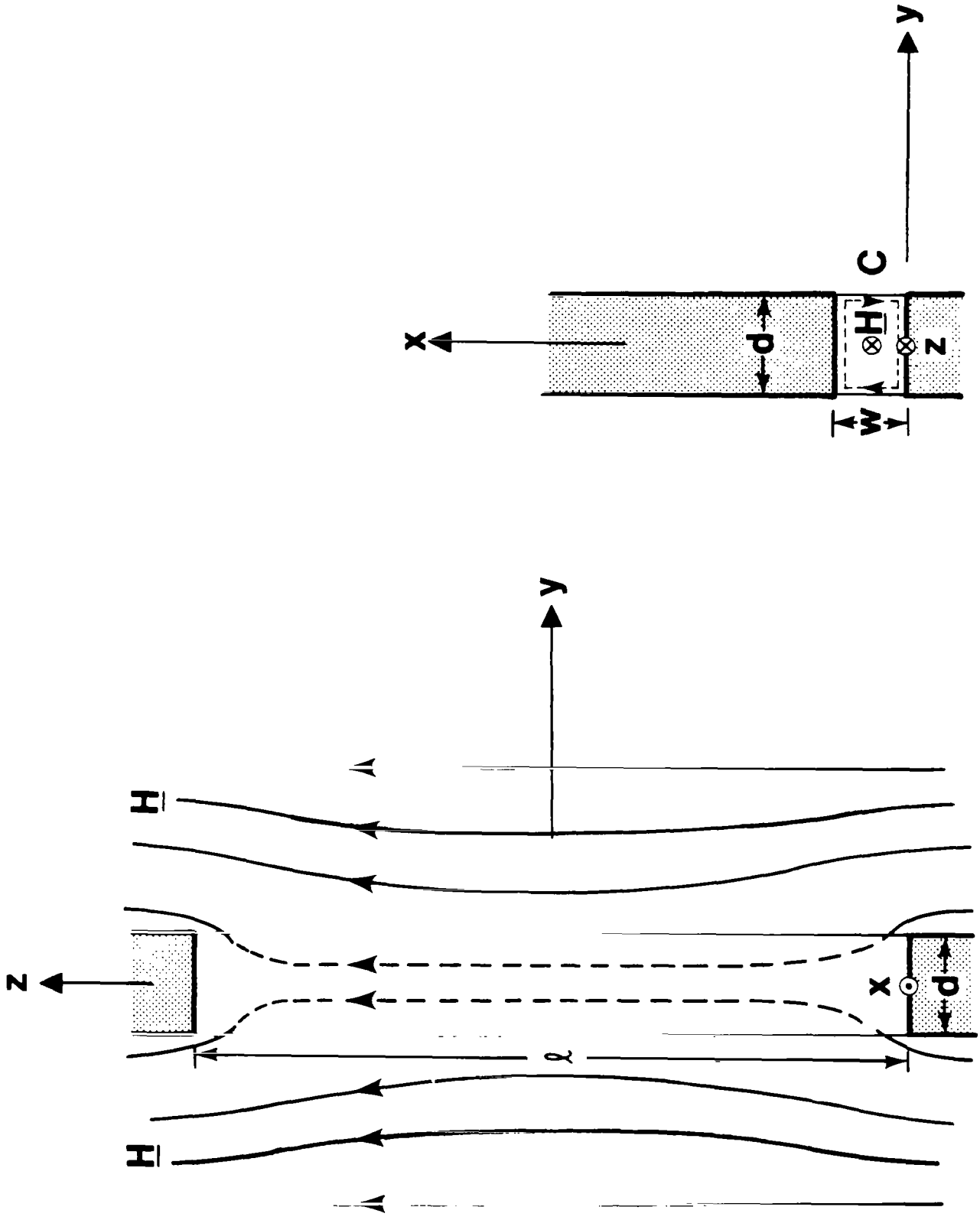

Figure 16. The magnetic field in the "odd" problem. (a) The magnetic field away from the ends of the slot is approximately the short circuit magnetic field. (b) Contour for application of Faraday's law.

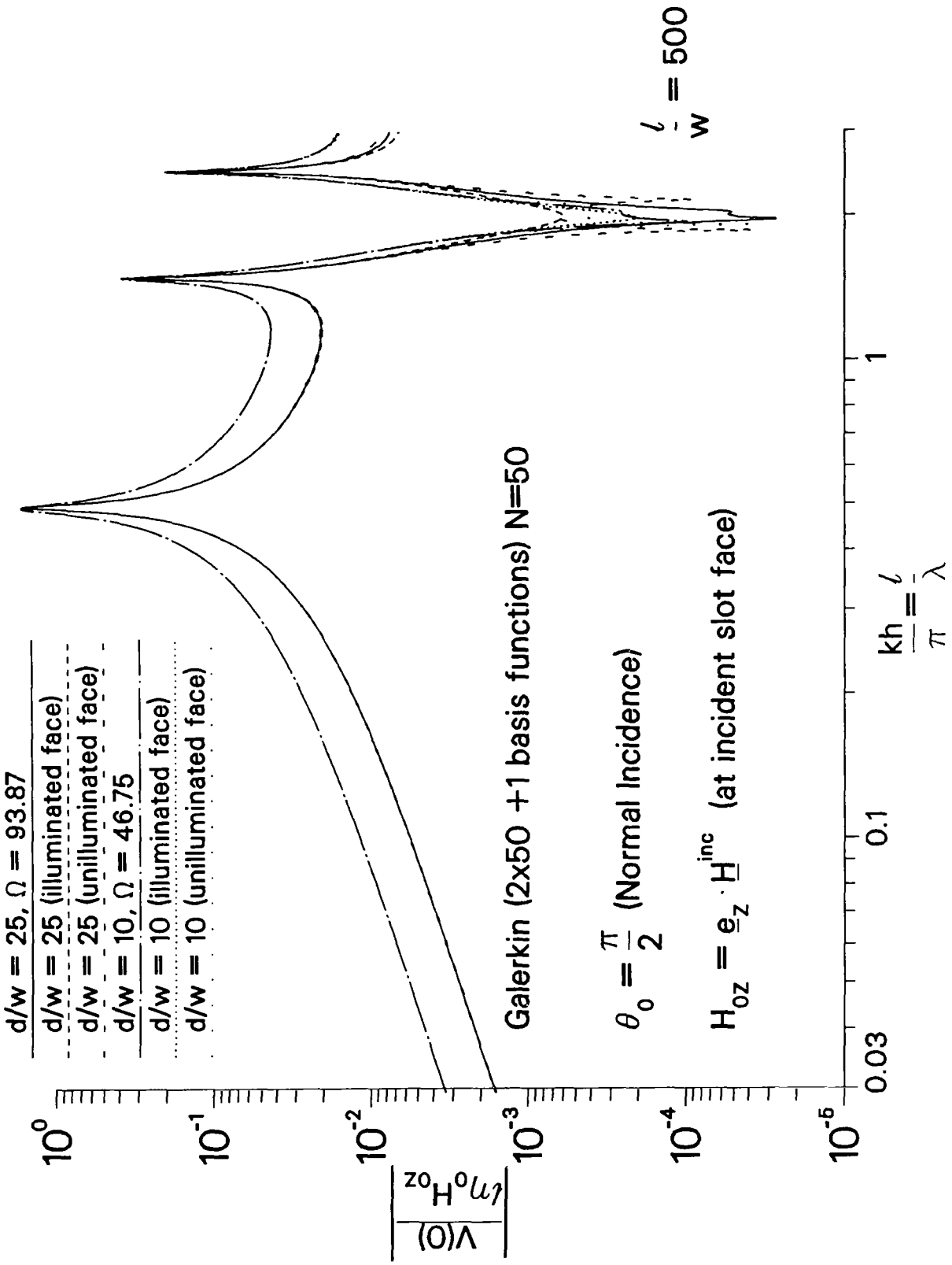

Figure 17. Comparison of "even" center voltage magnitude with combined, "odd" plus "even", center voltage magnitude. The curves labled illuminated and unilluminated represent the combined voltage at the incident and transmitted slot faces.

reasonable to infer that the exact solution is very close to these results. See the results at the end of Appendix I for a confirmation of this assertion.

VIII. CONCLUSIONS

The problem of electromagnetic penetration of the rectangular slot aperture shown in Figure 2 was reduced to the solution of Hallén's integral equation with an equivalent antenna radius. The conditions (3) and (14) are assumed to hold for this approach to be valid. The equivalent radius was evaluated in terms of the solution to the transverse static problem giving equation (37). Approximations for the equivalent radius were also found, see equations (40), (41), and (44). The solution of Hallén's integral equation was illustrated by King's three–term method and the Galerkin method. The low frequency axial magnetostatic dipole moment and polarizability were derived by means of Hallén's iteration method. Note that the theory of the long antenna [19] can be applied to determine the voltage along slots that are several wavelengths long.

Generalizations of these results can also be easily accomplished. For example, the approximate formula (44) for the equivalent radius, also applies to the slot cross section of Figure 18 provided that d>>w. This tortuous depth route is perhaps a reasonable approximation to the cross section of Figure 1. The effects of the slot bends may also be included. Figure 19a shows a right angle bend. The uniform field interior charge per unit length is

$$Q^{<}_{unif} = V\epsilon_o\left(\frac{d_1}{w_1} + \frac{d_2}{w_2}\right) . \qquad (75)$$

A correction due to the corner can be obtained from conformal mapping and is given by

$$\Delta Q^{<} = Q^{<} - Q^{<}_{unif} = \frac{V}{\pi}\epsilon_o \left[2\left(\frac{w_1}{w_2}\arctan\frac{w_2}{w_1} + \frac{w_2}{w_1}\arctan\frac{w_1}{w_2}\right)\right.$$

$$-\frac{\pi}{2}\left(\frac{w_1}{w_2}+\frac{w_2}{w_1}\right)+2\ell n\left\{\sqrt{(1+w_1^2/w_2^2)(1+w_2^2/w_1^2)}\,/4\right\}\Big] \quad , \tag{76}$$

where d_1, $d_2 >> w_1$, w_2, and $Q^<$ is the actual interior charge per unit length. Figure 19b shows a generalization of the slot of Figure 18. The above formula can be applied to each of the two bends of Figure 19b, as long as they are well separated. Because the slot is very thick, the exterior plus fringing (at the face edges) charge per unit length can be obtained from the limit (d>>w) of (34) minus (43). Generalizing this charge per unit length to two different end widths yields

$$Q_R^> \sim 2\epsilon_o \frac{V}{\pi}\,\ell n\left[\frac{R\pi e}{2\sqrt{w_1 w_3}}\right] \quad . \tag{77}$$

Applying these results to Figure 18 we obtain the more accurate equivalent radius

$$a \sim \frac{4w}{e\pi/2}\,e^{\frac{-\pi d}{2w}} \quad . \tag{78}$$

Slots with slowly varying width such as shown in Figure 20 can also be handled, yielding

$$a \approx \sqrt{\frac{w(0)w(d)}{e\pi/2}}\,e^{-\frac{\pi}{2}\int_o^d \frac{ds}{w(s)}} \quad . \tag{79}$$

The factor in the denominator ($e\pi/2$), of course, assumes that the slot is perpendicular to each half space at s=0,d. Gradual variations of d and/or w with the axial distance lead to a varying equivalent radius a(z). The equivalent radius (37) also applies to the hatch aperture of Figure 21. Introduction of the equivalent radius (37) can thus incorporate depth in existing zero depth magnetostatic polarizability formulas for hatch apertures [1].

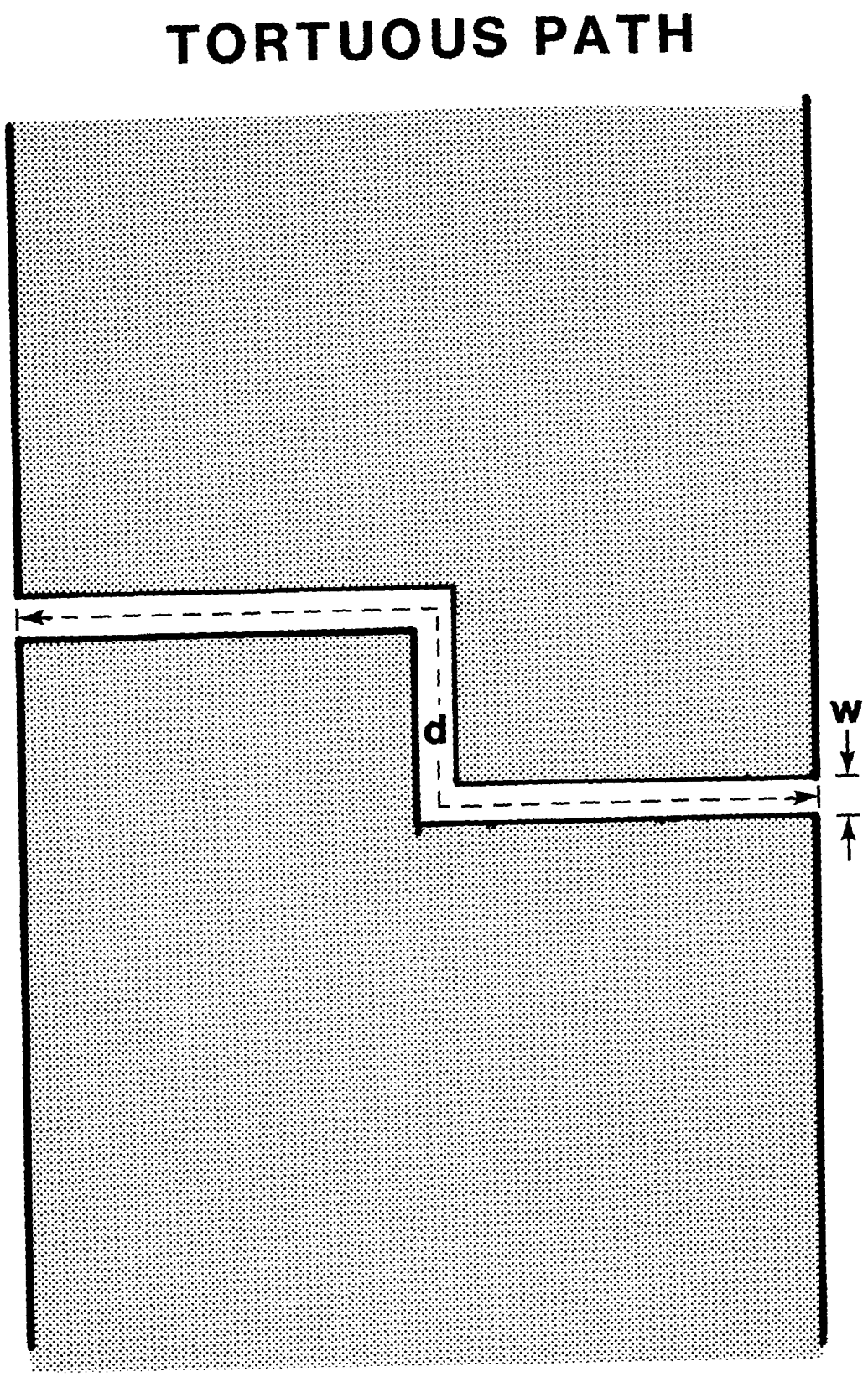

Figure 18. Slot with tortuous depth route.

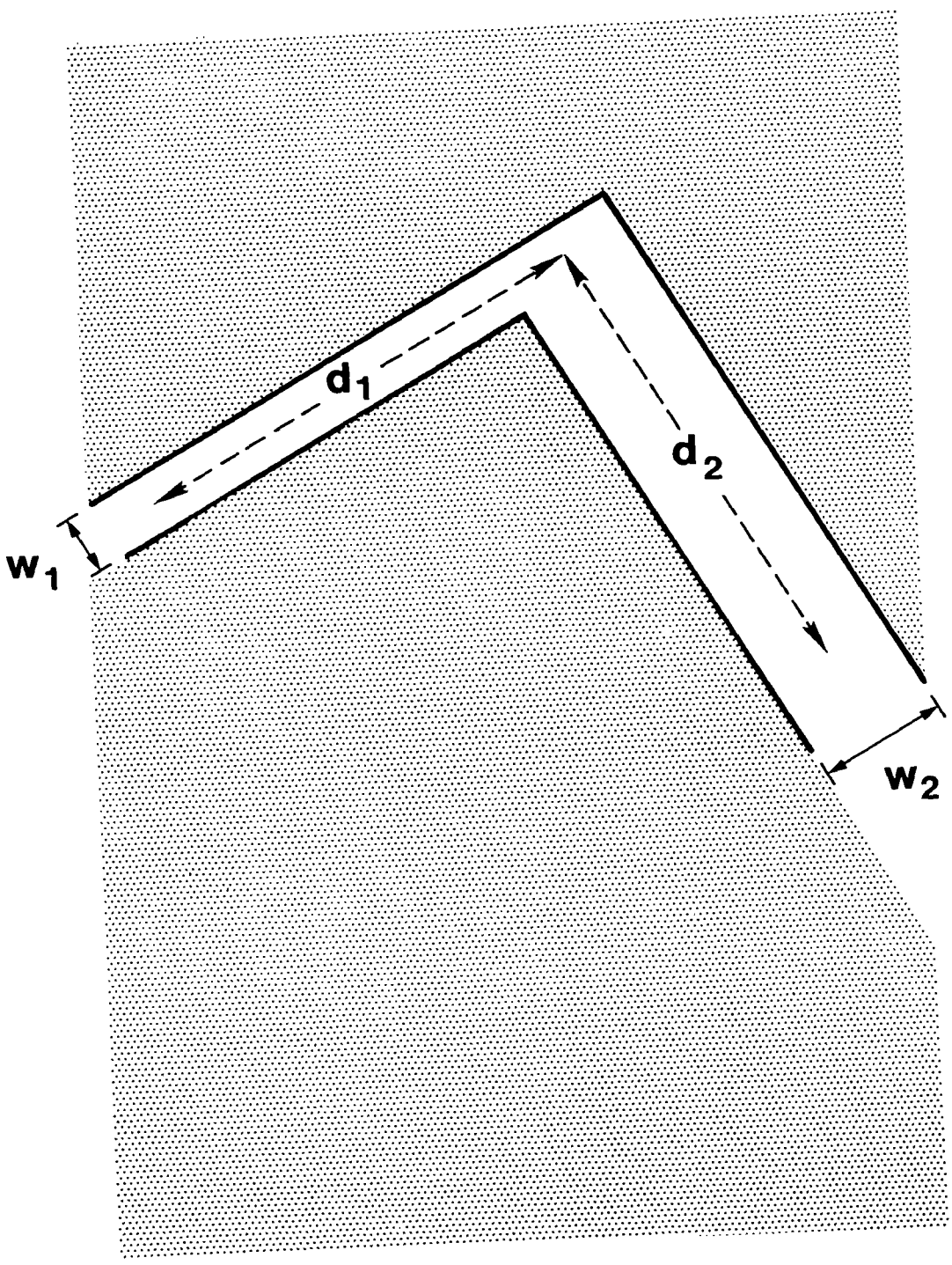

Figure 19. Geometry for slot bend corrections. (a) Single right angle bend in the depth.

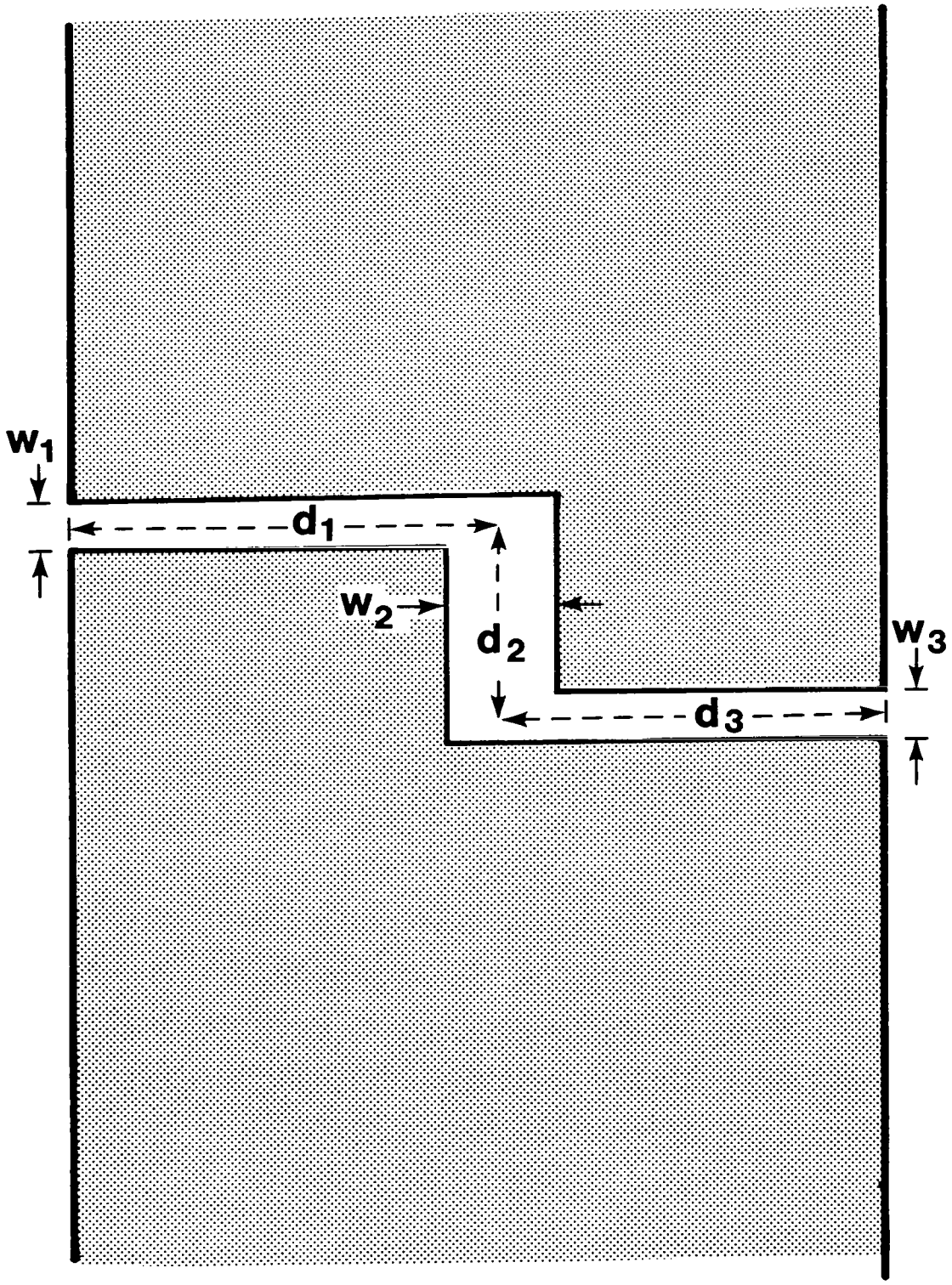

(b) Generalization of tortuous depth route to several different widths.

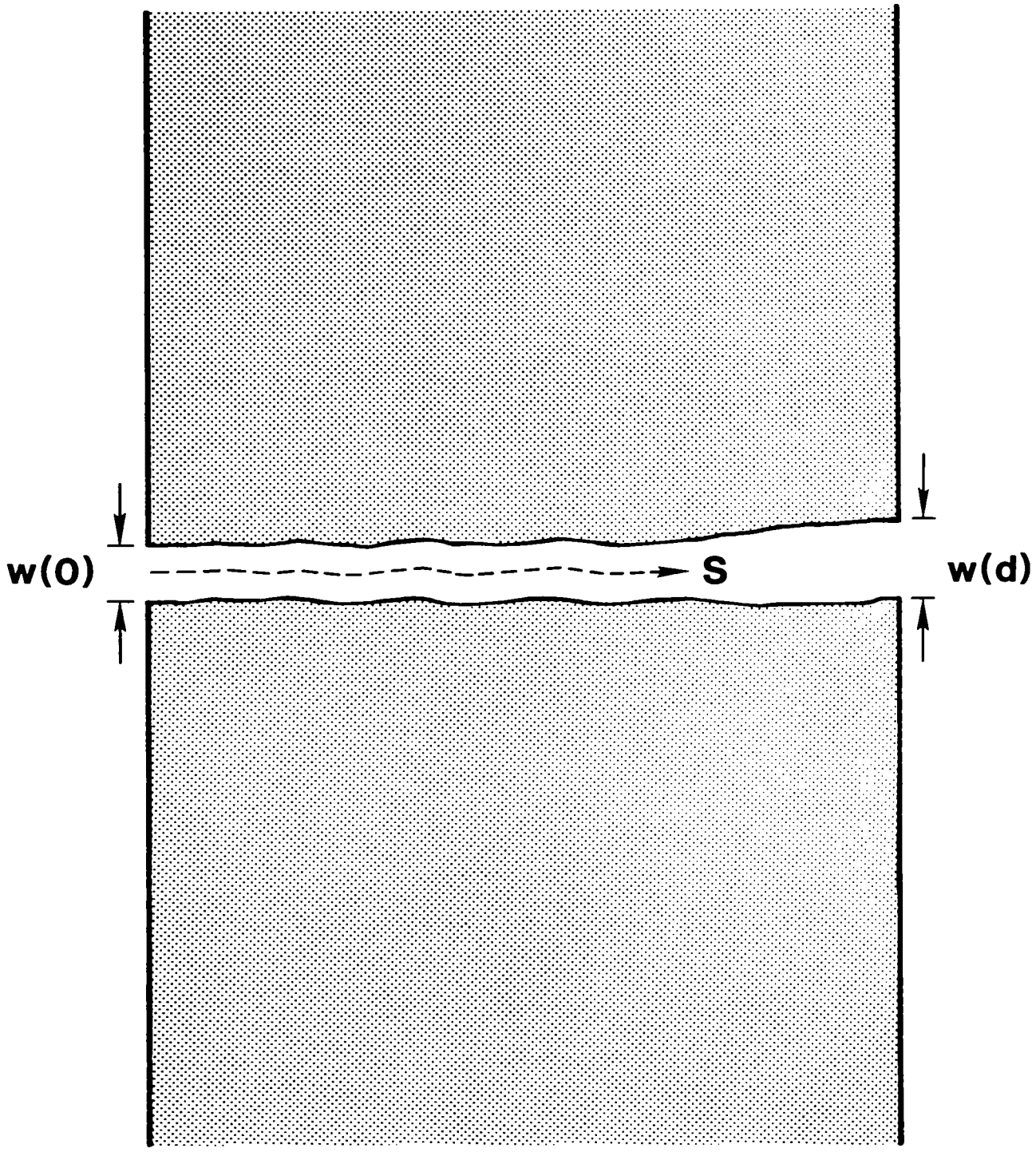

Figure 20. Slot with slowly varying width in the depth direction.

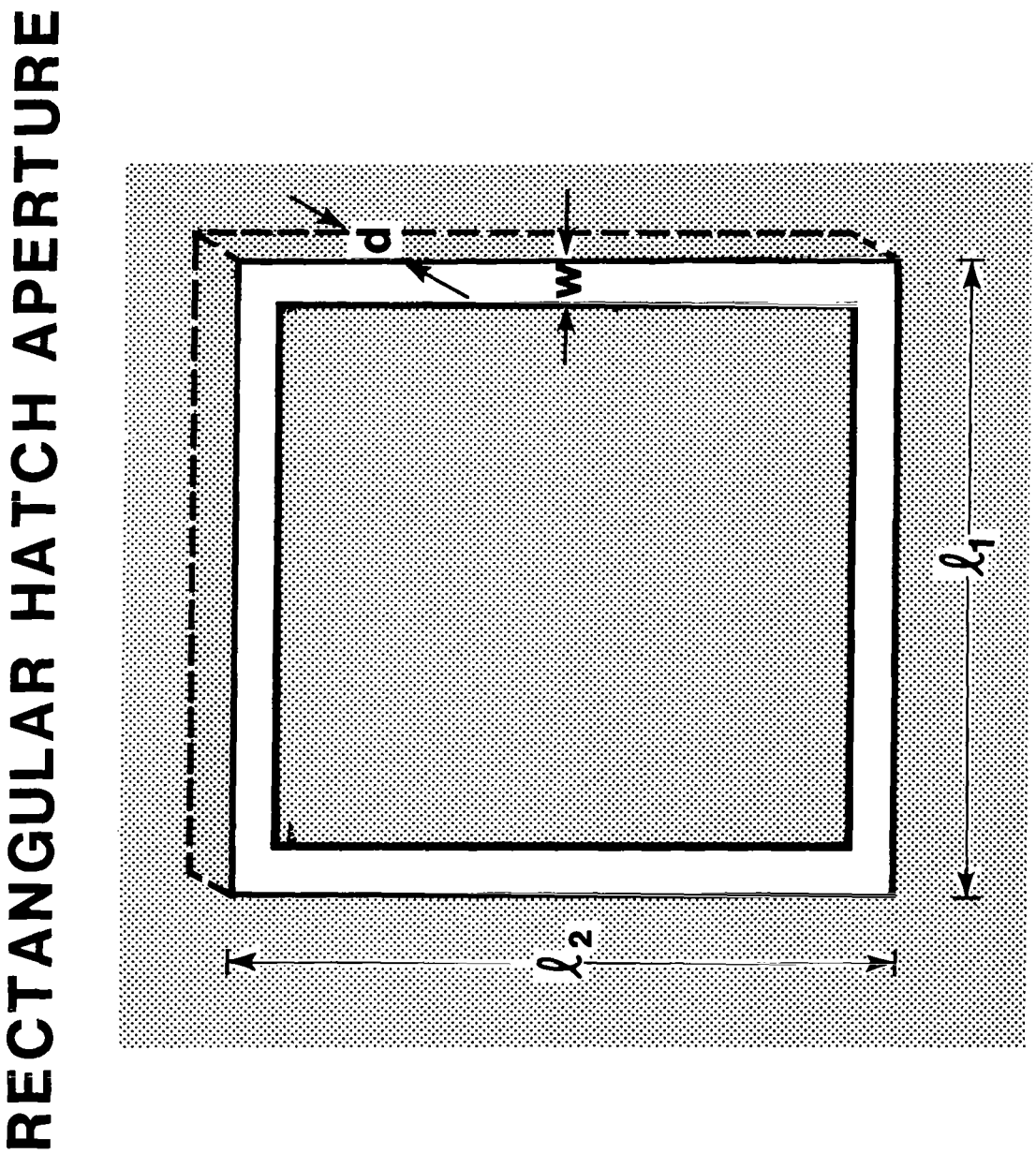

Figure 21. Rectangular hatch aperture having depth.

The induced current on a wire behind an electrically small slot aperture, having depth, can be easily determined [1] from the polarizability (72).

The rectangular slot problem was symmetrized and split into "even" and "odd" parts with respect to the depth. The "even" part is dominant in the limits (3) and (14), and is modeled by Hallén's integral equation. A simple approximate solution to the "odd" problem was found by means of Faraday's law. The addition of the "odd" solution relaxes the requirement that kd be very small compared to unity.

A rigorous splitting of the generalized problems mentioned above into "even" and "odd" parts is not always possible. However, as long as the slot cross section is small compared to both the slot length and the wavelength, the "local" fields are approximately static and Hallén's integral equation with the equivalent radius describes the major penetration of the slot. The "even" excitation (E_x^{inc} even with respect to y) still dominates and the above derivation for the equivalent radius is valid.

APPENDIX I. INTEGRAL EQUATION DERIVATION OF EQUIVALENT ANTENNA RADIUS

This appendix gives a mathematical derivation of the equivalent antenna radius starting from the integral equations for the slot with depth.

Part A formulates the "exact" integral equations under the restrictions that $kw<<1$ and $w<<\ell$, so that the electric field component along the length of the slot may be ignored. The integral equations are derived for both the "even" and the "odd" parity of E_x with respect to the depth. Part B makes use of the conditions $kw<<1$ and $w<<\ell$ to further simplify the integral equations. Part C approximates the integral equations in the additional limits $kd<<1$ and $d<<\ell$. Part C also gives the dominant odd solution. Part D defines the equivalent antenna radius by comparison with Hallén's integral equation. Part E determines the equivalent radius in terms of the "discontinuity" of interior and exterior static electric vector potentials at the slot face. This "discontinuity" is evaluated in Part F by use of the analytic conformal mapping solution. Part G simplifies the integral equations of Part B when the depth is much larger than the width but otherwise unrestricted. The integral equations of Part G can be used to investigate depth resonances [16]. Part H gives a comparison of the Galerkin solution of the integral equations of Part G with the Galerkin solution of the integral equations of Part D using the equivalent radius of Part F. Part H also gives Hallén type zero order solutions of the "even" and "odd" integral equations of Part D.

A. "Exact" Integral Equations

The limits $kw<<1$ and $w<<\ell$ are assumed to hold. The tangential electric fields at the slot faces, $y = \pm \frac{d}{2}$, can thus be replaced by z directed magnetic currents by means of

(4). The magnetic currents generate electric vector potentials satisfying the Helmholtz equation [7]. The vector potentials exterior and interior to the slot can be written as

$$A^{>}_{ez}(\underline{r}) = 2\epsilon_o \iint\limits_{S_{\pm}} K_{mz}(\underline{r}')\, G^{>}(\underline{r}, \underline{r}')\, dS' \quad , y \gtrless \pm \frac{d}{2}, \tag{80}$$

where

$$G^{>}(\underline{r},\underline{r}') = \frac{e^{ik|\underline{r} - \underline{r}'|}}{4\pi|\underline{r} - \underline{r}'|} \quad ,$$

$$K_{mz}(x', \pm \frac{d}{2}, z') = \pm E_x(x', \pm \frac{d}{2}, z') \quad ,$$

and

$$A^{<}_{ez}(\underline{r}) = \epsilon_o \int\limits_{S_+} \int\limits_{+S_-} K_{mz}(\underline{r}')\, G^{<}(\underline{r},\underline{r}')\, dS', -\frac{d}{2} \leq y \leq \frac{d}{2}, \tag{81}$$

where

$$G^{<}(\underline{r},\underline{r}') = -\sum_{m=1}^{\infty}\sum_{n=0}^{\infty} \epsilon_n \frac{2}{\ell w} \cos\frac{n\pi x'}{w} \cos\frac{n\pi x}{w} \sin\frac{m\pi}{\ell}(z'+h)$$

$$\sin\frac{m\pi}{\ell}(z+h)\, \frac{\cos\gamma_{mn}(y_< + \frac{d}{2})\, \cos\gamma_{mn}(y_> - \frac{d}{2})}{\gamma_{mn}\, \sin\gamma_{mn} d} \quad ,$$

$$K_{mz}(x', \pm \frac{d}{2}, z') = \mp E_x(x', \pm \frac{d}{2}, z') \quad ,$$

$$\gamma_{mn} = \sqrt{k^2 - (\frac{m\pi}{\ell})^2 - (\frac{n\pi}{w})^2} \quad ,$$

$$y_{\gtrless} = \min_{\max}(y,y') \quad .$$

Here ϵ_n is the Neumann number (equal to 1 if n=0; equal to 2 if $n \geq 1$), and $S_{\pm}$ are the slot faces at $y' = \pm \frac{d}{2}$, $-h < z' < h$, and $0 < x' < w$. The function $G^>$ is the free space Green's function and the factor of two, in (80), accounts for the magnetic current image in the planes $y = \pm \frac{d}{2}$. The function $G^<$ is the Green's function satisfying Neumann boundary conditions on the faces $y = \pm \frac{d}{2}$ and walls $x = 0$, w and Dirichlet boundary conditions on the walls $z = \pm h$.

The excitation of the slot is split into even and odd parts with respect to the depth coordinate y. We therefore assume the short circuit potential (13) excites the slot. Matching the z component of the magnetic field (50) at the face $y = -\frac{d}{2}$ leads to integro–differential equations for E_x. The resulting integral equation for E_x "even" with respect to y is

$$-\epsilon_o \int_{-h}^{h} \int_{o}^{w} 2\, E_x(x', -\tfrac{d}{2}, z') \left[\frac{e^{ikR_o}}{4\pi R_o} + \frac{1}{\ell w} \sum_{m=1}^{\infty} \sum_{n=0}^{\infty} \frac{\epsilon_n \tan \gamma_{mn} \frac{d}{2}}{\gamma_{mn}} \right.$$

$$\left. \sin \tfrac{m\pi}{\ell}(z+h) \sin \tfrac{m\pi}{\ell}(z'+h) \cos \tfrac{n\pi}{w} x \cos \tfrac{n\pi}{w} x' \right] dx'dz' =$$

$$-A_{ez}^{inc}(z) + C_1' \sin kz + C_o' \cos kz \quad , \qquad (82)$$

where $$R_o = \sqrt{(x-x')^2 + (z-z')^2} \quad ,$$

C_o' and C_1' are integration constants, and $A_{ez}^{inc}(z)$ is given below (13). The integration constants are taken to be independent of x so that H_x and D_y are also continuous at the slot faces.

Strictly speaking we are not permitted to additionally require continuity of H_x, and thus D_y, at the slot faces. This results from the fact that the small electric field component E_z was ignored at the slot faces. However the existence of exact solutions to the integral equations in this appendix will not concern us. As in the case of Hallén's integral equation, we assume that the integral equations will provide us with asymptotic approximations in the limits being considered. Alternatively, the differential operator of equation (50) may be applied to these integral equations, and only integrated after the transverse dependence has been eliminated. This alternative procedure leads to identical results.

The integral equation for E_x "odd" with respect to y is

$$-\epsilon_o \int_{-h}^{h} \int_{o}^{w} 2\, E_x(x', -\frac{d}{2}, z') \left[\frac{e^{ikR_o}}{4\pi R_o} - \frac{1}{\ell w} \sum_{m=1}^{\infty} \sum_{n=0}^{\infty} \epsilon_n \frac{\cot \gamma_{mn} \frac{d}{2}}{\gamma_{mn}} \right.$$

$$\left. \sin\frac{m\pi}{\ell}(z+h) \sin\frac{m\pi}{\ell}(z'+h) \cos\frac{n\pi}{w}x \cos\frac{n\pi}{w}x' \right] dx'dz' =$$

$$-A_{ez}^{inc}(z) + C_1'' \sin kz + C_o'' \cos kz \quad , \tag{83}$$

where C_o'' and C_1'' are integration constants independent of x.

The electric field vanishes at the ends of the slot

$$E_x(x, \pm\frac{d}{2}, \pm h) = 0 \quad , \tag{84}$$

which is used to find the constants C_o' and C_1' or C_o'' and C_1''.

B. "Approximate" Integral Equations

Because of the conditions $kw<<1$ and $w<<\ell$ the interior propagation constant can be approximated as

$$\gamma_{mn} \approx i\frac{n\pi}{w} \quad , n \neq 0. \tag{85}$$

Using (85) along with the identity [20]

$$\sum_{m=1}^{\infty} \sin\frac{m\pi}{\ell}z \sin\frac{m\pi}{\ell}z' = \frac{\ell}{2}\,\delta(z-z'),\ 0<z,z'<\ell\,, \tag{86}$$

and the product approximation [12]

$$E_x(x, -\frac{d}{2}, z) \approx V(z)\, f(x)\,,\ h-|z| >> w \quad , \tag{87}$$

where $V(z)$ is the slot voltage and the transverse field distribution, $f(x)$, satisfies

$$\int_0^w f(x)dx = 1 \quad ,$$

equation (82) reduces to

$$-\epsilon_o \int_{-h}^{h} 2\, V(z') \left[\frac{1}{\ell w} \sum_{m=1}^{\infty} \frac{\tan\gamma_m \frac{d}{2}}{\gamma_m} \sin\frac{m\pi}{\ell}(z+h) \sin\frac{m\pi}{\ell}(z'+h)\right.$$

$$+\int_o^w f(x')\left\{\frac{e^{ikR_o}}{4\pi R_o}+\delta(z-z')\sum_{n=1}^{\infty}\frac{\tanh(\frac{n\pi}{2}\frac{d}{w})}{n\pi}\cos\frac{n\pi}{w}x'\cos\frac{n\pi}{w}x\right.$$

$$\left.\right\}dx'\Big]dz' = -A_{ez}^{inc}(z) + C_1' \sin kz + C_o' \cos kz\,, \qquad (88)$$

where
$$\gamma_m = \sqrt{k^2 - (\frac{m\pi}{\ell})^2}\,.$$

The exterior term in the kernel is approximated as [11]

$$\int_{-h}^{h} V(z')\frac{e^{ikR_o}}{R_o}dz' \approx \int_{-h}^{h} V(z')\frac{e^{ik|z-z'|}-V(z)}{|z-z'|}dz'$$

$$+ V(z)\int_{-h}^{h}\frac{dz}{R_o}\,, \qquad (89)$$

where
$$\int_{-h}^{h}\frac{dz'}{R_o} \approx \ell n[4(h^2-z^2)]-2\ell n|x-x'|,\ h-|z|>>w\ . \qquad (90)$$

Applying (89) and (90) to (88) yields

$$-\epsilon_o\int_{-h}^{h} 2\Big[V(z')\frac{e^{ik|z-z'|}-V(z)}{4\pi|z-z'|}+V(z')\sum_{m=1}^{\infty}\frac{\tan\gamma_m\frac{d}{2}}{\ell w\gamma_m}\sin\frac{m\pi}{\ell}(z+h)$$

$$\sin\frac{m\pi}{\ell}(z'+h)\Big]\,dz' - \frac{\epsilon_o}{2\pi}V(z)\,\ell n[4(h^2-z^2)]$$

$$+\frac{\epsilon_o}{\pi}V(z)\int_o^w f(x')[\ell n|x-x'|-2\sum_{n=1}^{\infty}\frac{\tanh(\frac{n\pi}{2}\frac{d}{w})}{n}\cos\frac{n\pi}{w}x$$

$$\cos\frac{n\pi}{w}x']dx' = -A_{ez}^{inc}(z) + C_1' \sin kz + C_o' \cos kz \ . \qquad (91)$$

The above procedure applied to the "odd" equation (83) yields

$$-\epsilon_o \int_{-h}^{h} 2\left[\frac{V(z')e^{ik|z-z'|}}{4\pi|z-z'|} - V(z) - V(z')\sum_{m=1}^{\infty}\frac{\cot\gamma_m\frac{d}{2}}{\ell w\,\gamma_m}\sin\frac{m\pi}{\ell}(z+h)\right.$$

$$\left.\sin\frac{m\pi}{\ell}(z'+h)\right]dz' - \frac{\epsilon_o}{2\pi}V(z)\,\ell n[4(h^2-z^2)]$$

$$+\frac{\epsilon_o}{\pi}V(z)\int_{o}^{w} f(x')\left[\ell n|x-x'| - 2\sum_{n=1}^{\infty}\frac{\coth\left(\frac{n\pi}{2}\frac{d}{w}\right)}{n}\cos\frac{n\pi}{w}x\right.$$

$$\left.\cos\frac{n\pi}{w}x'\right]dx' = -A_{ez}^{inc}(z) + C_1'' \sin kz + C_o'' \cos kz \ . \qquad (92)$$

Conditions (84) become

$$V(\pm h) = 0 \ . \qquad (93)$$

C. "Shallow" Depth Integral Equations

The additional limits $kd << 1$ and $d << \ell$ will now be imposed on the integral equations of Part B.

Use of the approximation

$$\frac{\tan\gamma_m\frac{d}{2}}{\gamma_m} \approx \frac{d}{2} \ , \qquad (94)$$

along with the identity (86) in (91) yields

$$-\epsilon_o \int_{-h}^{h} \frac{V(z')e^{ik|z-z'|} - V(z)}{2\pi|z-z'|}\,dz' - \frac{\epsilon_o}{2\pi} V(z)\,\ell n[4(h^2-z^2)]$$

$$+ \frac{\epsilon_o}{\pi} V(z) \int_{o}^{w} f(x') \left[\ell n|x-x'| - \frac{d\pi}{2w} - 2\sum_{n=1}^{\infty} \frac{\tanh(\frac{n\pi}{2}\frac{d}{w})}{n} \cos\frac{n\pi}{w}x\right.$$

$$\left.\cos\frac{n\pi}{w}x'\right]dx' = -A_{ez}^{inc}(z) + C_1' \sin kz + C_o' \cos kz \ . \qquad (95)$$

Use of the approximation

$$\frac{\cot \gamma_m \frac{d}{2}}{\gamma_m} \approx \frac{2/d}{\gamma_m^2} - \frac{d}{6} \ , \qquad (96)$$

along with the identities [20]

$$\sum_{m=1}^{\infty} \frac{\cos\frac{m\pi x}{\ell}}{m^2 a^2 - b^2} = \frac{1}{2b^2} - \frac{\pi}{2ab} \frac{\cos[(\pi b/a)(1-\frac{|x|}{\ell})]}{\sin(\pi b/a)} \ , \ |x|<2\ell, \qquad (97)$$

and (86), in equation (92), yields

$$-\epsilon_o \int_{-h}^{h} 2\left[\frac{V(z')e^{ik|z-z'|} - V(z)}{4\pi|z-z'|} - \frac{\cos k\ell(1-\frac{|z-z'|}{\ell}) - \cos k(z+z')}{2kdw \sin k\ell}\right.$$

$$\left.V(z')\right]dz' - \frac{\epsilon_o}{2\pi} V(z)\,\ell n[4(h^2-z^2)]$$

$$+\frac{\epsilon_o}{\pi} V(z) \int_o^w f(x') \left[\ell n|x-x'| - \frac{d\pi}{6w} - 2 \sum_{n=1}^{\infty} \frac{\coth(\frac{n\pi}{2}\frac{d}{w})}{n} \right.$$

$$\left. \cos\frac{n\pi}{w}x \cos\frac{n\pi}{w}x' \right] dx' = -A_{ez}^{inc}(z) + C_1'' \sin kz + C_o'' \cos kz \, . \qquad (98)$$

The validity of approxmations (94) and (96) hinges upon the assumption that the unknown voltage does not vary appreciably over distances of order d. The solution of the "odd" equation, (98), violates this assumption near the end points, $h-|z| < d$. Nevertheless, interior to the interval, equation (98) does yield the correct solution. In fact (98) also yields a good approximation to the end behavior in the examples of Part H.

The dominant term in the kernel of the "odd" equation (98) is the second term

$$\epsilon_o \int_{-h}^{h} \frac{\cos k\ell(1 - \frac{|z-z'|}{\ell}) - \cos k(z+z')}{kdw \sin k\ell} V(z') \, dz' =$$

$$-A_{ez}^{inc}(z) + C_1'' \sin kz + C_o'' \cos kz \, . \qquad (99)$$

The solution to (99) is

$$V(z) \approx i\omega\mu_o \, w \frac{d}{2} H_{oz} e^{ikz\cos\theta_o} \, , \qquad (100)$$

where H_{oz} is now interpreted as the incident axial magnetic field at the center of the incident slot face. The solution (100) can be found by applying the operator $(\frac{\partial^2}{\partial z^2} + k^2)$ to both sides of (99). The fact that (100) violates the end conditions (93) can be corrected by retaining smaller terms in the kernel of (98).

D. Definition of Equivalent Radius

Consider Hallén's integral equation for a magnetic scattering antenna

$$\epsilon_o \int_{-h}^{h} I_m(z') \frac{e^{ikR_a}}{4\pi R_a} dz' = -A_{ez}^{inc}(z)$$

$$+ C_1 \sin kz + C_o \cos kz \ , \tag{101}$$

where

$$I_m(z') = -2V(z') \ , \tag{102}$$

$$I_m(\pm h) = 0 \ ,$$

$$R_a = \sqrt{a^2 + (z-z')^2} \ ,$$

$$A_{ez}^{inc}(z) = -\frac{i}{\omega} \frac{H_{oz}}{\sin^2\theta_o} e^{ikz\cos\theta_o} \ , \tag{103}$$

and θ_o is the incident wave direction with axial magnetic field amplitude H_{oz}. Using (89) and (90) this equation becomes

$$-\epsilon_o \int_{-h}^{h} \frac{V(z')\ e^{ik|z-z'|} - V(z)}{2\pi|z-z'|} dz' - \frac{\epsilon_o}{2\pi} V(z)\ \ell n[4(h^2-z^2)]$$

$$+ \frac{\epsilon_o}{\pi} V(z)\ \ell n\ a = -A_{ez}^{inc}(z) + C_1 \sin kz + C_o \cos kz \ . \tag{104}$$

Comparing (104) with (95) we see that the choice of equivalent radius

$$\ell n\, a = \int_o^w f(x') \left[\ell n|x-x'| - \frac{d\pi}{2w} - 2\sum_{n=1}^{\infty} \frac{\tanh(\frac{n\pi}{2}\frac{d}{w})}{n} \right.$$

$$\left. \cos\frac{n\pi}{w}x \cos\frac{n\pi}{w}x' \right] dx' \quad , \qquad (105)$$

reduces equation (95) to Hallén's integral equation, provided H_{oz} in (103) is interpreted as the incident axial magnetic field at the center of the incident slot face, as in (13).

The solution (100) to the approximate "odd" equation (99) is a good approximation to the "odd" problem when the observation point is several depth and width measures from the ends of the slot, $z=\pm h$. A very small part of the interval is excluded when the depth is comparable to the width. When the depth is much larger than the width, it is of interest to determine the form the voltage takes as the ends of the slot are approached.

Taking the limit $d/w>>1$ in the hyperbolic cotangent of (98) we see that equation (98) can be replaced by

$$\epsilon_o \int_{-h}^{h} I_m(z') \left[\frac{e^{ikR_a}}{4\pi R_a} - \frac{\cos k\ell(1-\frac{|z-z'|}{\ell}) - \cos k(z+z')}{2\, kdw\, \sin k\ell} \right] dz'$$

$$= -A_{ez}^{inc}(z) + C_1'' \sin kz + C_o'' \cos kz \quad , \qquad (106)$$

where the equivalent radius in this "odd" "very thick" case is

$$\ell n\, a = \int_o^w f(x') \left[\ell n|x-x'| - \frac{d\pi}{6w} - 2\sum_{n=1}^{\infty} \frac{1}{n} \cos\frac{n\pi}{w}x \right.$$

$$\cos\frac{n\pi}{w}x'\Big]dx' \quad . \tag{107}$$

E. Equivalent Radius in Terms of "Discontinuity" of Static Potentials

The integral equation for the static problem of Figure 4 is formulated by matching the electric vector potential at the slot face $y = -\frac{d}{2}$. The static electric vector potential satisfies a Poisson type equation. The solution exterior to the slot is

$$A^{>}_{ez}(\underline{\rho}) = 2\epsilon_o \int_{C_{\pm}} G^{>}(\underline{\rho}, \underline{\rho}')\, K_{mz}(\underline{\rho}')d\ell', \; y \gtrless \pm\frac{d}{2} \quad , \tag{108}$$

where $$G^{>}(\underline{\rho},\underline{\rho}') = -\frac{1}{2\pi}\ell n|\underline{\rho}-\underline{\rho}'| \quad ,$$

$$K_{mz}(x', \pm\frac{d}{2}) = \pm E_x(x', -\frac{d}{2}) \quad ,$$

$\underline{\rho} = x\underline{e}_x + y\underline{e}_y$ is the position vector, and $C_{\pm}$ are the slot faces $y' = \pm\frac{d}{2}$ and $0<x'<w$.

The electric field component in the x direction is "even" with respect to y. The potential (108) is thus odd with respect to y. The potential interior to the slot in Figure 4 can be found by separation of variables in Laplace's equation as

$$A^{<}_{ez}(\underline{\rho}) = \epsilon_o \sum_{n=1}^{\infty} A_n \sinh\frac{n\pi}{w}y \cos\frac{n\pi}{w}x + \epsilon_o A_o\, y \quad , \tag{109}$$

where matching tangential $\underline{E}$ at the slot face, $y = -\frac{d}{2}$, yields

$$A_n = -\frac{2}{\pi}\int_o^w E_x(x', -\frac{d}{2})\,\frac{\cos\frac{n\pi}{w}x'}{n\,\cosh(\frac{n\pi}{w}\,\frac{d}{2})}\,dx' \quad ,$$

$$A_o = -\frac{1}{w}\int_o^w E_x(x', -\frac{d}{2})\,dx' \quad .$$

The tangential electric field derived from (109), of course, vanishes on the walls x = 0, w. Matching the normal component of the electric displacement D_y at $y = -\frac{d}{2}$ yields the integral equation

$$A^{<}_{ez}(x, -\frac{d}{2}) - A^{>}_{ez}(x, -\frac{d}{2}) = -C_a \, , \tag{110}$$

or

$$\frac{\epsilon_o}{\pi}\int_o^w \left[\ell n\,|x-x'| - \frac{d\,\pi}{2w} - 2\sum_{n=1}^{\infty}\frac{\tanh(\frac{n\pi}{2}\,\frac{d}{w})}{n}\cos\frac{n\pi}{w}x\,\cos\frac{n\pi}{w}x'\right]$$

$$E_x(x', -\frac{d}{2})\,dx' = C_a \, , \tag{111}$$

where

$$\int_o^w E_x(x', -\frac{d}{2})\,dx' = V \, , \tag{112}$$

and 0<x<w. Comparing (105) and (111) we see that the equivalent radius for the "even" problem is

$$\ell n\, a = \frac{\pi}{\epsilon_o}\frac{C_a}{V} = \frac{\pi}{\epsilon_o V}\left[A^{>}_{ez}(x, -\frac{d}{2}) - A^{<}_{ez}(x, -\frac{d}{2})\right] \quad . \tag{113}$$

The "very thick" "odd" problem requires use of the "very thick" static problem shown in Figure 22. The potential in the half space $y<0$ is given by (108) with C_- now interpreted as the surface $y=0$. The potential interior to the slot is

$$A^{<}_{ez}(\rho) = \epsilon_o \sum_{n=1}^{\infty} A_n \cos\frac{n\pi}{w}x \, e^{\frac{-n\pi}{w}y} + \epsilon_o A_o y \ , \qquad (114)$$

where

$$A_n = \frac{2}{n\pi}\int_o^w E_x(x', 0) \cos\frac{n\pi}{w}x' \, dx' \ ,$$

$$A_o = -\frac{1}{w}\int_o^w E_x(x', 0) \, dx' \ .$$

The integral equation at the slot face is

$$A^{<}_{ez}(x,0) - A^{>}_{ez}(x,0) = -C_a \ , \qquad (115)$$

or

$$\frac{\epsilon_o}{\pi}\int_o^w E_x(x',0) \left[\ell n|x-x'| - 2\sum_{n=1}^{\infty}\frac{1}{n}\cos\frac{n\pi}{w}x' \cos\frac{n\pi}{w}x\right]$$

$$dx' = C_a \ , \qquad (116)$$

where

$$\int_o^w E_x(x',0) \, dx' = V \ . \qquad (117)$$

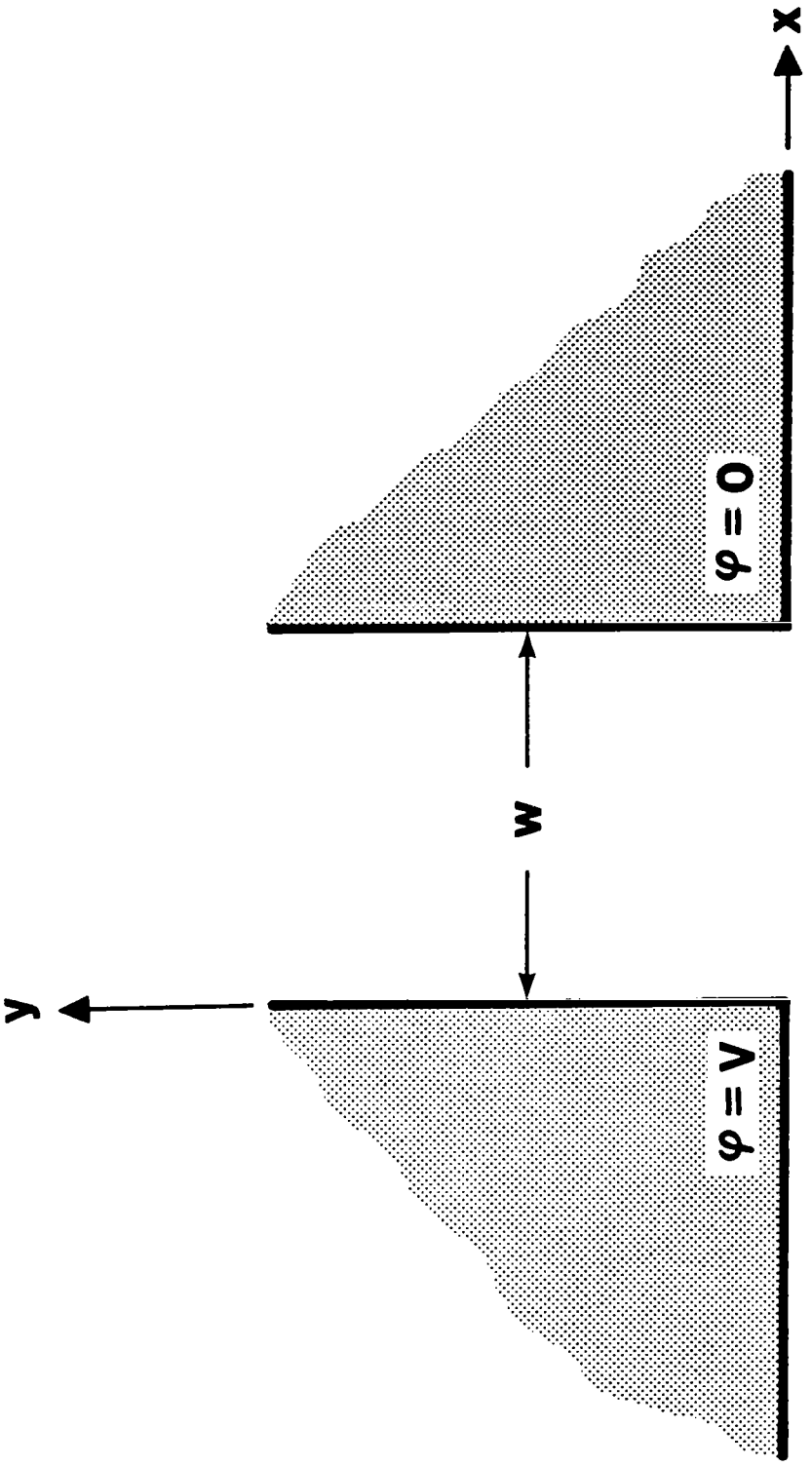

Figure 22. Very thick slot geometry.

Comparing (116) with (107) the equivalent radius in the "odd" "very thick" case is

$$\ell n\, a = \frac{\pi}{\epsilon_o V}\left[A^{>}_{ez}(x,0) - A^{<}_{ez}(x,0)\right] - \frac{d\,\pi}{6w} \quad . \tag{118}$$

F. Conformal Mapping Evaluation of Equivalent Radius

The conformal mapping solution given in Section III can be used to evaluate the "discontinuity" in electric vector potential in equation (113). The exterior electric vector potential can be written as

$$A^{>}_{ez}(\varrho) = A_{ez}(z) + \left[A^{>}_{ez}(-R, -\tfrac{d}{2}) - A_{ez}(-R - i\,\tfrac{d}{2})\right] \quad , \tag{119}$$

where $A_{ez}(z)$ is the conformal mapping solution (26), and R is a large positive quantity. The interior electric vector potential can be written as

$$A^{<}_{ez}(\varrho) = A_{ez}(z) + \left[A^{<}_{ez}(0,0) - A_{ez}(0+i0)\right] \quad . \tag{120}$$

The bracketed quantities are constants relating the conformal mapping solution to the interior and exterior potentials. The conformal mapping solution is analytic, external to the metal, and thus continuous at the slot face. From (113),(119), and (120) we obtain

$$\ell n\, a = \frac{\pi}{\epsilon_o V}\left[A^{>}_{ez}(-R, -\tfrac{d}{2}) - A^{<}_{ez}(0,0) - \Delta A_{eT}\right] \quad , \tag{121}$$

where $\Delta A_{eT} = A_{ez}(-R - i\,\frac{d}{2}) - A_{ez}(0+i0)$. The interior vector potential (109) vanishes at the origin. The exterior vector potential (108), at a large distance from the slot, R>>w, is

$$A^{>}_{ez}(-R, -\frac{d}{2}) \sim \frac{\epsilon_o}{\pi} V \ell nR \ . \qquad (122)$$

The symmetry of the field in Figure 6a means that $E_y(x,0) = 0$. This fact can be used to find the location $z = 0 + i0$ in the z_1 plane

$$z_1 = -1/\sqrt{p} \ . \qquad (123)$$

Using (123) and (33) in the conformal mapping solution, (18) and (26), we obtain

$$\Delta A_{eT} = \epsilon_o \frac{V}{\pi} \ell n\left[\frac{R}{-C_1\sqrt{p}}\right] \ , \qquad (124)$$

which from symmetry is also one half the charge between $z = -R-i\frac{d}{2}$ and $z = -R + i\frac{d}{2}$, given by (34). The equivalent radius in the "even" case is therefore

$$a = -C_1\sqrt{p} \ . \qquad (125)$$

The "very thick" "odd" problem requires the conformal mapping solution to Figure 22. The transformation between the upper half of the z_1 plane and the z plane of Figure 22 can be written as [21]

$$\frac{z}{w} = \frac{1}{\pi}(\arctan\zeta - \zeta) \ , \qquad (126)$$

where $$\zeta = \sqrt{z_1^2 - 1} \ ,$$

$$\arctan\zeta = \frac{\pi}{2} + \frac{1}{2i} \ell n\left(\frac{i\zeta+1}{i\zeta-1}\right) \ ,$$

and the principal branch is taken for each of the linear factors of the square root and the logarithm.

The exterior and interior potentials are related to the conformal mapping solution by means of

$$A^{>}_{ez}(\varrho) = A_{ez}(z) + [A^{>}_{ez}(-R, 0) - A_{ez}(-R + i0)] ,$$

$$A^{<}_{ez}(\varrho) = A_{ez}(z) + [A^{<}_{ez}(0, R) - A_{ez}(0 + iR)] .$$

The equivalent radius in the "odd" "very thick" case (118) can thus be written as

$$\ell n\, a = \frac{\pi}{\epsilon_o V} [A^{>}_{ez}(-R,0) - A^{<}_{ez}(0,R) - \Delta A_{eV}] - \frac{d\pi}{6w} , \qquad (127)$$

where $\Delta A_{eV} = A_{ez}(-R+i0) - A_{ez}(0 + iR)$.

The transformation (126) can be expanded for R>>w as

$$z_1 \sim \pi \frac{R}{w} \quad , z = -R ,$$

$$z_1 \sim 2e^{-\pi R/w-1} \quad , z= iR .$$

Using these locations in minus (18) and (26) we obtain

$$\Delta A_{eV} = \epsilon_o \frac{V}{\pi} [\ell n(\frac{\pi R}{2w}) + \pi \frac{R}{w} + 1] . \qquad (128)$$

From (114)

$$A^{<}_{ez}(0,R) \sim -\frac{\epsilon_o}{w} V R \quad ,$$

and $A^{>}_{ez}(-R,0)$ is given by (122). The equivalent radius in the "odd" "very thick" case from (127) is thus

$$a = \frac{2w}{\pi e} e^{\frac{-d\pi}{6w}} \quad . \tag{129}$$

G. "Deep" Slot Integral Equations

We now simplify the integral equations of Part B, (91) for the "even" case and (92) for the "odd" case, when $d/w>>1$ but kd and d/ℓ are unrestricted.

The hyperbolic functions in (91) and (92) are thus replaced by unity and the transverse integration is carried out by means of the procedure used on the "very thick" "odd" equation in the previous two parts of this appendix.

The "deep" equations can thus be written in the compact form

$$\epsilon_o \int_{-h}^{h} I_m(z') \left[\frac{e^{ikR_a}}{4\pi R_a} + \sum_{m=1}^{\infty} \frac{\tan \gamma_m \frac{d}{2}}{\ell w \gamma_m} \sin\frac{m\pi}{\ell}(z+h) \sin\frac{m\pi}{\ell}(z'+h) \right]$$

$$dz' = -A^{inc}_{ez}(z) + C'_1 \sin kz + C'_o \cos kz \quad , \tag{130}$$

for the "even" case; and for the "odd" case as

$$\epsilon_o \int_{-h}^{h} I_m(z') \left[\frac{e^{ikR_a}}{4\pi R_a} - \sum_{m=1}^{\infty} \frac{\cot \gamma_m \frac{d}{2}}{\ell w \gamma_m} \sin\frac{m\pi}{\ell}(z+h) \sin\frac{m\pi}{\ell}(z'+h) \right.$$

$$\left. \right] dz' = - A_{ez}^{inc}(z) + C_1'' \sin kz + C_o'' \cos kz \ , \qquad (131)$$

where $\gamma_m = \sqrt{k^2 - \left(\frac{m\pi}{\ell}\right)^2}$, and the equivalent radius is in both cases

$$a = \frac{2w}{\pi e} \ . \qquad (132)$$

An alternative representation for the sums in the kernels of (130) and (131) can be obtained by either beginning with an alternative representation for the interior Green's function appearing in (81), or by use of the Watson transformation. The resulting integral equations become

$$\epsilon_o \int_{-h}^{h} I_m(z') \left[\frac{e^{ikR_a}}{4\pi R_a} - \frac{1}{dw} \sum_{q,\text{odd}} \frac{2}{\gamma_q} \frac{\sin\gamma_q(h-z_>) \ \sin\gamma_q(h+z_<)}{\sin\gamma_q \ell} \right] dz'$$

$$= - A_{ez}^{inc}(z) + C_1' \sin kz + C_o' \cos kz \ , \qquad (133)$$

for the "even" case; and for the "odd" case

$$\epsilon_o \int_{-h}^{h} I_m(z') \left[\frac{e^{ikR_a}}{4\pi R_a} - \frac{1}{dw} \sum_{q,\text{even}} \frac{\epsilon_q}{\gamma_q} \frac{\sin\gamma_q(h-z_>) \ \sin\gamma_q(h+z_<)}{\sin\gamma_q \ell} \right] dz'$$

$$= - A_{ez}^{inc}(z) + C_1'' \sin kz + C_o'' \cos kz \ , \qquad (134)$$

where $\gamma_q = \sqrt{k^2 - \left(\frac{q\pi}{d}\right)^2}$. This representation is somewhat more efficient when kd and d/ℓ

are relatively small.

H. Solution of Integral Equations

The solution of the various integral equations in this appendix can be accomplished by means of the Galerkin method described in Appendix IV. The only thing required is an additive modification of the matrix elements G_{jn}. These matrix elements are replaced by the elements $\tilde{G}_{jn}$.

The "even" problem with "shallow" depth has been replaced by Hallén's integral equation (101) and equivalent radius (125). The matrix elements of Appendix IV are thus not modified for this case.

The "very thick" "odd" problem with "shallow" depth, equation (106), with equivalent radius (129), uses matrix elements

$$\tilde{G}_{jn} = G_{jn} - \frac{4\pi}{dw} \int_{-h}^{h} F_j(z)\, F_n(z)\, dz \quad . \tag{135}$$

The "deep" "even" problem, equation (130), uses matrix elements

$$\tilde{G}_{jn} = G_{jn} + \frac{4\pi}{\ell w} \sum_{m=1}^{\infty} \frac{\tan \gamma_m \frac{d}{2}}{\gamma_m} F_{jn}^{(m)} \quad , \tag{136}$$

and the "deep" "odd" problem, equation (131), uses matrix elements

$$\tilde{G}_{jn} = G_{jn} - \frac{4\pi}{\ell w} \sum_{m=1}^{\infty} \frac{\cot \gamma_m \frac{d}{2}}{\gamma_m} F_{jn}^{(m)} \quad , \tag{137}$$

where

$$F_{jn}^{(m)} = \int_{-h}^{h} F_j(z)\left(\frac{\partial^2}{\partial z^2} + k^2\right) \sin\frac{m\pi}{\ell}(z+h)$$

$$\int_{-h}^{h} F_n(z') \sin\frac{m\pi}{\ell}(z'+h)\, dz' dz \quad , \tag{138}$$

and the equivalent radius (132) is used for both "even" and "odd" cases.

The alternative integral equations (133) and (134) will be used here for the "deep" case. The matrix elements for the "even" problem are

$$\tilde{G}_{jn} = G_{jn} - \frac{4\pi}{dw} \sum_{q,odd} \frac{2 F_{jn}^{(q)}}{\gamma_q \sin \gamma_q \ell} \quad , \tag{139}$$

and for the "odd" problem are

$$\tilde{G}_{jn} = G_{jn} - \frac{4\pi}{dw} \sum_{q,even} \frac{\epsilon_q F_{jn}^{(q)}}{\gamma_q \sin \gamma_q \ell} \quad , \tag{140}$$

where

$$F_{jn}^{(q)} = \int_{-h}^{h} F_j(z) \left(\frac{\partial^2}{\partial z^2} + k^2 \right) \int_{-h}^{h} F_n(z') \sin\gamma_q(h-z_>) \sin\gamma_q(h+z_<)\, dz'dz \quad , \tag{141}$$

and the same equivalent radius (132) is used. The q=0 term in (140) is identical to the contribution in (135).

To give some insight into the behavior of the "even" and particularly the "odd" solutions, we give the crude Hallén zero order asymptotic solutions to equations (101) and (106). The zero order approximation [18] uses the crude approximation

$$\int_{-h}^{h} I_m(z') \frac{e^{ikR_a}}{R_a} dz' \approx \Omega\, I_m(z) \quad . \tag{142}$$

Using (142) in (101) we obtain for the "even" problem

$$\frac{\epsilon_o}{4\pi} \Omega\, I_m(z) = - A_{ez}^{inc}(z)$$

$$+ \tfrac{1}{2}[A_{ez}^{inc}(h) + A_{ez}^{inc}(-h)] \frac{\cos kz}{\cos kh}$$

$$+ \tfrac{1}{2}[A_{ez}^{inc}(h) - A_{ez}^{inc}(-h)] \frac{\sin kz}{\sin kh} \quad , \tag{143}$$

where the equivalent radius (125) is used in (45) to define Ω. Of course (143) is not valid near resonances where the next order is required.

For the "odd" problem, once (142) is used in (106), we then apply the operator of equation (50) to solve the resulting approximate equation, yielding

$$\frac{i\Omega}{4\pi\omega\mu_o}\left(\frac{\partial^2}{\partial z^2} - \alpha^2\right) I_m(z) = -H_z^{inc}(z) \quad , \tag{144}$$

where $$\alpha = \sqrt{\frac{4\pi}{\Omega dw} - k^2} \quad ,$$

$$H_z^{inc}(z) = H_{oz}\, e^{ikz\cos\theta_o} \quad ,$$

and again H_{oz} is interpreted as incident magnetic field at the center of the incident slot face.

The solution to (144), which vanishes at the ends of the interval, is

$$I_m(z) = \frac{-i\ \omega\mu_o\ dw}{1 - \frac{\Omega}{4\pi}\, k^2\, dw\, \sin^2\theta_o} \left[H_z^{inc}(z) \right.$$

$$\left. - H_z^{inc}(h)e^{-\alpha(h-z)} - H_z^{inc}(-h)e^{-\alpha(h+z)} \right] \quad , \tag{145}$$

where the fact that $\alpha h >> 1$ has been used. The equivalent radius (129) is used to define Ω for the "odd" problem.

We give one example at normal incidence to illustrate the "even" and "odd" solutions. The example is taken from the final value of $\frac{kh}{\pi} = 3$ on Figure 17 with $d/w = 25$ and $\ell/w = 500$.

Figure 23 shows a comparison of the "deep" Galerkin solution using matrix elements

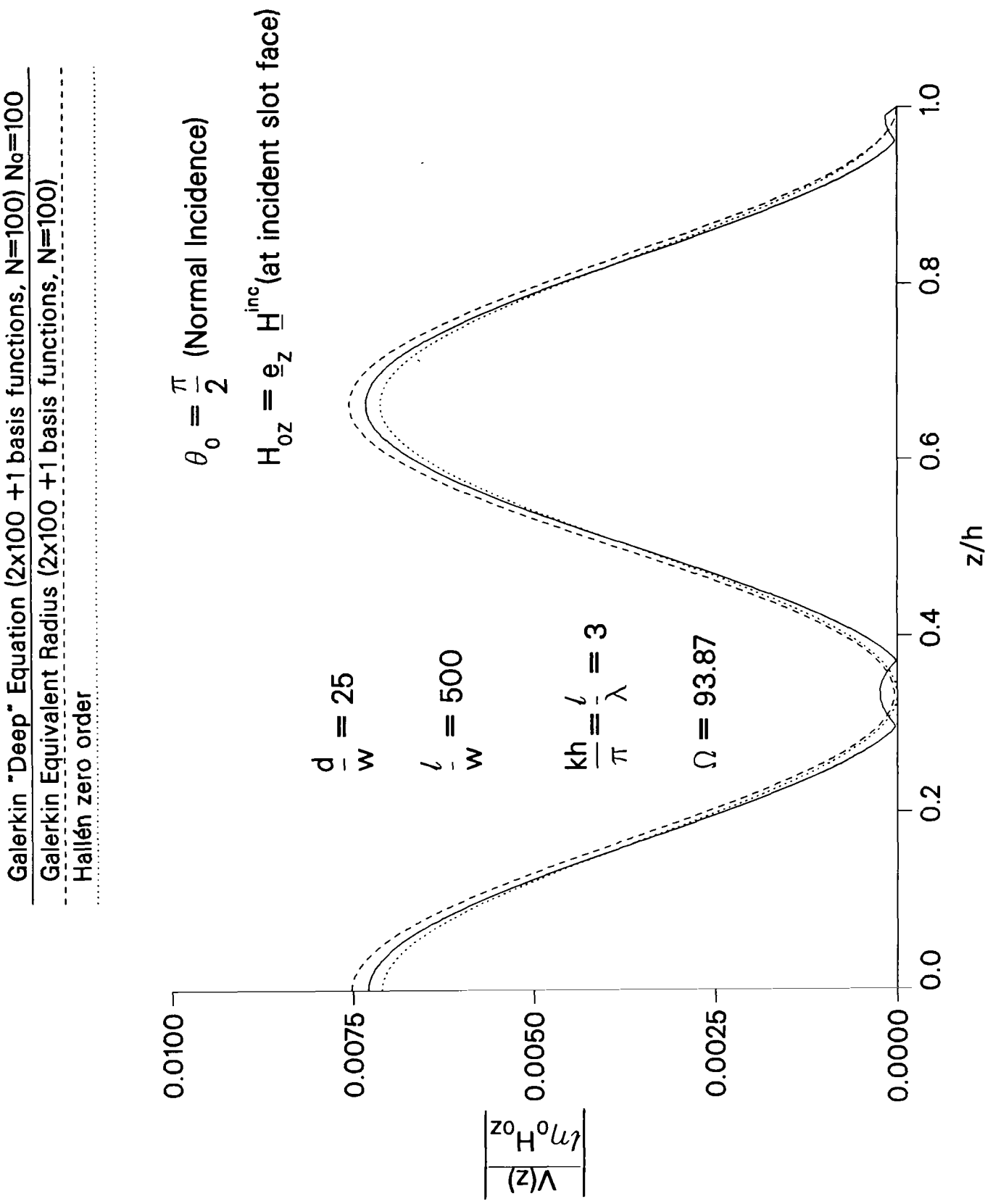

Figure 23. Comparison of voltage magnitude distributions for the "even" problem. The Galerkin solutions to the "exact deep" integral equation and Hallén's integral equation as well as the Hallén zero order solution are shown.

(139) (N_Q is the number of terms of the sum over q that have been included), the Galerkin solution of Hallén's integral equation (101), and the Hallén zero order solution (143). Note for normal incidence the final term of (143) is absent and no resonance occurs at $kh = 3\pi$.

Figure 24 shows a comparison of the "deep" Galerkin solution using matrix elements (140), the Galerkin solution of the "shallow" equation (106) using matrix elements (135), Hallén's zero order solution (145), and the Faraday's law result (74) or (100).

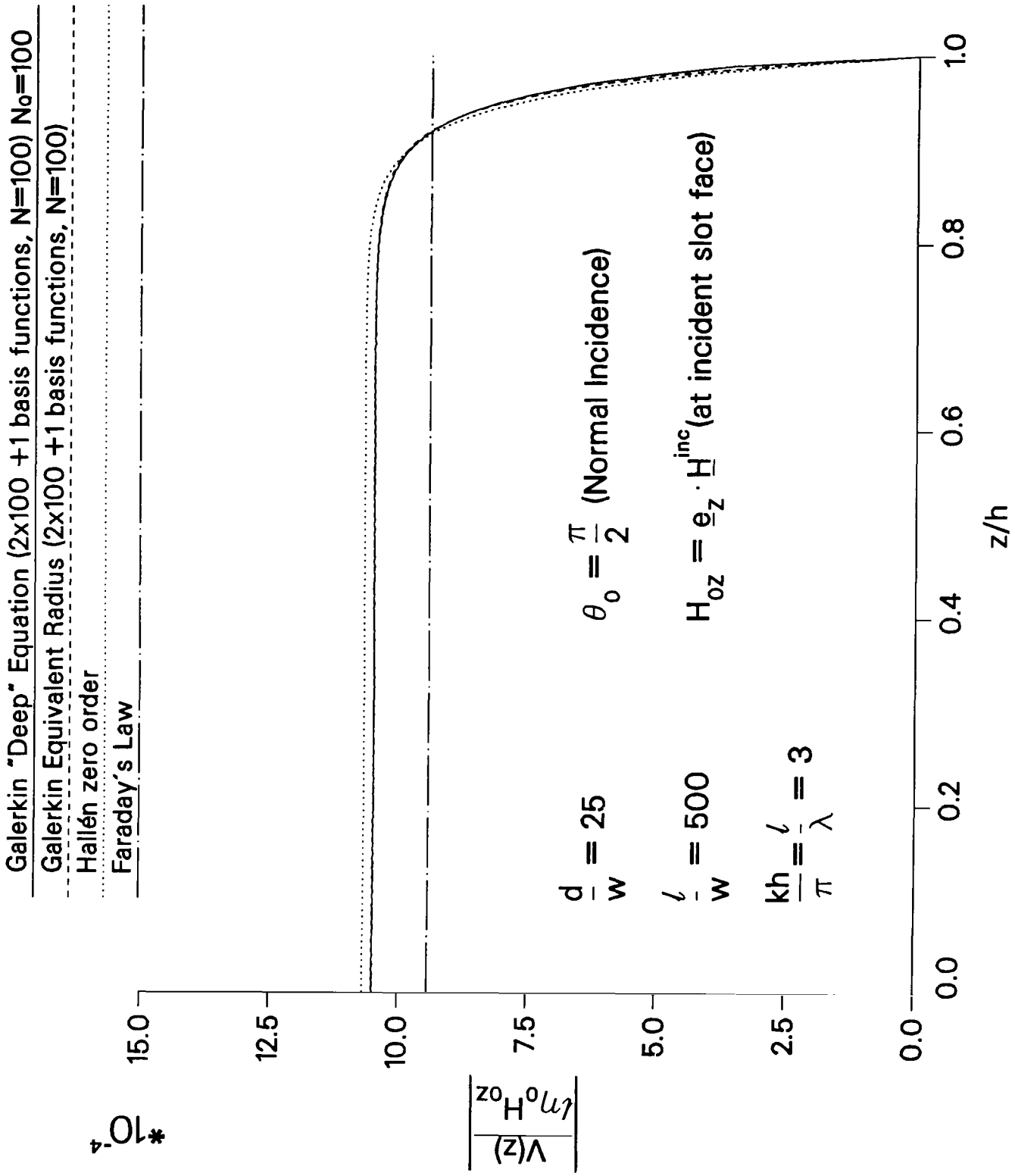

Figure 24. Comparison of voltage magnitude distributions for the "odd" problem. The Galerkin solutions to the "exact deep" integral equation and the approximate equivalent radius integral equation as well as the Hallén zero order solution and the result from Faraday's law are shown.

APPENDIX II. PARAMETERS OF CONFORMAL MAPPING SOLUTION

The transcendental equation (20) can be expanded for large and alternatively small d/w, yielding solutions [5]

$$p \sim \nu \left[1 + \frac{3}{4}\nu^2 + \frac{159}{128}\nu^4 + \frac{4021}{1536}\nu^6 + \frac{407349}{65536}\nu^8 \right.$$

$$\left. + \frac{20778821}{1310720}\nu^{10} + \ldots \right] , \qquad (146)$$

where $$\nu = 4/e^{(2+\pi d/w)} \quad , d/w >> 1 \quad ,$$

and

$$p \sim 1 - 4\nu' + 8\nu'^2 - \{11 - 4\ \ell n(\tfrac{\nu'}{2})\}\nu'^3 + \{3 - 4\ \ell n(\tfrac{\nu'}{2})\}4\nu'^4$$

$$- \{\tfrac{95}{8} - 29\ \ell n(\tfrac{\nu'}{2}) + 6\ \ell n^2(\tfrac{\nu'}{2})\}\nu'^5 + \ldots \quad , \qquad (147)$$

where $$\nu' = \sqrt{\frac{d}{\pi w}} \quad , d/w << 1 \quad .$$

The intersection of these two approximations, with the number of terms shown, occurs at

$$\frac{d}{w} = .06589225619 \quad ,$$

at which point the relative error in the value of p is four tenths of one percent.

Corresponding expansions for the constant $-C_1/w$ are

$$-\frac{C_1}{w} \sim \frac{1}{\pi}\Big[1 - \frac{\nu^2}{4} - \frac{21}{64}\nu^4 - \frac{81}{128}\nu^6 - \frac{70519}{49152}\nu^8$$

$$- \frac{466405}{131072}\nu^{10} - \frac{24499121}{2621440}\nu^{12} + \ldots\Big] \,, \qquad (148)$$

and

$$-\frac{C_1}{w} \sim \frac{1}{4}\Big[1 + 2\nu' + \{1 + 2\,\ell n(\frac{\nu'}{2})\}\nu'^2$$

$$- \{\frac{1}{2} - 2\,\ell n(\frac{\nu'}{2})\}\nu'^3 - \{\frac{3}{4} + 2\,\ell n(\frac{\nu'}{2})\}\nu'^4$$

$$- \{\frac{1}{16} + \frac{3}{2}\,\ell n(\frac{\nu'}{2}) + \ell n^2(\frac{\nu'}{2})\}\nu'^5 + \ldots\Big] \,. \qquad (149)$$

The maximum relative error in $-C_1/w$, with the number of terms shown, at the intersection point of the approximations for p, is six one–hundredths of one percent.

APPENDIX III. KING THREE–TERM Ψ PARAMETERS

The Ψ parameters used in the King three–term method are defined by the integral representations [13]

$$\Psi_{dUR} = \frac{1}{1 - \cos kh} \int_{-h}^{h} (\cos kz' - \cos kh) \left[\frac{\cos kR_{ao}}{R_{ao}} - \frac{\cos kR_{ah}}{R_{ah}} \right] dz' \quad , \tag{150}$$

$$\Psi_{dUI} = \frac{1}{1 - \cos \frac{1}{2}kh} \int_{-h}^{h} (\cos kz' - \cos kz) \left[\frac{\sin kR_{ao}}{R_{ao}} - \frac{\sin kR_{ah}}{R_{ah}} \right] dz' \quad , \tag{151}$$

$$\Psi_{dD} = \frac{1}{1 - \cos \frac{1}{2}kh} \int_{-h}^{h} (\cos \tfrac{1}{2}kz' - \cos \tfrac{1}{2}kh) \left[\frac{e^{ikR_{ao}}}{R_{ao}} - \frac{e^{ikR_{ah}}}{R_{ah}} \right] dz' \quad , \tag{152}$$

$$\Psi_{U}(h) = \int_{-h}^{h} (\cos kz' - \cos kh) \frac{e^{ikR_{ah}}}{R_{ah}} dz' \quad , \tag{153}$$

$$\Psi_{D}(h) = \int_{-h}^{h} (\cos \tfrac{1}{2}kz' - \cos \tfrac{1}{2}kh) \frac{e^{ikR_{ah}}}{R_{ah}} dz' \quad , \tag{154}$$

where

$$R_{ao} = \sqrt{a^2 + z'^2} \ ,$$

$$R_{ah} = \sqrt{a^2 + (h - z')^2} \ .$$

These integrals can be evaluated numerically, or for very small a, can be approximated in terms of standard sine and cosine integrals [5].

The power radiated by the magnetic current on the antenna can be evaluated by the Poynting vector method [7]. Assuming the current (54) is concentrated along a filament at the z axis, the radiated power can be written as [5]

$$P_{rad} = \eta_o \, |H_{oz}|^2 \frac{\pi}{k^2 \, |Q|^2} \left[\, |\Psi_{dD}|^2 \, 2P_{FF} \right.$$

$$\left. - 2 \, \Psi_{dDI} \, \Psi_{dUI} \, P_{FG} + \Psi_{dUI}^2 \, P_{GG} \right] \ , \qquad (155)$$

where

$$P_{FF} = Cin(4kh) + 4 \, Si(2kh) \, \cos kh \, (kh \, \cos kh - \sin kh)$$

$$- \sin^2 2kh \ ,$$

$$P_{FG} = 4 \cos^3 \tfrac{1}{2}kh \, [Cin(3kh) - Cin(4kh)]$$

$$+ 4 \sin^3 \tfrac{1}{2}kh \, [Si(3kh) + Si(kh)]$$

$$+4Si(2kh) \, [2kh \, \cos kh \, \cos \tfrac{1}{2}kh - \sin \tfrac{1}{2}kh \, (1 + 3 \, \cos kh)]$$

$$+2\cos\tfrac{1}{2}kh\,(\cos 3kh - \cos kh) \quad ,$$

$$P_{GG} = (4 + \tfrac{3}{2}\cos kh)[Cin(3kh) - Cin(kh)]$$

$$+ \tfrac{3}{2}(kh - \sin kh)[Si(3kh) + Si(kh)]$$

$$+4Si(2kh)[kh(1 + \cos kh) - 2\sin kh] - 4$$

$$+ 2\cos 2kh + \tfrac{3}{2}\cos 3kh + \tfrac{1}{2}\cos kh \quad ,$$

Ψ_{dDI} is the imaginary part of Ψ_{dD}, and Q is defined below (54). The sine and cosine integrals are defined by

$$Si(x) = \int_0^x \frac{\sin t}{t}\,dt \quad ,$$

$$Cin(x) = \int_0^x \frac{1 - \cos t}{t}\,dt \quad .$$

Note that a much simpler formula can be obtained for P_{rad} [5] by approximating the scattered axial magnetic field, resulting from the magnetic current (54), by minus the incident axial magnetic field and then using the EMF method [7].

APPENDIX IV. GALERKIN ANTENNA SOLUTION

The magnetic current basis functions are the piecewise sines (56). Applying equation (50) to Hallén's integral equation (51), and substituting the expansion (55), yields the axial magnetic field equation

$$H_z^{scatt}(z) = \frac{i}{4\pi\omega\mu_o} \sum_{n=-N}^{N} I_{mn} \left(\frac{\partial^2}{\partial z^2} + k^2 \right)$$

$$\int_{-h}^{h} F_n(z') \frac{e^{ikR_a}}{R_a} dz' = -H_z^{inc}(z) \quad . \tag{156}$$

The application of the operator, $\int_{-h}^{h} F_j^*(z)\, dz$, where the asterisk denotes complex conjugate, to the magnetic field equation yields the linear system for I_{mn}

$$\frac{i}{4\pi\omega\mu_o} \sum_{n=-N}^{N} G_{jn} I_{mn} = -H_{oz} H_j \quad , \tag{157}$$

where
$$G_{jn} = \int_{-h}^{h} F_j(z) \left(\frac{\partial^2}{\partial z^2} + k^2 \right) \int_{-h}^{h} F_n(z') \frac{e^{ikR_a}}{R_a} dz' dz \quad , \tag{158}$$

$$j = -N, \ldots, 0, \ldots, N \quad ,$$

$$H_j = \int_{-h}^{h} F_j(z)\, e^{ikz\cos\theta_o}\, dz \quad . \tag{159}$$

The z integral of G_{jn} can be eliminated by integration by parts yielding

$$G_{jn} = \frac{-\sin U_{j+1,\,j-1}}{\sin U_{j,j-1}\,\sin U_{j+1,j}} A_n(z_j) + \frac{1}{\sin U_{j,j-1}} A_n(z_{j-1})$$

$$+ \frac{1}{\sin U_{j+1,j}} A_n(z_{j+1}) \quad , \tag{160}$$

where $$U_{j,n} = k(z_j - z_n) \quad ,$$

$$A_n(z) = \int_{-h}^{h} F_n(z') \frac{e^{ikR_a}}{R_a} k\, dz' \quad . \tag{161}$$

The remaining z' integral $A_n(z)$ can be evaluated in terms of generalized sine and cosine integrals [12], which can in this case be reduced exactly to standard sine and cosine integrals [5], [12], [14].

To calculate the radiated power, the EMF method [7], in its complementary form, is applied to a slender antenna, yielding

$$P_{rad} = -\tfrac{1}{2}\,\mathrm{Re} \int_{-h}^{h} H_z^{*scatt}\, I_m\, dz \quad . \tag{162}$$

Using (156) for H_z^{scatt} and (55) for I_m, we obtain

$$P_{rad} = \frac{1}{8\pi\omega\mu_o}\,\mathrm{Re}\left[i \sum_{j=-N}^{N} \sum_{n=-N}^{N} I_{mj}\, I_{mn}^{*}\, G_{jn}^{*} \right] \quad . \tag{163}$$

Note that the system for I_{mn} can be broken into even and odd parts (in the antenna length) to reduce computation time [5].

REFERENCES

[1] K. S. H. Lee, editor, EMP Interaction: Principles, Techniques, and Reference Data. New York: Hemisphere Pub. Corp., 1986.

[2] J. Van Bladel, Electromagnetic Fields. New York: Hemisphere Pub. Corp., 1985.

[3] R. F. Harrington and David T. Auckland, "Electromagnetic Transmission Through Narrow Slots in Thick Conducting Screens," IEEE Trans. Antennas Propagat., Vol. AP–28, pp 616–622, Sept. 1980.

[4] G. A. Seely, "An Approximate Method of Incorporating the Wall Thickness Into Aperture Calculations," presented at Nat. Radio Sci. Meet., U. R. S. I. B–15–10, Vancouver, CANADA, June 1985.

[5] L. K. Warne and K. C. Chen, "Electromagnetic Penetration of Narrow Slot Apertures Having Depth and Losses," Sandia National Laboratories Report, to be published.

[6] J. A. Stratton, Electromagnetic Theory. New York: McGraw–Hill Inc., 1941.

[7] C. H. Papas, Theory of Electromagnetic Wave Propagation . New York: McGraw–Hill Inc., 1965.

[8] W. R. Smythe, Static and Dynamic Electricity. New York: McGraw–Hill Inc., 1968, pp 72–93.

[9] H. Kaden, Wirbelstrome und Schirmung in der Nachrichtentechnik. Berlin:

Springer–Verlag, 1959, pp 236–254.

[10] S. A. Schelkunoff and H. T. Friis, Antennas Theory and Practice. New York: John Wiley and Sons, 1952, Section 8.4.

[11] E. Hallén, Electromagnetic Theory. London: Chapman and Hall Ltd., 1962, Section 35.3.

[12] R. W. P. King, The Theory of Linear Antennas. Cambridge, Mass.: Harvard University Press, 1956, Sections I.7, II.19.

[13] R. E. Collin and F. J. Zucker, editors, Antenna Theory: Part 1. New York: McGraw–Hill Inc., 1969, Chapter 9.

[14] W. L. Stutzman and G. A. Thiele, Antenna Theory and Design. New York: John Wiley and Sons, 1981, Section 7.5.

[15] R. W. P. King, "The Linear Antenna – Eighty Years of Progress," Proc. of the IEEE, Vol. 55, No. 1, Jan. 1967.

[16] L. K. Warne and K. C. Chen, "Electromagnetic Penetration of Narrow Slot Apertures Having Depth Resonances and Losses," Sandia National Laboratories Report, to be published.

[17] M. Born and E. Wolf, Principles of Optics. New York: Pergaman Press, 1980, Section 11.3.

[18] J. D. Kraus, Antennas. New York: McGraw–Hill, Inc., 1950, Section 9–5.

[19] D. C. Chang, S. W. Lee, and L. Rispin, "Simple Formula for Current on a Cylindrical Recieving Antenna," IEEE Trans. on Ant. and Prop., Vol. AP–26, No. 5, Sept. 1978.

[20] F. Oberhettinger, Fourier Expansions. New York: Academic Press, 1973, pp 13, 19, 20.

[21] S. Flugge, editor, Elektrische Felder Und Wellen. Handbuch Der Physik Band XVI, Berlin: Springer Verlag, 1958, p75.